# Wearable Active Directionally-sensitive Radiation Dosimeter

Submitted by

Le Huu Hai

Bachelor of Telecommunication
Master of Electronic Engineering

A thesis submitted in total fulfillment
of the requirements for the degree of
Doctor of Philosophy

Department of Engineering
College of Science, Health and Engineering

La Trobe University
Victoria, Australia

November 2018

# Declaration of Authorship

Except where reference is made in the text of the thesis, this thesis contains no material published elsewhere or extracted in whole or in part from a thesis submitted for the award of any other degree or diploma.

No other person's work has been used without due acknowledgement in the main text of the thesis.

The thesis has not been submitted for the award of any degree or diploma in any other tertiary institution.

Signed:

Date: *11$^{st}$ November 2018*

# *Abstract*

The International Atomic Energy Agency (IAEA) has warned of the threat of "dirty" bomb attacks resulting from inadequate management of radioactive sources world-wide. Since 1996, approximately 1500 radioactive sources have been lost in America and Europe every year, which has led to a very high risk of radioactive material being used to produce dirty bombs for terrorist purposes. The consequence of such a bomb would be not only as deadly as a regular bomb but radiation spread out from a dirty bomb explosion could cause long-term health effects to the public as well as social disruption and economic crisis to society.

Radiation is energy that travels in the form of waves or high-speed particles. It can exist naturally in the environment or is man-made for use in diagnostic X-rays, nuclear weapons, nuclear power plants, and cancer treatment. Radiation exposure can damage human tissues and organs, sometimes resulting in disease. The effects of radiation exposure to human health depend on the amount and duration of exposure, but are different for different body regions as well as the types of radioactive sources. Health effects can be chronic (long-term effects) or acute (short-term effects). The biggest risk for long-term human health after radiation exposure is cancer: the unborn, neonates, children and adolescents are particularly at risk, as they are more sensitive to radiation than adults.

Ionizing radiation cannot be detected by human senses, so we are dependent on instruments to observe its existence in the environment. Radiation dosimeters are instruments designed for detecting and measuring particles emitted by radioactive materials produced by particle accelerators or observed in cosmic rays. Recently, the problem of detecting and locating radioactive sources has gained increased importance due to the threat to public safety and homeland security from radiation attacks by terrorists. In addition, the localization of radioactive sources is also a critical issue within the nuclear industry, including nuclear power plant decommissioning, radioactive waste management and radiation protection.

In practice, measurements of radiation intensity acquired at multiple locations are often used to estimate the location and strength of a radioactive source. Currently, to improve the accuracy of detecting and locating radioactive materials, researchers have been attempting to design detectors with better measurement characteristics, as well as developing new mathematical models for automatic source localization.

This thesis proposes a novel wearable directionally-sensitive radiation dosimeter that can provide the real-time identification, direction estimation, and intensity of a radioactive source. It commences with a literature review of existing radiation detectors and the current state-of-the-art of directionally-sensitive radiation dosimeters. Next, the proposed dosimeter is modeled in Geant4, a Monte Carlo simulation package for radiation dosimetry, followed by the development of an algorithm to estimate the emission direction of radioactive sources based on the radiation intensity measured by four closest detectors in an array of eight detectors, arranged in a circular pattern. The performance of the proposed system is then analyzed in terms of radioactive source emission direction, estimation speed and accuracy at different source-to-detector (STD) distances. Finally, the ability of the proposed dosimeter to determine the source direction in a 3D environment is evaluated using different shaped detectors. Although the proposed dosimeter is intended for human use, with minor modifications, it can be adapted for use in other platforms (such as a robot) to meet the requirements of different situations.

# *Acknowledgements*

This thesis would not have been completed without support and encouragement from many people, to whom I am extremely grateful.

Firstly, I would like to express my deepest gratitude and special thanks to Mr. Paul Junor, my principal supervisor at La Trobe University, for his supervision and academic guidance throughout my research. Paul has been an excellent source of knowledge, a very supportive supervisor as well as a great encouragement for me to overcome every single obstacle during my PhD journey. I could not come to this final state to finish my research without his support.

Special thanks to Adjunct Professor Richard Kirsner, my co-supervisor, for his support when proofreading my thesis, papers and providing me valuable feedback throughout my research. I also would like to thank to Dr. Graeme O'Keefe, medical physicist at the Department of Molecular Imaging and Therapy at Austin Health, for his valuable contribution to my research.

Special thanks to Associate Professor Moshi Geso, of the School of Medical Radiations, RMIT University, for his extremely supportive contribution to my thesis. He has spent a lot of time and effort to help me at the hardest time during my research even though I am not actually one of his students. Together with Paul, he always provided me with valuable academic advice and motivation to keep going until this final state of my research.

I also would like to gratefully acknowledge the valuable support of the Program 165 of Vietnam and The Graduate School of La Trobe University for providing scholarship and financial support. The scholarship and support have given me a wonderful opportunity to study, to do research and to expand my knowledge as well as to satisfy my desire to complete my research degree. I also would like to extend my special thanks to all the staff in the Department of Engineering at La Trobe University for being a supportive team in my daily work.

Special thanks to my parents who have sacrificed everything for my education and always encouraged me to complete my PhD degree. Without their support and encouragement, I would not be able to come to this state. I owe them in every achievement I have got in my life.

Finally, special thanks to Van Anh, my wife. I am deeply grateful for your sacrifice, patience and encouragement throughout my research. Special thanks to my daughters, Thu Ngan and Ngoc Diep, who are always a wonderful motivation for me to overcome

every challenge in my life. You might not be aware, but you all actually make a huge contribution to my study and my life. *This thesis is for you all!*

Above all, my special thanks to everyone who were involved into my study:

**"IF I HAVE SEEN FURTHER THAN OTHERS, IT IS BY STANDING UPON THE SHOULDERS OF GIANTS"** - ***Sir Isaac Newton*** -

# Contents

# List of Figures

# List of Tables

# Abbreviations

| | |
|---|---|
| **BGO** | **B**ismuth **G**ermanium **O**xide |
| **CdMnTe** | **C**admium **M**anganese **T**elluride |
| **CdTe** | **C**admium **T**elluride |
| **CdZnTe** | **C**admium **Z**inc **T**elluride |
| **CERN** | The **E**uropean **C**ouncil for **N**uclear **R**esearch |
| **DRLs** | The **D**iagnostic **R**eference **L**evels |
| **FOV** | **F**ield of **V**iew |
| **FWHM** | **F**ull **W**idth at **H**alf **M**aximum |
| **GaAs** | **G**allium **A**rsenide detector |
| **Geant4** | for **G**Eometry **A**Nd **T**racking |
| **GUI** | **G**raphic **U**ser **I**nterface |
| **IAEA** | **I**nternational **A**tomic **E**nergy **A**gency |
| **ICRP** | **I**nternational **C**ommission on **R**adiological **P**rotection |
| **LD** | **L**ethal **D**ose |
| **MCA** | **M**ulti **C**hannel **A**nalyzer |
| **MURA** | **M**odified **U**niformly **R**edundant **A**rray |
| **NaI** | **S**odium **I**odide |
| **NIST** | **N**ational **I**nstitute of **S**tandards |
| **PRD** | **P**ersonal **R**adiation **D**etector |
| **RIID** | **R**adioactive **I**sotope **I**dentification **D**evice |
| **RPM** | **R**adiation **P**ortal **M**onitor |
| **SNR** | **S**ignal to **N**oise **R**atio |
| **STD** | **S**ource to **D**etector |
| **TLD** | **T**hermoluminescent dosimeter |
| **UAV** | **U**nmanned **A**erial **V**ehicle |

# Chapter 1

# Introduction

In 2011, the release of radioactive material into the environment from the Tokyo Electric Power Company's Fukushima Daiichi nuclear power plant due to earthquakes and a tsunami led to increased public concern about the potential for acute and long-term health effects on human beings [1]. The adverse effects from the accident may have been reduced if emergency responders were equipped with radiation dosimetry capable of identifying areas or direction having the strongest radiation activity, so that evacuation or isolation processes could be conducted more effectively by giving priority responses to the highest risk region.

According to the International Atomic Energy Agency (IAEA), radioactive materials for building so-called "dirty" bombs are easy to find in many countries worldwide. Since 1996, in America approximately 1500 radioactive sources have gone missing each year; within Europe that number is 70. Initially the consequence of a dirty bomb would be only as deadly as a regular bomb, but spread-out radiation might poison those attempting to help the injured or inhaling contaminated air. As a result, the nearby area including airports or subway stations might need to be closed for months with a costly cleanup process after such an attack [2]. The direct impacts of a dirty bomb would depend on many factors, but social disruption and economic crisis would be an inevitable consequence after any explosion [3].

The threat of smuggled radioactive materials has increased due to their appeal for producing dirty bombs for terrorist purposes [4]. In a speech in Prague in 2009, U.S.A President Obama has stated his deep concern about the probability of a nuclear attack

by terrorists: “Black market trade in nuclear secrets and nuclear materials abound. The technology to build a bomb has spread. Terrorists are determined to buy, build or steal one.” [5]. Radiation detectors provide a useful tool against nuclear smuggling by detecting, tracking and identification of radioactive sources during any use, storage and/or transport of nuclear materials.

In response to the threat of a nuclear attack by terrorists, and to monitor civilian use of nuclear materials, the ability to detect, identify and localize radioactive sources is of extreme importance for homeland security for every country [6]. This thesis proposes a directionally-sensitive personal wearable radiation dosimeter that can provide real-time dose rate measurement, identification as well as emission direction estimation of radioactive sources. In practical operation, real-time dose rate is measured and provided to users by each individual detector. A measurement time frame of 15 seconds or longer was used to allow each detector to record an appropriate number of interacted particles, in order to accurately perform an estimation of source direction. In fact, the main aim is to design a personal wearable dosimeter; however, in practice, the proposed system can be easily integrated into other platforms for different applications without major modifications.

## 1.1 Radiation Exposure and Health Effects

Radiation is energy that can be considered as traveling in the form of waves or high-speed particles. It can exist naturally in the environment, or is man-made for use in diagnostic radiography, nuclear weapons, nuclear power plants and cancer treatment. The two main pathways for human radiation exposure are external and internal. External exposure happens when radiation is emitted by radioactive substances (referred to as radiation sources) outside the body, and internal exposure occurs when radiation is emitted from radiation sources taken into the body (for example, by injection or through wounds).

In general, health effects of radiation exposure depend on the amount and duration of exposure. Health effects can be chronic (long-term effects) and acute (short-term effects).

- **Chronic** exposure is continuous or intermittent exposure to radiation over a long period, and there is often a delay between the exposure and the observed health

effect with chronic exposure that can include cancer and other pathologies such as benign tumors, cataracts, and potentially harmful genetic changes.

- **Acute** health effects occur when particular parts of the body are exposed to a large amount of radiation. The large exposure can occur instantaneously or from multiple brief exposures such as accidentally handling a strong industrial radiation source, or extreme events such as nuclear explosions.

Radiation can damage human tissue and organs, sometimes resulting in disease. The effects of radiation exposure are different for different body regions and types of radioactive sources. There are several factors that determine the potential health effects but the most important is the absorbed dose - the actual amount of energy deposited in the body [7]. The variety of possible health effects based on different effective dose (measured in rem) is shown in Table 1.1

In a population subjected to high levels of radiation, cancer and cardiovascular disease are significant long-term risks to human health, increasing in proportion to exposed dose [8]. Among the exposed population, the unborn, neonates, children and adolescents are at highest risk as they are more sensitive to radiation than adults. Long-term and large scale epidemiological studies have showed that at doses above 100 mSv the risk of developing cancer increases significantly [9].

## 1.2 Radiation Interaction Process

Interaction of $\gamma$-rays with matter can occur in different processes, including: the Photoelectric Effect, Compton Scattering, Pair Production, Rayleigh (coherent) Scattering and Photonuclear Interactions. The first three processes are the most important as they result in radiation energy being deposited in matter [10].

### 1.2.1 Photoelectric Effect

Of interaction mechanisms for low-energy photons with matter, the Photoelectric Effect is the most important. During this process, a photon interacts either with an electron that is bound in an individual atom, or with an electron in condensed matter (usually

| **Dose (rem)** | **Effects** |
|---|---|
| 5-20 | Possible late effects; possible chromosomal damage. |
| 20-100 | Temporary reduction in white blood cells. |
| 100-200 | Mild radiation sickness within a few hours: vomiting, diarrhea, fatigue; reduction in resistance to infection. |
| 200-300 | Serious radiation sickness effects as in 100-200 rem and hemorrhage; exposure is a Lethal Dose (LD) to 10-35% of the population after 30 days (LD 10-35/30). |
| 300-400 | Serious radiation sickness; also marrow and intestine destruction; LD 50-70/30. |
| 400-1000 | Acute illness, early death; LD 60-95/30. |
| 1000-5000 | Acute illness, early death; LD 100/10. |

TABLE 1.1: Possible health effects of radiation exposure [7]

a solid) that is not bound to an individual atom but may be shared among many atoms [11].

When interacting with matter, the photon transfers all of its energy to an electron, and then disappears. The electron is ejected with a kinetic energy equal to the difference between the photon energy and its own binding energy. The photo-electron will then undergo interactions with atoms in its path, transferring energy to the atoms until it comes to rest. if the absorbing medium is water or biological tissue, Photoelectric absorption is most important for photons below 0.1 MeV.

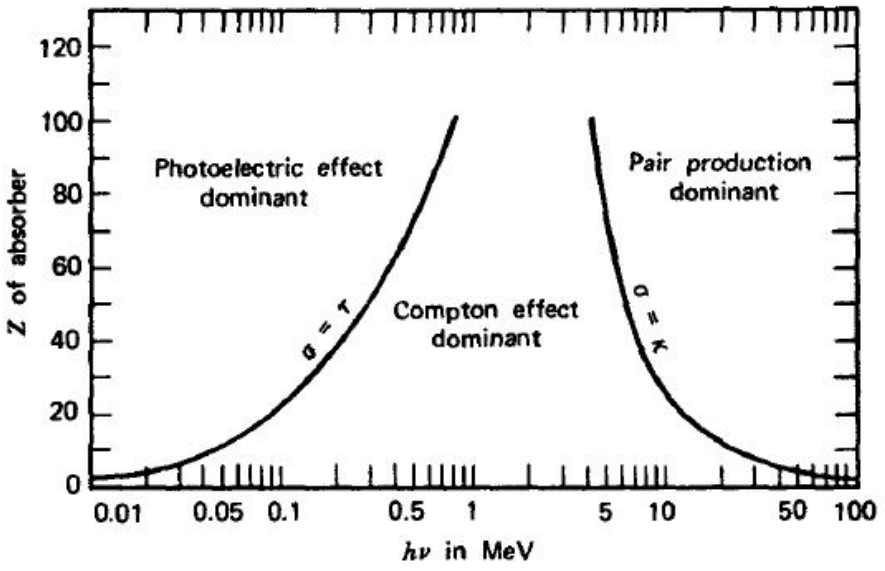


FIGURE 1.1: The relative importance of the three major types of $\gamma$-ray interaction (reproduced from [10]).

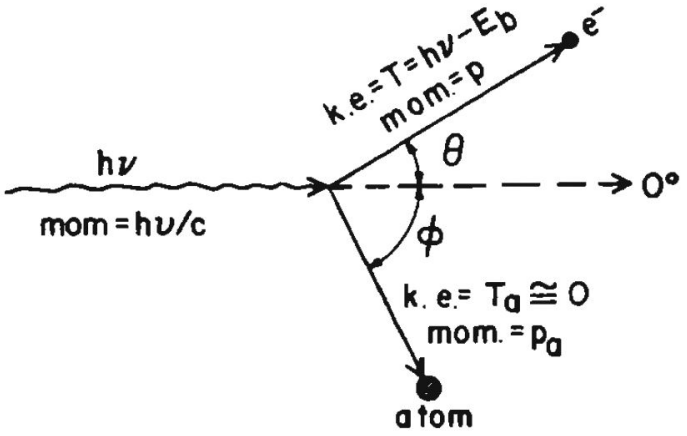


FIGURE 1.2: Kinematics of the Photoelectric Effect (reproduced from [11]).

### 1.2.2 Compton Scattering

The Compton Effect is the predominant interaction of medium-energy photons (0.3 to 3 MeV). A gamma ray will transfer a portion of its energy to an electron and then continue moving in a new direction, at a lower energy (longer wavelength). Thus, the Compton Effect has an absorption component and scattering component. The amount of energy lost by the photon can be related to the angle at which the scattered photon travels relative to the original direction of travel.

The scattered photon may then interact again, but since its energy has decreased, it

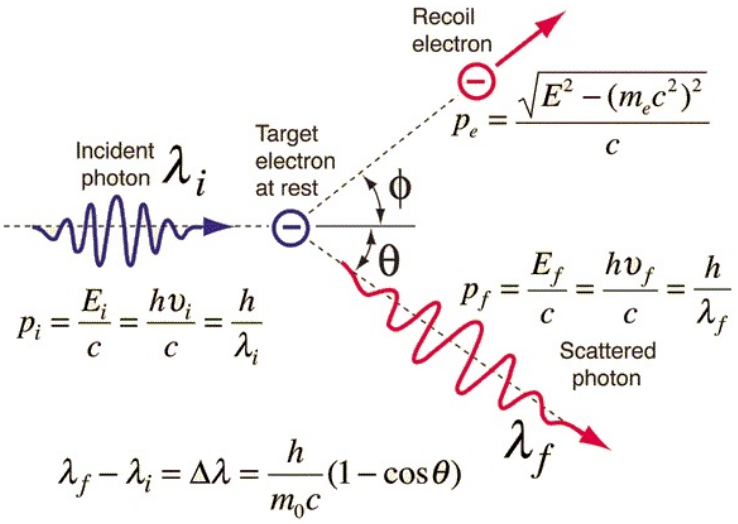


FIGURE 1.3: Compton Scattering (reproduced from [12]).

becomes more probable that it will enter into a Photoelectric or Rayleigh Interaction (see below). The free electron produced by the Compton process may be quite energetic and behave like a beta particle of similar energy, producing secondary ionization and excitation before coming to rest.

### 1.2.3 Pair Production

Under the influence of the electromagnetic field of a nucleus, a $\gamma$-ray with energy greater than 1.022 MeV, can have all of its energy converted into electron and positron. The $\gamma$-ray energy must be greater than 1.022 MeV for pair production, because the energy equivalent of the rest mass of the electron and positron is 0.51 MeV each. The available kinetic energy to be shared by the electron and the positron is the photon energy minus 1.02 MeV, or that energy needed to create the pair. The probability of pair production increases with Z (atomic mass number) of the absorber and with the photon energy.

### 1.2.4 Rayleigh Scattering

During a Rayleigh Scattering (or Coherent Scattering) process, a photon can also scatter from a complete atom. During the process, the atom will recoil, taking some of the energy and leaving the scattered photon with a slightly smaller energy. Rayleigh Scattering is the main scattering process for very low photon energies (typically below a few hundred

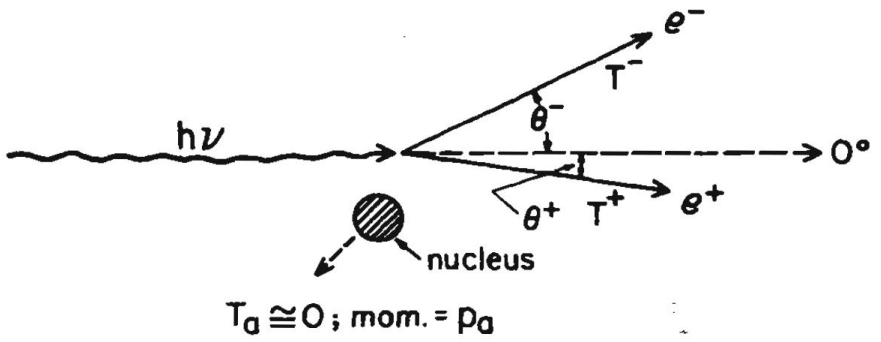


FIGURE 1.4: Pair Production of an atomic nucleus (reproduced from [11]).

keV for common materials) and is important for visible light. The deflection angle of scattered photon decreases with a higher energy photon which further limits the importance of Rayleigh scattering to low energy photons only.

### 1.2.5 Photonuclear Interactions

A photonuclear interaction process occurs when a photon with energy exceeding a few MeV enters and excites a nucleus and releases a proton or neutron. The probability of photonuclear interactions is very low (less than 5%) due to pair production. Therefore, the process is often neglected in radiation dosimetry.

## 1.3 Radiation Detection and Protection

Gamma radiation cannot be observed directly by human senses: it must interact with matter in order to be detected. Gamma-ray photons can interact with the charged electrons in the atoms of all matter due to their strong electromagnetic nature. Ionization, in which the gamma photon loses part or all of its energy to an electron, is the main process in detecting gamma rays. To detect the presence and to measure the energy of $\gamma$-rays, the liberated charge needs to be collected by detectors. Finally, how this energy is determined will depend on the detector type and its function [13] .

Radiation protection is the protection of people and the environment from the harmful effects of ionizing radiation. While the application of radiation in imaging and radiotherapy have offered many benefits, it is still a very high risk to the public if unsafe forms or excessive amounts of radiation exist in the environment. Protection from radiation used

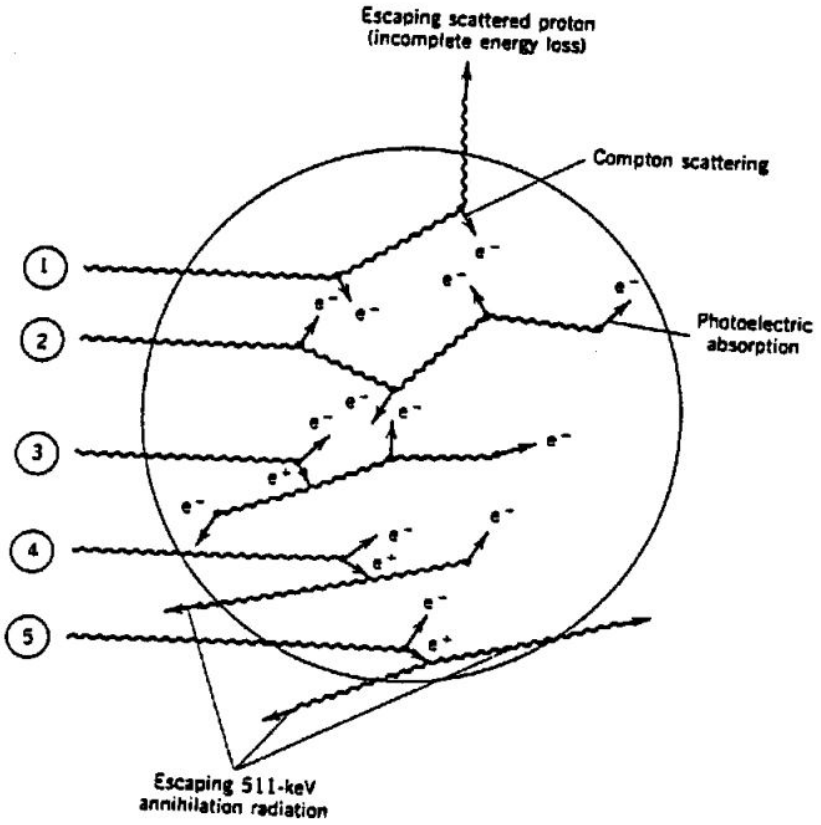


FIGURE 1.5: Processes occurring in the detection of gamma radiation (reproduced from [13]).

for treatment purposes in radiotherapy facilities is critical for workers, medical staff and patients. It is also very important to protect the general public from unintentional radiation exposure such as in accidents. An effective and appropriate radioactive material management policy will help to reduce the dangers to the public from radiation [14].

## 1.4 Identification and Localization of Radioactive Sources

Increasing security concerns regarding dirty bomb attacks has led to intense engineering efforts in the identification and localization of radioactive sources. In defence strategy, it is critical to identify the signatures of such sources before explosion or during transportation, enabling first responders to react more effectively [15].

In the medical use of radioisotopes, the ability to identify and locate radioactive sources is also a vital safety requirement. The use of these sources often includes transportation

and disposal, which are the two most sensitive steps due to the high probability of losing sources [16].

Radioactive materials can vary in appearance and exist in different physical states, including liquids and gases. They are also physically indistinguishable from other (non-radioactive) materials. In addition, ionizing radiation cannot be detected by any human senses: it cannot be seen, heard, smelled, tasted, or felt. Therefore, simple visual inspection is not sufficient to identify radioactive materials, and an instrument is required to detect and measure radiation [17]. There are four major types of handheld and laboratory equipment available on the market for detecting and identifying radioactive materials:

- **Personal Radiation Detector (PRD)**: the PRD is a wearable gamma and neutron radiation detector providing alarms with flashing lights, tones, and vibrations when exposed to elevated radiation levels. Most PRDs display the detected radiation intensity numerically (on a scale of 0 to 9) and can be used to locate a radiation source; however, they typically are not as sensitive as handheld survey meters and cannot identify the type of radioactive source.
- **Handheld Survey Meter**: the survey meter is a handheld radiation detector, which usually measures the amount of radiation present and provides this information on a numerical display in units of counts per minute, counts per second, or micro-roentgen ($\mu$R), or micro-rem ($\mu$rem) per hour. Most of these devices detect beta and gamma radiation only, while some models can detect alpha, beta, gamma, and neutron radiation emitted from radioactive materials.
- **Radioactive Isotope Identification Device (RIID)**: the RIID is a radiation detector that enables the identification of the specific radioactive material by analyzing the energy spectrum of the emitted radiation.
- **Radiation Portal Monitor (RPM)**: the RPM is a pass-through radiation monitor (or portal) for personnel, vehicles, container boxes, or trains. These monitors alarm to indicate the presence of radioactive materials, including low-radiation materials like uranium.

Localization is the most important and difficult task in the regulatory control of radioactive sources. The task often includes the collection and rapid analysis of spectrometric

data from multiple detectors in order to give an estimation of the location of a radioactive source. Therefore, in any localization system there is always a trade-off that needs to be balanced between measurement time and the accuracy of the source's location [18].

## 1.5 Problem Statement

Despite major efforts toward researching and producing new detectors for identifying and localizing radioactive sources, there are still limitations with those devices in terms of speed, accuracy, efficiency and cost. The reasons for those limitations are that radioactive materials vary widely in their concentration and compositions [19], and that they are often hidden from detection by different shielding materials. In addition, background radiation in the environment is not always stable and can vary in intensity over a wide range of both time and space [20]. Moreover, although there are many detectors available on the market, their technical specifications are not always consistent, especially in quality and sensitivity [21].

Together with all these practical challenges, a theoretical limitation also exists due to the nature of the properties of radioactivity in any radioactive isotope. The emission of particles from radioactive sources is a discrete process, characterized by a Poisson Distribution, which leads to an irreducible amount of randomness and uncertainty associated with radiation measurements [22].

There are many research publications on radiation dosimeters to localize radioactive sources, but each of them still has limitations. An example of these attempts is a self-collimating BGO detector system [23] that enables determination of the direction of a 1 mCi source placed 5 m away from the detectors, at 10 degrees angular resolution, using a measurement duration of 300 seconds. The long measurement window is a shortcoming that could make the dosimeter unusable when the source is moving. Another proposed approach [24], uses pixelated CdZnTe arrays and coded-mask apertures to detect and provide orientation information of radioactive sources. The results show that a 2 mCi source at 5 m can be detected and localized with an accuracy of less than 3 degrees. Despite the shorter measurement time, the large size of the system is a disadvantage that limits the number of situations where it can be used.

A directional radiation detector based on an array of semiconductor sensors has been presented in [25]. This system attempts to derive the source direction by comparing the count rates measured at different detectors, but only achieves 9 degrees of angular resolution. Another system, using four scintillation detectors placed in a four-quadrant formation to localize a radioactive source, was proposed by Willis et al [26] who devised a fuzzy logic algorithm to calculate the source position based on the relative measured signal intensity in the arrays of detectors. Simulation results have shown that the position of a radioactive source, placed 50 cm away, can be determined with accuracy of less than 1 degree. Unfortunately, the estimation of source position using the proposed algorithm depends on a set of pre-determined calibration data, so that re-calibration is required whenever the measurement conditions change, making it unsuitable for use as a fast response device.

The focus of this thesis is, therefore, to develop a wearable active directionally-sensitive radiation dosimeter that allows the estimation of a radioactive source in a short measurement time and with high angular resolution. The proposed dosimeter is presented in Chapter 5, where a new and simple algorithm is developed to estimate the direction of the source based on the number of interacting particles recorded in the 4 closest detectors of a circular array of 8 detectors.

## 1.6 Objectives

It is proposed that radioactive source direction can be estimated by comparing the radiation intensity measured by several detectors. Consequently, the first goal of this thesis is to review the existing range of radiation detectors and to evaluate their performance. The second and primary goal of this thesis, is to develop a wearable directionally-sensitive dosimeter, together with an algorithm to estimate the direction of radioisotope at high angular resolution.

The objectives of this thesis are as follows:

1. Review radiation detectors and dosimeters
2. Introduction to Monte Carlo simulation (Geant4 package) in radiation physics
3. Develop a method for a wearable dosimeter to estimate radioactive source direction

4. Evaluate the effectiveness of the proposed dosimeter method over varying source-to-detector (STD) distances

5. Compare the source direction estimation accuracy of different detector shapes

6. Evaluate the ability of the proposed dosimeter to estimate the direction of a radioactive source in a 3D environment

## 1.7 Thesis structure

The thesis contains seven chapters, including this chapter. Each chapter begins with a short introduction of its contents and ends with a discussion/summary of the main ideas.

**Chapter 2** provides background information on available radiation detectors. It then introduces concepts of radiation detection and measurement along with a literature review of solid-state CdZnTe semiconductor detectors as the vehicle of the proposed dosimeter.

**Chapter 3**. In this chapter, a review of relevant literature related to radioactive source localization is provided. The chapter also presents a report on the existing directionally-sensitive radiation dosimeter approaches, analyzing their strengths and disadvantages to highlight the need for further research.

**Chapter 4** provides an introduction to Monte Carlo simulation (Geant4 package) in radiation dosimetry, including the toolkit fundamentals, main elements of a simulation, pre-defined physical models and processes, materials and methods in Geant4.

**Chapter 5** gives detailed information about the proposed directionally-sensitive radiation dosimeter using multiple CdZnTe detectors, together with the algorithm developed to estimate radioactive source direction based on the number of interacted particles recorded in the 4 closest detectors of a circular array of 8 detectors. This is then followed by a performance evaluation of the proposed dosimeter at different STD distances. Finally, the ability of the proposed dosimeter to determine radioactive source direction in a 3D environment is assessed with different physical detector shapes.

**Chapter 6** discusses the critical findings and observations throughout this thesis. It then concludes with a summary of the main contributions of the research.

**Chapter 7** shows the limitations of the study, indicates directions for future research and conclusions.

## 1.8 Publications

Much of the material contained in this thesis has been published or has been submitted for publication and is discussed in various chapters. The publications are listed below.

1. Hai Huu Le, Paul Junor, Moshi Geso, and Graeme O'Keefe, Directionally-sensitive Personal Wearable Radiation Dosimeter, *International Journal of Mathematical, Computational, Physical, Electrical and Computer Engineering*, Vol 11, No 5, 2017.

2. Hai Huu Le, Paul Junor, Moshi Geso, Graeme O'Keefe and Richard Kirsner, The Directional Emission Estimation of a Radioactive Source Using a Wearable Dosimeter, under reviewed in *Australasian Physical and Engineering Sciences in Medicine Journal*, October, 2018.

3. Hai Huu Le, Paul Junor, and Richard Kirsner, A Study of the state-of-the-art Radioactive Source Localization, submitted to *The 2019 International Conference of Electrical and Electronics Engineering (ICEEE'19)*.

# Chapter 2

# Radiation Dosimeters

This chapter provides background information on currently available radiation detectors. It then discusses radiation measurement and protection, followed by a summary of the general properties of radiation dosimeters. Finally, a brief review of current development of the CdZnTe solid-state semiconductor detectors, that are used in our proposed dosimeter, will be provided.

As radiation cannot be detected by human senses, we must depend on instruments to observe the existence of ionizing radiation in the environment. Radioactivity is a natural process where the unstable atoms of an element emit or radiate excess energy in the form of particles or waves. For such ionizing radiation emissions, either a lower energy atom of the same form, or a completely different nucleus or atom, will be formed depending on how the nucleus loses this excess energy. When it interacts with materials, ionizing radiation can remove electrons from the atoms in the material thus providing the means for radiation detection, but also potentially causing a health hazard.

## 2.1 Radiation Detectors

Radiation detectors are instruments designed to detect and measure particles emitted by radioactive materials, produced by particle accelerators or observed in cosmic rays. Such particles can include electrons, protons, neutrons, $\alpha$-particles, $\gamma$-rays, and numerous mesons and baryons. Unfortunately, there is no device that can detect all kinds

of radiation in every situation. Therefore, an understanding of the principles of radiation detection and the characteristics of the commonly encountered detection devices is essential in radiometry. Currently, most radiation detector systems share the characteristic that the radiation incident on the transducer produces ionization effects that are not directly observable.

### 2.1.1 Detector Characteristics

As previously noted, there is no detector that is perfectly suited for all possible applications: depending on the application, radiation detector systems are designed according to several criteria such as radiation type, energy range, operating voltage and detector size. In general, there are several characteristics specifying the features of a detector, as follows:

#### 2.1.1.1 Detector Sensitivity

Detector sensitivity is defined as the ability to detect and measure the radiation of interest in the presence of noise and signals caused by other radiation. The sensitivity of a detector often depends on many factors such as the interaction cross section of the detector material, detector mass, detector noise and protection material around the detector.

#### 2.1.1.2 Energy Resolution

The energy resolution of a radiation detector is the exactness with which the system can measure the energy of a particle, and its capability to distinguish radiations of slightly different energy.

The energy resolution $R$ is given by the full width at half maximum (FWHM) divided by the location of the signal peak centroid $H_0$. For a Gaussian distribution with standard deviation $\sigma$, we have:

$$FWHM = 2.35\sigma \tag{2.1}$$

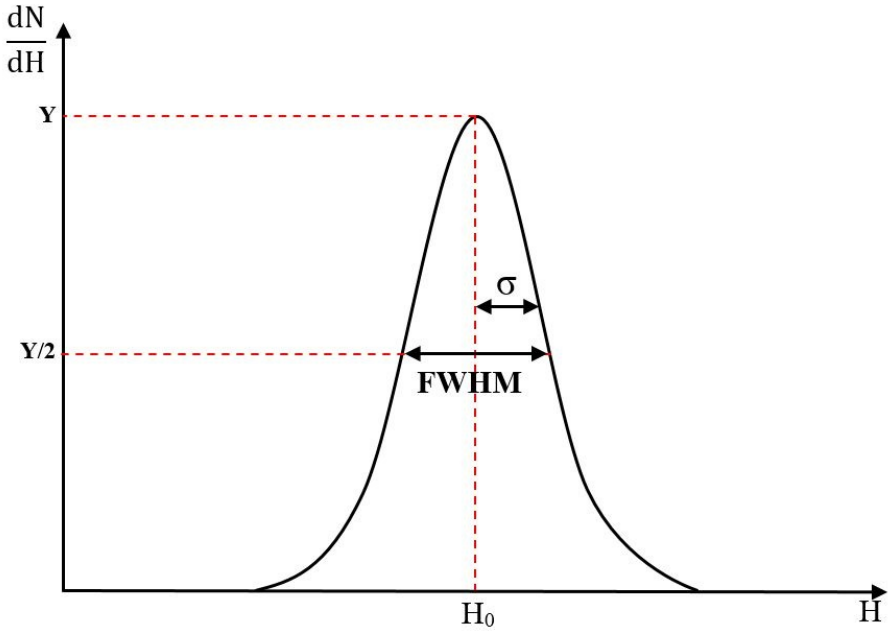


FIGURE 2.1: Definition of energy resolution of radiation detector (after [10]).

In general, the average energy needed to produce an ionization is a constant and depends only on the detector material. Therefore, the average number of ionizations increases with the deposited energy. When the full energy of a particle is absorbed in the detector, Poisson statistics will no longer be applicable since the number of ionizations is constrained by this energy value. As a consequence, the detector resolution may be reduced by the so-called Fano Factor $F < 1$ resulting in improved resolution [27].

#### 2.1.1.3 Detection Efficiency

The absolute efficiency of a detector is defined by the fraction of pulses registered at the detector with respect to the number of events emitted by a radiation source.

$$\epsilon_{abs} = \frac{number\ of\ pulses\ registered}{number\ of\ events\ emitted\ by\ source} \tag{2.2}$$

In addition, the intrinsic efficiency is given by the fraction of pulses registered by the detector with respect to the number of particles striking the detector.

$$\epsilon_{int} = \frac{number\ of\ pulses\ registered}{number\ of\ particles\ hitting\ detector} \tag{2.3}$$

While the absolute efficiency of a detector depends on detector properties and counting geometry (primarily the distance from source to detector), the intrinsic efficiency is mainly dependent on detector material, radiation energy and the thickness of the detector [28].

#### 2.1.1.4 Response Time

Detector response time is the time between the arrival of the radiation, and the formation of an output signal. If the signal is formed in a very short time-scale with a fast rising flank, a precise moment in time can be marked by the signal. This characteristic is of importance if timing information is crucial, for example in Time-Of-Flight measurements with scintillators, or in space determinations using a drift chamber through drift time measurements [29].

#### 2.1.1.5 Dead Time

In most detector systems, the process of energy (charge) deposition and readout information takes a finite time in which the detector and its associated electronics is not able to register a subsequent signal. This finite time is usually referred to as the dead time of the counting system. If the detector is insensitive to other events during the readout time, these events are lost. On the other hand, if the detector is sensitive to additional events, these events may pile up, resulting in distortion of the signal [30].

Due to the random nature of radioactive decay process, there is always the chance that a true event was unrecorded because it happened too soon after the preceding event. These dead time losses can become even worse when operating at high counting rates. Therefore, under such conditions, some correction might be required in the counting system to achieve an accurate measurement [31].

### 2.1.2 Type of Detectors

A radiation detector is a device that responds informatively to the phenomena to which it is exposed. Detection of radiation starts with the interaction of the radiation with matter, resulting in a conversion of the energy of the radiation into the generation of

photons (light), electrical charge, or heat. Radiation detectors have been continuously developed and improved since the first attempts using photographic plates by Henri Becquerel in 1896 to demonstrate the phenomenon of radioactivity. Together with the invention of new materials and manufacturing technologies, different types of detectors have been made with many improvements in physical size and properties.

#### 2.1.2.1 The Ionization Chamber

The ionization chamber is a device that measures the amount of ionization created by charged particles passing through a volume of gas enclosed in a vessel. If an electric field is maintained in a gas by a pair of electrodes, the positive and negative ions will drift apart, inducing charges on the electrodes. In their traversal, the ions may undergo recombination processes, and the charge collected by the electrodes alone will result in an ionization current measured in the external circuit. When all ions are collected, with no loss due to recombination, the maximum current obtained is called saturation current, which will be proportional to the intensity of radiation.

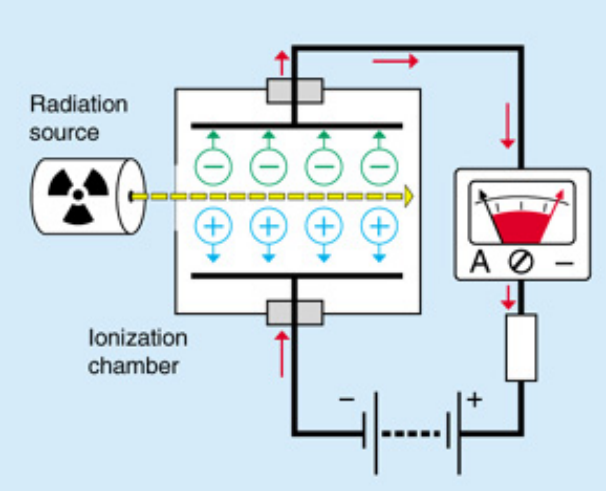


FIGURE 2.2: Principle of an ionization chamber (reproduced from [32]).

Ionization chambers are often portable. The ability of the ion chamber to measure the exposure rate from a radioactive source is based upon the ability of the emission to reach the active portion of the meter and the energy of the emission. Ion chambers are used where there is measurable exposure to or potential for measurable exposure to X-rays and $\gamma$-rays.

#### 2.1.2.2 Proportional Counter

Proportional counters are photon-counting devices, meaning that the detection of each photon results in a discrete signal in the associated electronics. A typical counter usually consists of a gas-filled chamber fitted with one or more X-ray transparent windows.

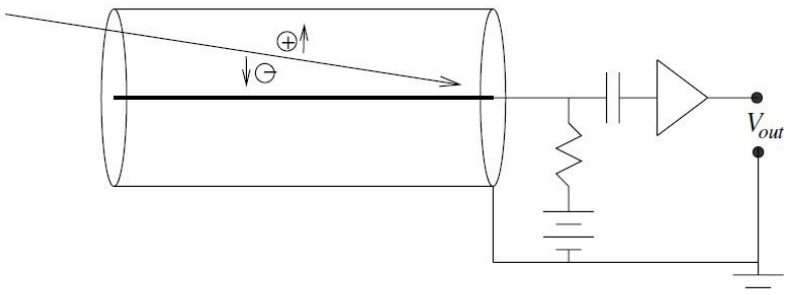


FIGURE 2.3: Schematic of a cylindrical proportional counter (reproduced from [28]).

Photons penetrate the window and pass into the gas inside where interactions with the gas atoms result in the creation of a number of ion pairs (electrons and partially ionized gas atoms). Anodes in the detector volume are held at a positive potential with respect to the rest of the detector. The anodes are usually thin metal wires, and their electric field causes the electrons to drift towards them where the field strength is highest. The energy of the electrons increases, and collisions with other gas atoms cause further ionization producing more electrons. These secondary electrons themselves drift and acquire enough energy to cause further ionization (and electrons), and so a large cloud of electrons arrives at the anode in a process known as an avalanche. The quantity of charge produced in the avalanche is large enough to be detectable in an amplifier connected to the anode.

#### 2.1.2.3 Geiger-Müller Counter

A Geiger-Müller counter (Geiger tube) is a device used for the detection and measurement of all types of ionizing radiation: alpha, beta and gamma radiation. Basically it consists of a pair of electrodes surrounded by low-pressure gas (usually Helium or Argon) sealed in a metal cylinder by a plastic or ceramic window at one end. The electrodes are connected to a high magnitude, positive voltage so there is a strong electric field between it and the outside tube.

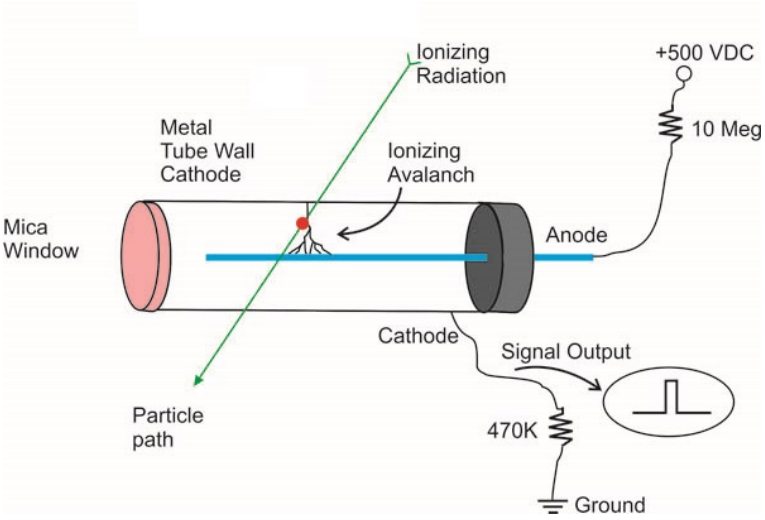


FIGURE 2.4: A cutaway drawing of a Geiger-Müller tube (reproduced from [33]).

When it enters the tube, radiation will cause ionization, splitting gas molecules into ions and electrons. Being negatively charged, the electrons are instantly attracted to the high potential positive wire. The result is that many electrons suddenly arrive at the wire, producing a pulse of electricity that can be measured on a meter. The ions and electrons are quickly absorbed among the billions of gas molecules in the tube, so the counter effectively resets itself in a fraction of a second and is ready to detect more radiation.

#### 2.1.2.4 Scintillation Detectors

Scintillation detectors consist of a scintillator material, an optical relay (optional) and a photodetector. When a charged particle interacts with a scintillator, its atoms are excited and photons are emitted. These photons are directed to the photocathode of a photomultiplier tube that emits primary electrons by the photoelectric effect. The primary electrons, accelerated by an electric field, strike the first dynode of the tube and release a number of secondary electrons. Each subsequent dynode impact in the tube will release further electrons, and so there is a current-amplifying effect at each dynode stage. The output signal at the anode is in the form of a measurable pulse for each photon detected at the photocathode, and is passed to the processing electronics. The output pulse also carries information about the energy of the incident radiation, which allows both the intensity and energy of the radiation to be measured.

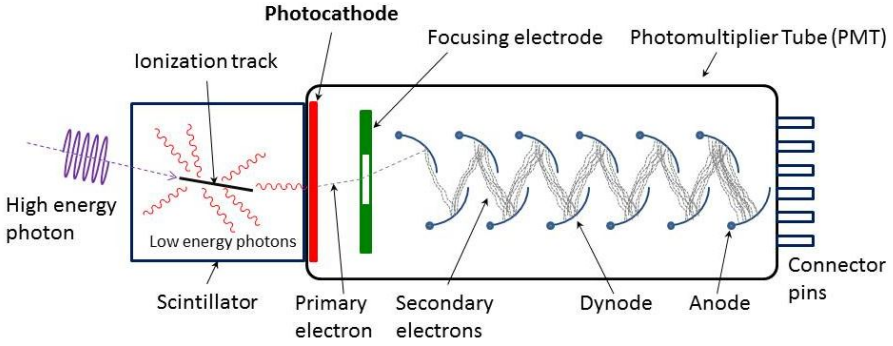


FIGURE 2.5: Schematic diagram of a scintillation detector (reproduced from [34]).

In practice, many organic and inorganic scintillation materials are available and chosen based on the type of radiation to be measured. The trade-offs include light yield, speed, long-term material stability, and ease of integration with light-collection optics. Although scintillation detectors allow for spectroscopic measurements of ionizing radiation, because the energy resolution of scintillation detectors is limited, the identification of radioisotopes might not be accurate with closely spaced energy signatures [35].

#### 2.1.2.5 Semiconductor Detectors

In general, semiconductor detectors can be considered as solid-state ionization chambers in which the conventional gas has been replaced by a high purity semiconductor material. In these detectors, radiation is measured by means of the number of charge carriers set free in the detector, which is arranged between two electrodes. The greatest advantage of semiconductor detectors over ionization chambers is that the energy required for production of electron-hole-pairs is much lower compared to the energy required for production of paired ions in a gas detector. Consequently, the statistical variation of the pulse height is smaller, the energy and time resolution is higher in semiconductor detectors. Because the density of a semiconductor detector is very high, charged particles of high energy can give off their energy in a semiconductor of relatively smaller dimensions than in a gaseous ionization chamber [36].

The advantages of semiconductor detectors are their excellent energy resolution, and fast and linear energy response. In addition, they are relatively cheap to construct and easily adaptable into special configurations as well as having lower power supply requirements [37]. The radiation energy is directly converted into electrical charge carriers without

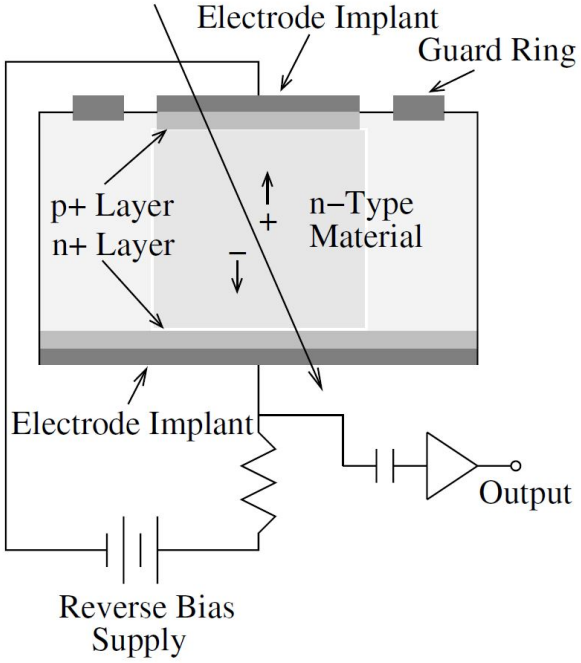


FIGURE 2.6: A simple diagram of semiconductor detector (reproduced from [28]).

the need of any optical stages, so a compact radiation dosimeter based on semiconductor detectors can be built for measurement in confined spaces [38].

## 2.2 Radiation Measurement and Protection

Radioactive materials consist of unstable atoms that spontaneously transform into more stable atoms by emitting charged particles during radioactive decay processes. Source activity and radiation exposure are the two of the most important aspects when measuring radiation. While source activity is defined as the amount of radiation emitted by a radioactive source, radiation exposure measures the effect of radiation on a substance that absorbs it [39].

### 2.2.1 Radiation Activity Measurement

The strength of a radioactive source is called its activity, which is defined as the rate at which the isotope decays. Radiation activity is measured by the number of atoms that decay and emit radiation in a given period of time. The standard international unit of radioactivity is called a becquerel (Bq), which is equal to one disintegration per second

| **Unit** | **Description** | **Equivalent** |
|---|---|---|
| Rem | A unit of equivalent absorbed dose of radiation that takes into account the relative biological effectiveness of different forms of ionizing radiation, or the varying ways in which they transfer their energy to human tissue. The dose in rem equals the dose in rad multiplied by the quality factor (Q). The quality factor is different for different types of radiation, for beta and gamma radiation, it is taken as one, for alpha radiation is 20 and for neutron is 10. Rem is essentially a measure of biological damage. | rem = rad x Q |
| Sievert (Sv) | A unit of equivalent absorbed dose equal to 100 rem. | 1 Sv = 100 rem Sv = Gy x Q |
| Rad (radiation absorbed dose) | A unit of absorbed dose of radiation. Rad is a measure of the amount of energy deposited in tissue. | 1 rad = 100 erg/gram |
| Gray (Gy) | A unit of absorbed radiation dose equal to 100 rad. Gray is a measure of deposition of energy in tissue. | 1 Gy = 100 rad |
| Curie (Ci) | The traditional unit of radioactivity, equal to the radioactivity of one gram of pure Radium-226. | 1 Ci = 37 billion dps = 37 billion Bq |
| Becquerels (Bq) | The standard international unit of radioactivity equal to one disintegration per second. | 1 Bq = 27 pCi |
| Disintegrations per second (dps) | The number of subatomic particles (e.g. alpha particles) or photons ($\gamma$-rays) released from the nucleus of a given atom over one second. One dps = 60 dpm (disintegrations per minute) | 1 dps = 1 Bq |

TABLE 2.1: Some units used in measuring radiation activity and dose [40]

(dps). The becquerel is a small unit, normally radioactivity is quantified in kilobecqerels (kBq) or megabecquerels (MBq). The curie (Ci) is another unit commonly used for activity of a particular source material, and is equal to 3.7 x $10^{10}$ atoms disintegrations per second [41].

The activity of a radioactive source decreases with time and does not depend on the mass of material. For example, two sources of the same activity might have different masses based on the relative proportion of non-radioactive atoms present in each source. The relationship between the mass of radioactive material and the source activity is called the specific activity. Specific activity is defined as the number of curies or becquerels per unit mass or volume. The higher the specific activity of a material, the smaller the

physical size of the source with the same strength [42].

### 2.2.2 Radiation Exposure Measurement

One way to measure the intensity of radiation is to measure the exposure, the amount of ionization it causes in air. Exposure is expressed in terms of a scientific unit called a roentgen (R or r). The unit roentgen is equal to the amount of radiation that produces in one cubic centimetre of dry air at $0^0$C and standard atmospheric pressure ionization of either sign equal to one electrostatic unit of charge.

Radiation exposure is expressed in several ways to account for the different levels of harm caused by different forms of radiation and the different sensitivity of body tissues. The most important thing to understand about radiation exposure is that it is measured by what radiation does to substances, not anything particular about the radiation itself.

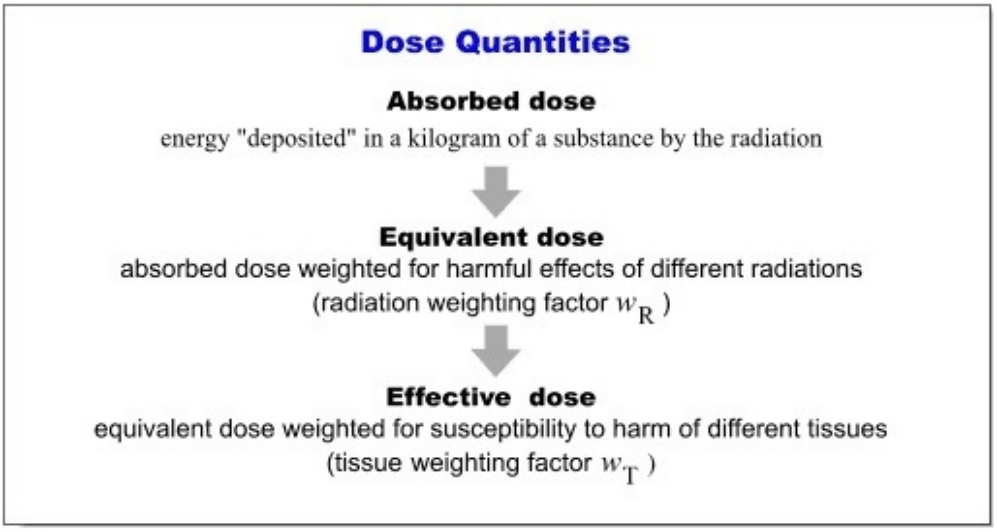


FIGURE 2.7: Radiation dose quantities (reproduced from [43]).

#### 2.2.2.1 Absorbed Dose

When a person is exposed to radiation, energy is deposited in the tissues of the body. The amount of energy deposited per unit of weight of human tissue is called the absorbed dose, which is measured using the traditional rad or the gray (Gy), the international (SI) unit, where 1 Gy is equivalent to 100 rad.

The absorbed dose $\boldsymbol{D}$ is defined as:

$$\boldsymbol{D} = \frac{\boldsymbol{d\bar{\varepsilon}}}{\boldsymbol{dm}} \tag{2.4}$$

where:

$\boldsymbol{d\bar{\varepsilon}}$ is the mean energy imparted to matter in an infinitesimal volume $\boldsymbol{dV}$.

$\boldsymbol{dm}$ is the mass in $\boldsymbol{dV}$.

Normally, absorbed dose is used to assess the potential for biochemical changes in specific tissues. However, absorbed dose is not a good indicator of the biological effect, because with different types of radiation, under different exposure conditions, the same absorbed dose can cause different biological effects on the human body.

#### 2.2.2.2 Equivalent Dose

Equivalent dose ($\boldsymbol{H}_T$) is a measure of the radiation dose to tissue that allows for the different biological effects of ionizing radiation of different types and energy levels. In quantitative terms, equivalent dose is less fundamental than absorbed dose, but it is more biologically significant. Equivalent dose is measured in the international (SI) unit, the Sievert (Sv).

Equivalent dose ($\boldsymbol{H}_T$) is calculated as:

$$\boldsymbol{H}_T = \sum_R \boldsymbol{W}_R \cdot \boldsymbol{D}_{T,R} \tag{2.5}$$

where:

$\boldsymbol{H}_T$ is the equivalent dose in sieverts (Sv) absorbed by tissue $T$.

$\boldsymbol{W}_R$ is the radiation weighting factor defined by regulation.

$\boldsymbol{D}_{T,R}$ is the absorbed dose in grays (Gy) in tissue $T$ by radiation type $R$.

The radiation weighting factor $\boldsymbol{W_R}$ takes into account that some kinds of radiation are inherently more dangerous to biological tissue, even if their energy deposition levels are the same. The radiation weighting factor is also dependent on the type and energy of the incident radiation. In practice, $\boldsymbol{W_R}$ is an approximation value and can change periodically as new research refines the approximations. In 2007, the International Commission on Radiological Protection (ICRP) published a new set of radiation weighting factors as in Table 2.2 below [44]:

| **Radiation types** | **The radiation weighting factor $\boldsymbol{W_R}$** |
|---|---|
| photon, all energies | 1 |
| electron, muons, all energies | 1 |
| protons, charged ions | 2 |
| alpha particles, fission fragments, heavy ions | 20 |
| neutrons | continuous function of neutron energy calculated using 3 complex equations depending on energy (see Figure 2.8) |

TABLE 2.2: The radiation weighting factor $\boldsymbol{W_R}$ published by ICRP in 2007 [45]

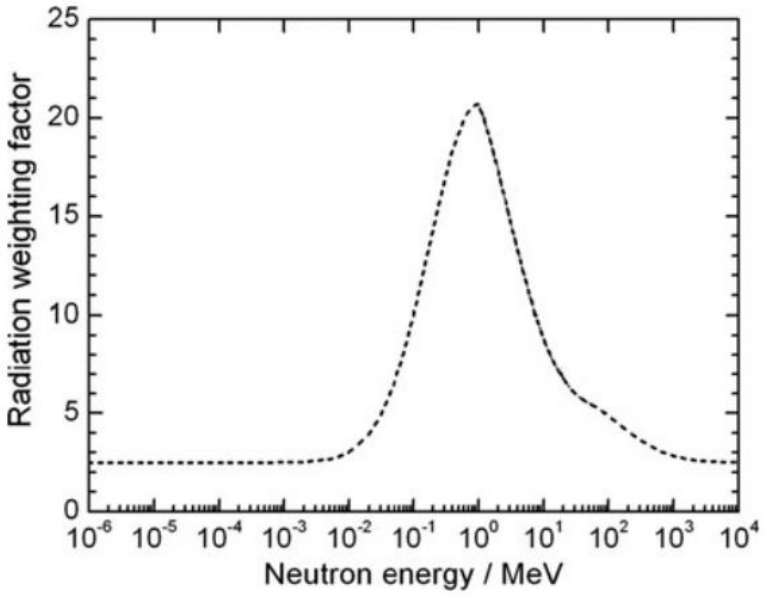


FIGURE 2.8: Radiation weighting factors $\boldsymbol{W_R}$ for external neutron exposure with various energies (reproduced from [44]).

#### 2.2.2.3 Effective Dose

The probability of a harmful effect from radiation exposure depends on what part or parts of the body are exposed. Because some organs are more sensitive to radiation than others, a tissue weighting factor ($\boldsymbol{w_t}$) is used to take this into account. The effective dose ($\boldsymbol{E}$) to an organ is calculated by multiplying equivalent dose to the tissue by a weighting factor for that organ. The unit of effective dose is the Sievert (Sv). Because particular body tissues react differently to radiation, the effective dose is used to compare the risk of developing malignancy (cancer) of the tissue when exposed to radiation.

Effective dose ($\boldsymbol{E}$) is calculated as:

$$\boldsymbol{E} = \sum_{T} \boldsymbol{w_t} \ . \ \boldsymbol{H_T} \tag{2.6}$$

The tissue weighting factor (shown in Table 2.3) is a relative measure of the risk of stochastic effects that might result from irradiation of that specific tissue. It accounts for the variable sensitivities to ionizing radiation for organs and tissues in the body. The sum of the weighting factors of all organs in the body is 1.

| **Organ/tissue** | **The tissue weighting factor $w_t$** | **Sum of tissue weighting factors** |
|---|---|---|
| Bone marrow, colon, lung, stomach, breast | 0.12 | 0.6 |
| Gonads | 0.08 | 0.08 |
| Bladder, oesophagus, liver, thyroid | 0.04 | 0.16 |
| Bone surface, brain, salivary glands, skin | 0.01 | 0.04 |
| Remainder | 0.12 | 0.12 |
| **Whole body** | **Total** | **1.00** |

TABLE 2.3: The tissue weighting factor $\boldsymbol{w_R}$ pulished by ICRP in 2007 [45]

#### 2.2.2.4 Dose Rate

The dose rate indicates the amount of radioactive dose received by a person within a certain period of time. So the actual dose received depends upon both the dose rate and the exposure time. Because the Sievert is a very large unit, radiation dose rate is normally expressed in microSieverts per hour ($\mu$Sv/hr) or milliSieverts per year (mSv/year).

### 2.2.3 Radiation Protection

Radiation protection (radiological protection) is defined by the International Atomic Energy Agency (IAEA) as "The protection of people and the environment from harmful effects of exposure to ionizing radiation, and the means for achieving this" [46].

Radiation protection can be categorised as:

- **Medical radiation protection**: the protection of patients exposed to radiation as part of their diagnosis or treatment.
- **Occupational radiation protection**: the protection of workers in situations where their exposure is directly related to or required by their work.
- **Public radiation protection**: the protection of individual members of the public and of the population in general.

#### 2.2.3.1 Radiation Protection in Medical Environments

The use of radiation in the diagnosis and treatment of human diseases has increased rapidly as providing significant benefits for patients and the development of modern health technology makes new applications safer. However, inappropriate use can lead to unnecessary or unintended radiation exposures with potential health hazards for patients and staff.

Radiation protection in medical environments consists of three principles:

- **Application of dose limit**: the diagnostic reference levels (DRLs) are applied to medical exposure as advisory and contribute to good radiological practice in

medicine. The DRL values should be reviewed at intervals that represent a compromise between the necessary stability and the long-term changes in the observed dose distributions, and could be specific to a country or region.

- **Justification of practices/procedures**: there are three levels of justification of radiological practice in medicine: firstly, the use of radiation in medicine should do more good than harm to society; secondly, the procedure with specified objective is defined and justified; and finally, the application of the procedure to an individual patient should be justified, taking into account the specific objectives of the exposure and the characteristics of the individual involved.

- **Optimization of protection**: optimization of protection for patients is usually applied at two levels: design, selection, construction of equipment and installations; and day-to-day methods of working. The aim of this optimization of protection is to keep the dose as low as reasonably achievable while maximizing the benefit.

Radiation exposures of patients can occur in diagnostic, intervention, and therapeutic procedures. Therefore, radiation protection in medicine is aimed at providing an appropriate level of protection for people, and the environment, against the detrimental effects of radiation exposure without limiting the benefits associated with such exposure.

#### 2.2.3.2 Occupational Exposures Radiation Protection

The term "occupational exposures" refers to the exposure of personel to ionizing radiation from radioactive sources within a workplace. It is recommended for workers exposed to radiation sources to follow and apply all the requirements established in the International Basic Safety Standards for Protection against Ionizing Radiation, and the Safety of Radiation Sources. Dose estimation is an important factor for government and organizations to evaluate radiation risks and establish protective measures against any harmful effects to radiation workers [47][48].

An occupational radiation protection program for radiation workers often includes [51]:

- The surveillance and monitoring of workers engaged in radiation work, monitoring of working area, assessment of working methods with respect to health and safety, and classification of workers engaged in radiation work.

| | |
|---|---|
| **Effective dose limit** | 20 mSv per year, averaged over a period of 5 consecutive calendar years |
| **Effective dose limit in a single year** | 50 mSv |
| **Equivalent dose limit** | |
| in the lens of the eye | 150 mSv per year (from 2011, reduce to 20 mSv in a year, averaged over defined periods of 5 years, with no single year exceeding 50 mSv [49]) |
| in the skin | 500 mSv per year |
| in the hands and feet | 500 mSv per year |

TABLE 2.4: Occupational dose limits for radiation workers in Australia (Adapted from "National standard for limiting occupational exposure to ionizing radiation", NOHSC, 1995 [50] and "Statement on changes to occupational dose limit for lens of the eye", ARPANSA, 2011 [49]).

- The establishment of contaminated areas, assessment of protective measures, provision of advice on decontamination procedures, and any other appropriate measures.
- Periodic review of the program, and in the event of any new installations or practices or of any major modifications made to installations or practices, to ensure that it may continue to meet its objectives.
- Ensuring that equipment and instruments function correctly, procedures are properly established and implemented, analyses are correctly performed, records are correctly and promptly maintained, and personnel are properly trained.

Radiation protection training is an important component of any protection program which aims at providing the workers with a clear understanding of what is presently known about the biological risks associated with exposure to radiation. It will allow workers to make informed decisions regarding these risks rather than excessive fear or indifference. In addition, it will also help to improve the effectiveness of a protection program by encouraging workers to comply with radiation protection standards [51].

#### 2.2.3.3 Radiation Protection for the Public

Protecting the general public from unintentional radiation exposure is an essential aspect of a radiation protection program. Radiation exposure incurred by members of the public might be due to an accident, a malicious act, or any other unexpected event, and requires prompt action in order to avoid or reduce adverse consequences. In addition, by managing radioactive materials and radioactive waste appropriately the dangers of radiation exposure to the general public can be greatly reduced [52].

For general public, safe management of radiation exposure can be achieved through a variety of methods, including [14]:

- **Shielding** radioactive materials can intercept radiation traveling away from its source and appropriate packaging makes it safe for staff and the public during storage and transport. The requirement of shielding, including packaging, depends on the type of radioactive sources or waste and its emitting radiation.
- **Limiting** the exposure to radioactive materials, or isolating the materials to eliminate the chance of exposure to the public.
- **Disposing** of radioactive waste in a responsible way including construction of specially designed facilities and appropriate containment barriers.

In the case of a radiological emergency (a large release of radioactive material into the environment), using the principles of exposure time, distance and shielding, can help protect and limit harmful effects of radiation exposure to the public [53]:

- **Time:** limiting or minimizing the exposure time will reduce the dose from the radiation source.
- **Distance:** the dose of radiation decreases dramatically as the distance from the source increases.
- **Shielding:** inserting appropriate shielding material can greatly reduce or eliminate the received dose.

## 2.3 Properties of Radiation Dosimeters

A radiation dosimeter is a device that measures, either directly or indirectly, the quantities exposure, kerma, absorbed dose, equivalent dose, or other related quantities of ionizing radiation. In order to be useful, a radiation dosimeter must exhibit several desirable characteristics such as: low energy, angular and dose rate dependence, high accuracy and precision, linearity, high spatial resolution and convenience in use. Unfortunately, there is no dosimeter which can satisfy all these desirable characteristics, so the choice of a radiation dosimeter must be judicious, taking into account the requirements of the specific measurement situation [54].

### 2.3.1 Energy Dependence

The response of a dosimetry system is generally a function of the radiation energy. Since dosimetry systems are calibrated at a specified radiation beam quality and used over a much wider energy range, the response of a dosimetry system with radiation quality (energy dependence) should be corrected if the user's beam quality is not identical to the calibration beam quality.

Energy dependence is an important characteristic of a dosimetry system. It is expected that the energy response of the dosimetry system is flat over a certain range of radiation qualities. However, in reality, energy correction often has to be included in most measurement situations.

### 2.3.2 Angular Dependence

The variation in response of a dosimeter with changing angle of incidence of radiation is known as the angular dependence of the dosimeter. Dosimeters usually exhibit a certain angular dependence due to details of construction, energy of the incident radiation and physical size. In order to limit the effect of angular dependence, in some applications radiation dosimeters are used in the same geometry as that in which they are calibrated.

### 2.3.3 Dose Rate Dependence

It is expected that the response of a dosimeter should be constant for different dose rates. However, in reality the dose rate may influence the dosimeter readings, and appropriate corrections are necessary, for example recombination corrections for ionization chambers in pulsed beams.

### 2.3.4 Accuracy and Precision

The accuracy of dosimeters specifies the proximity of the mean value of their measurement to the true value of the measured quantity. The accuracy and precision associated with a measurement is often expressed in terms of its uncertainty. The combined standard uncertainty $u_C$ associated with the quantity $Q$, is a quadratic summation of type A ($u_A$) and type B ($u_B$) uncertainties [55]:

$$u_C = \sqrt{u_A^2 + u_B^2} \tag{2.7}$$

The precision of dosimetry measurements specifies the degree of reproducibility of the measurements under similar conditions and can be estimated from the data obtained in repeated measurements. High precision is associated with a small standard deviation of the distribution of the measurement results.

### 2.3.5 Linearity

The dosimeter reading should be linearly proportional to the dosimetric quantity. However, beyond a certain dose range, there is always non-linearity. The linearity range and the non-linearity behavior depend on the type of dosimeter and its physical characteristics.

In general, non-linear behavior should be corrected for. A dosimeter and its reader may both exhibit non-linear characteristics, but their combined effect could produce linearity over a wider range.

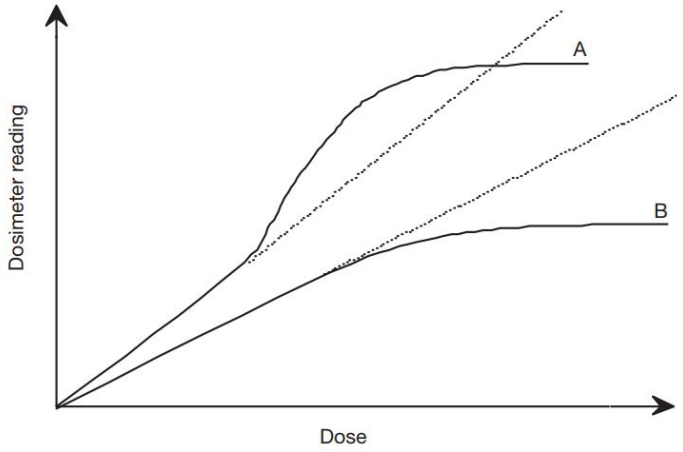


FIGURE 2.9: Response characteristics of two dosimetry systems. Curve A first exhibits linearity with dose, then supralinear behaviour and finally saturation. Curve B first exhibits linearity and then saturation at high doses (reproduced from [56]).

### 2.3.6 Spatial Resolution

Because the dose is a point quantity, the dosimeter should allow the determination of the dose from a very small volume, ideally a point-like detector to characterize the dose at a point. The position of the point where the dose is determined (spatial location) should be well defined in a reference coordinate system. In practice, a measurement result can be attributed to a point within the volume, referred to as effective point of measurement.

### 2.3.7 Readout Convenience

Direct reading dosimeters are more convenient than passive dosimeters. Although active dosimeters (such as ionization chambers or solid-state detectors) can provide instant and continuous reading, passive dosimeters (such as films and TLDs) require processing after the exposure.

### 2.3.8 Convenience of Use

Some dosimeters are reusable either with little or no change in sensitivity (such as ionization chambers) or with a gradual loss of sensitivity (such as with semiconductor dosimeters). However, some dosimeters (such as film or gel) are not reusable at all.

While some dosimeters are more rugged (sensitivity is not affected by handling), others (for example TLDs) are more sensitive to handling.

## 2.4 Solid-state Semiconductor Detector CdZnTe

In the last few years, solid-state semiconductor nuclear radiation detectors have had a rapid improvement in their performance. Compound semiconductors are often formed by elements of groups III and V (GaAs) and groups II and VI (CdTe) of the periodic table. A variety of binary and ternary compounds have been also produced, such as CdZnTe and CdMnTe, to meet the requirement in different application. A summary of the physical properties of the most common compound semiconductor materials is shown in Table 2.5 [57].

Among the compound semiconductors, Cadmium Telluride (CdTe) and Cadmium Zinc Telluride (CdZnTe) are the most promising detectors for X-ray and $\gamma$-ray measurement. Improvements in fabrication processes have allowed production of these detectors with a number of advanced physical properties (such as high energy resolution, room temperature operation, excellent spatial resolution, high stopping-power and fast response time) which made them suitable to a wide range of applications including nuclear physics, X-ray and $\gamma$-ray astronomy and nuclear medicine. Another important property of CdZnTe material is that it can be easily grown into different shapes and sizes. In practice, CdZnTe detectors with large area and complicated geometry can be fabricated to meet the requirements of different applications [58].

| **Material** | **Si** | **Ge** | **GaAs** | **CdTe** | **CdZnTe** | **Hg$I_2$** | **TlBr** |
|---|---|---|---|---|---|---|---|
| **Crystal structure** | Cubic | Cubic | Cubic (ZB) | Cubic (ZB) | Cubic(ZB) | Tetragonal | Cubic (CsCl) |
| **Growth method** | C | C | CVD | THM | HPB,THM | VAM | BM |
| **Atomic number** | 14 | 32 | 31, 33 | 48, 52 | 48, 30, 52 | 80, 53 | 81, 35 |
| **Density ($g/cm^3$)** | 2.33 | 5.33 | 5.32 | 6.20 | 5.78 | 6.4 | 7.56 |
| **Band gap (eV)** | 1.12 | 0.67 | 1.43 | 1.44 | 1.57 | 2.13 | 2.68 |
| **Pair creation energy (eV)** | 3.62 | 2.96 | 4.2 | 4.43 | 4.6 | 4.2 | 6.5 |
| **Resistivity (Ωcm)** | $10^4$ | 50 | $10^7$ | $10^9$ | $10^{10}$ | $10^{13}$ | $10^{12}$ |
| $\mu_e\tau_e(cm^2/V)$ | $> 1$ | $> 1$ | $10^{-5}$ | $10^{-3}$ | $10^{-3} - 10^{-2}$ | $10^{-4}$ | $10^{-5}$ |
| $\mu_h\tau_h(cm^2/V)$ | ∽ ffl1 | $> 1$ | $10^{-6}$ | $10^{-4}$ | $10^{-5}$ | $10^{-5}$ | $10^{-6}$ |

TABLE 2.5: Physical properties of the common compound semiconductor materials [57]

### 2.4.1 Principles of Operation

CdZnTe is a room temperature solid-state semiconductor that converts X-ray and $\gamma$-ray photons directly into electrons. They are fabricated with very thin metalized electrode geometries deposited on the detector surfaces. These electrodes are electrically biased to create a difference in electrical potential within the detector volume. When ionizing radiation interacts with the CdZnTe crystal, electron-hole pairs are created in proportion to the energy of the incoming photon. The negatively-charged electrons and positively-charged holes then migrate to the oppositely-charged electrode where they are collected. The resulting charge pulse is then detected by the preamplifier, which produces a voltage pulse whose height is proportional to the energy of the incoming photon [59].

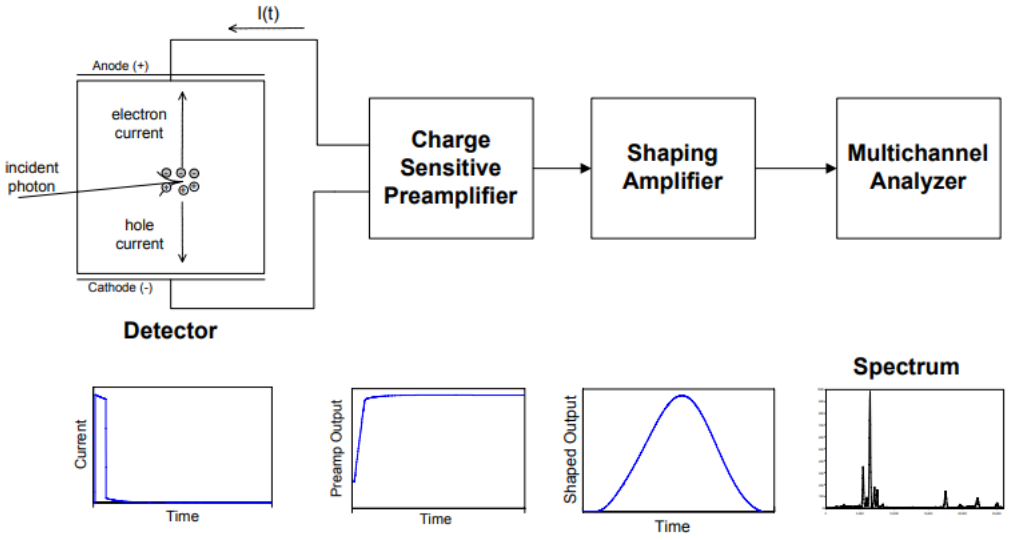


FIGURE 2.10: Block diagram of a typical spectroscopy system with outputs from each stage of the processing electronics sketched below (reproduced from [60]).

The typical process to obtain an energy spectrum of an incident photon is shown in Figure 2.10. After being amplified by a charge-sensitive preamplifier (CSP), the voltage pulse is fed into a shaping amplifier that converts the signal into a Gaussian pulse and amplifies it. Finally, the energy spectrum of the incoming photons will be generated by a standard counting system or Multi Channel Analyzer (MCA) [61].

### 2.4.2 Material Properties

X-ray and $\gamma$-ray radiation applications often require detectors with high resistivity and a minimum quantity of carrier traps. CdZnTe material has the desirable intrinsic properties of a wide band gap and high average atomic number, allowing room-temperature operation and efficient $\gamma$-ray stopping. Currently, the advantages of compound semiconductors growth techniques have enabled CdZnTe to be produced with negligible polarization effects, high resistivity, and good electron-collection properties, making them suitable for almost any radiation applications [62].

In CdZnTe crystal, the addition of a few percent of Zinc to the melt results in an increased band gap as well as the energy of defect formation. The increased bandgap ensures high bulk resistivities and reduces the dislocation density, resulting in lower leakage currents and higher temperature operation. With their low leakage currents (less than 10 nA at room-temperature), CdZnTe detectors are usually fabricated with ohmic contacts to achieve better energy resolution [63].

### 2.4.3 Method of Growth

The fabrication of CdZnTe solid-state semiconductor detectors involves a number of critical steps, including growth of high resistivity material, slicing and polishing of the device volume, the application of metal contacts, surface passivation and packaging. Currently, several techniques have been employed successfully in the growth of CdZnTe crystal including the Bridgman (BR) method [64], Vertical Gradient Freeze (VGF) method [65], Traveling Heater (THM) method [66] , Physical Vapour Transport (PVT) method [67], and Liquid Phase Epitaxy (LPE) method[68]. Among different growth techniques, the primary goal of the fabrication process is to produce defect-free detectors with high resistivity at low cost [62].

The Bridgman (BR) growth method [64] is a controlled freezing process occurring at the liquid-solid equilibrium condition, that involves the movement of a crucible containing the melt through a furnace designed to provide a suitable temperature profile. The furnace may be either vertical or horizontal. The crucible may be transported through the heater, or the crucible stationary with a moving heater, or alternatively, both stationary and the temperature profile altered by a programmed temperature controller. The

growth happens under a temperature gradient in order to produce a single nucleus from which a single crystal will propagate and grow. In the growth stage, the starting materials are melted and cooled to solidify into a crystalline form by allowing the solid-liquid to move slowly until the whole molten charge is solidified.

The High Pressure Bridgman (HPB) and Low Pressure Bridgman (LPB) methods are two variations of the BR method which have been applied in practice. The HPB method is often used to produce commercial CdZnTe detectors, where the material is typically grown under Te-rich conditions. In the HPB method, high pressure gas is used to suppress the loss of cadmium in the molten materials whereas the CdZnTe crystal can be grown without the use of high gas pressure in the LPB method using either horizontal or vertical configuration. In practice, it is usually difficult to obtain long-term stability at the growth interface for the BR method due to the charge and the furnace moving relative to each other. The other limitation of the BR method is the temperature profile is not modified during the whole process, which leads to a non uniform process [67].

These limitations of the BR technique can be eliminated by the Vertical Gradient Freeze (VGF) method [65], where the heat transport can be stabilized, and the variation of temperature across the melt is operated by temperature programming in a multi-zone furnace [69]. In the VGF method, several heaters are used to achieve the desired temperature profile along the ampoule. The temperature profile is then gradually displaced when the ampoule and the heaters are fixed, moving the solid-liquid interface (SLI) upwards across the charge [70]. The challenge of obtaining a stable growth arises from the continuous variations in the temperature profile with the probability of varying the temperature gradient during the crystal growth [71].

Another method that has been used successfully to grow binary compound semiconductor detectors used in radiation applications is Physical Vapour Transport (PVT) [72]. The greatest advantages of the PVT growth method are the lower growth temperature and minimal contact area with walls of the ampoule which results in reduction of stress-related impurity imperfections, easier to control stoichiometry, and greater material uniformity [73].

The Travelling Heater method (THM) is a seeded-growth process of CdZnTe crystals. It operates by precipitation of grown material from a solution. The CdZnTe seed is placed in the growth crucible and molten Te is added as a solvent while polycrystalline CdZnTe

is supplied as a feed material. In consequence, the polycrystalline CdZnTe dissolves into molten Tellurium. When the travelling heater is moved, the CdZnTe crystal precipitates from Te solvent and then grows onto the CdZnTe seed; thus homogeneous single grains of CdZnTe crystal are achieved [65].

The advantage of THM compared with the BR and VGF methods is the possibility of growing the crystal at a lower temperature, because it uses Te as solvent. Generally, the crystals grown by the THM technique often achieve better crystalline quality and homogeneity with Zn concentration than in the BR or VGF methods [64]. In addition, although low levels of impurities are exhibited as in grown ingots, these can be slowly eliminated with each subsequent pass of the heater. One of the limitations of the THM method is the difficulty to grow large diameter crystals, due to the existence of the large macro defects in the last-to-freeze region of the ingot [65].

Unfortunately, despite being considered as the most promising room-temperature radiation detectors, there are still several major limitations in the performance of CdZnTe materials such as the low hole mobility (and hence short lifetime) and crystal defects [66].

The low hole mobility is caused by hole-trapping mechanisms, and is more or less intrinsic to the material. Increasing the detector bias voltage can help to improve the hole lifetime, but it might not always be practical or even desirable in certain applications. A novel method to compensate for low hole mobility is to use ohmic contacts at the electrodes. The advantage of that method is that the holes get recombined with the electrons released into the material by the ohmic contacts, which effectively stops the leakage current, while the signal current is carried predominantly by electrons. Therefore, ohmic contacts can eliminate the need for external circuitry to compensate for low hole mobility or operating the detector at high voltages [57].

Theoretically, an ideal crystal will have all its atoms in a perfect, exactly repeating pattern. However, in reality, most crystalline materials have a variety of crystallographic defects, places where the crystal's pattern is interrupted. The types and structures of these defects may have a profound effect on the properties of the materials and the performance of semiconductor devices. The most common crystallographic defects presented in CdZnTe materials are grain boundaries, twins, cracks, dislocations and Te precipitates. In fact, as crystal defects will further deteriorate the hole mobility, it is

desirable to reduce crystal defects as much as possible during the crystal growth process [66].

## 2.5 Summary

This chapter has provided background information on available radiation detectors, including the detector classifications and characteristics. In addition, a general theory in radiation measurement and protection has been presented, followed by an introduction to the general properties of radiation dosimeters. In conclusion, the chapter has also provided a brief review of current development of CdZnTe solid-state semiconductor detectors, which will be featured in our proposed dosimeter.

# Chapter 3

# Literature Review: Localization of Radioactive Sources

Over the last few years, the problem of locating a radioactive source has gained increased importance due to the threat to public safety and homeland security of a terrorist attack with radiation [74] [75]. Localization of radioactive sources is also a critical issue within the nuclear industry including decommissioning of nuclear power plants, radioactive waste management and radiation protection [76]. Despite the expenditure of considerable engineering effort, the ability of current commercially available radiation dosimeters to localize a radioactive source accurately is still limited. The main factors influencing this are background radiation noise and the variation in source concentrations and composition [77].

This chapter provides a brief review of the literature related to radioactive source localization. It also includes a report of the current developments of directionally-sensitive radiation dosimeters, analyzing their strengths and disadvantages and highlighting the need for further research.

## 3.1 Introduction

Localization is a critical requirement in the regulatory control of radioactive materials but because they require spectrometric data together with advanced data analysis

techniques, these tasks are often extremely difficult to achieve in practice [78] [79]. Radioactive source localization can be classified into different cases depending on the status of the source (stationary or moving) as well as the configuration of the detectors (single, multiple stationary or moving). Futhermore, locating the position of a radioactive source also depends on the nuclide involved, its activity, the detector properties, the source-to-detector (STD) distance and the material of the medium between the source and the detectors [18]. Generally, localizing a source can be divided into different cases as presented in Table 3.1 below.

| **Detector Configuration** | **Source Status** | |
|---|---|---|
| | **Stationary source** | **Moving source** |
| **Multiple stationary detectors** | • Require minimum of 3 detectors<br>• Long measurement times possible<br>• Asymmetric shielding complicates localization | • Require minimum of 3 detectors<br>• Short measurement times or event-based data processing |
| **Single moving detector** | • Require minimum of 3 detectors<br>• Short measurement times or event-based data processing | • Event-based data processing or very short measurement times |
| **Multiple moving detectors** | • Expert system | • Expert system |

TABLE 3.1: Classification of the source localization problem [18]

In practice, measurements of radiation intensity acquired at multiple locations are often used to estimate the locations and strengths of a radioactive source [80]. Therefore, due

to the nature of the radioactive decay process, which follows a Poisson emission distribution, there is always an uncertainty associated with source intensity measurement and localization. To improve the accuracy of detecting and locating radioactive materials, researchers have been working towards new fabrication methods for producing detectors with better measurement characteristics, and developing new mathematical models for automatic source localization.

## 3.2 Network of Distributed Sensors

Given the availability of small, low cost radiation detectors [81], the use of a network of distributed sensors to track and localize radioactive sources is a promising research direction. The number of interacted particles collected by detectors from a radioactive source depends on the STD distance as well as source intensity. By combining data from a network of sensors, the location of a radioactive source can be estimated using a sensor fusion algorithm [82] [83].

Los Alamos National Laboratory has attempted to evaluate the use of distributed sensor networks for tracking radioactive materials [81]. When examining the signal-to-noise ratio (SNR) characteristic of distributed sensor networks, the Los Alamos group has pointed out that there is a considerable difference between the measured SNR of a stationary and a moving source. However, to compensate for the low efficiency of small detectors compared with larger detectors, the sensor networks must be able to measure the speed of a moving source in order to determine the appropriate time lag for a coherent addition process [81].

Another issue when localizing a radioactive source, especially for a low intensity source, is due to the nature of radioactive disintegration, background noise, and limitations in existing sensing hardware which can make a single instantaneous reading potentially unreliable for determining the true source activity. To overcome that issue, an iterative pruning (ITP) algorithm has been proposed in [84] to allow fast and accurate position estimation of a low-level point source using network of N sensors, under realistic noise and measurement conditions, by fusing the estimated position by groups of 3 sensors. However, as a consequence, such systems will often require a powerful and expensive

computation unit to analyze the large amount of data required to calculate the location of the source.

The accuracy of a radioactive source localization using sensor networks is also dependent on the number of reference nodes within the network. In [85], the authors have designed a wireless sensors network based on ZigBee techniques to monitor and localize radioactive materials. The system has been tested with different numbers of reference nodes under the same measuring conditions to evaluate whether that has any effect on the positioning accuracy. Experimental results have shown that the accuracy is improved when increasing the number of reference nodes. Unfortunately, that improvement also comes with higher costs and requires a more complex communication link, which will limit the application of the system.

In [86], the author has analyzed the advantages and challenge of working with large sensor networks for radiation detection. According to the author, even providing added benefits to the localization process, data fusion is still an obstacle for the application of sensor networks. Even if every sensor in the network is completely identical (which is not always possible in practice), aligning and combining the measurement data of each sensor as they move through space is still a challenging task that can introduce more errors in the whole localizing process.

Localization of radioactive source in a 3D environment is still a challenge as it is not always possible to deploy the sensors close enough to the source. Unmanned aerial vehicles (UAV) have been considered as a promising platform to deal with the issue as they offer the greatest flexibility for placing sensors at desired locations for data collection. The high mobility and portability of UAV will allow a faster response in emergency situations and will enable observation to be conducted in contaminated areas without exposing personnel to radioactive materials [83].

In [83], a network of drones fitted with radiation detectors using a two-stage adaptive algorithm to localize radioactive source in 3D space was proposed. Firstly, an approximate radiation source location is estimated while the UAVs remain in the middle of the observation area. Secondly, based on the initially-obtained location of the sources, the UAVs will move to additional locations to collect more data. Finally, more accurate location of the radiation source will be estimated by combining the data from the two previous steps. Simulation has shown that using only five sensors, the proposed system

can accurately localize a radioactive source with average errors of a hundredth of a metre, in under five minutes. The proposed system has also proved to outperform all other networks of distributed of fixed-position sensors [83].

Despite having many advantages, such as flexible and expandable configurability, and automatic continuous operation, as well as the facility to incorporate with existing sensor networks for quick deployment, using a network of distributed sensors for monitoring and localizing radioactive sources still faces some other challenges such as the requirement of a high speed, wide bandwidth communication linkage and a powerful centre processing node to store and analyse a massive amount of data from every sensor within the network. In addition, aligning and combining measurement data algorithms, SNR characteristics of sensor networks also need to be improved to achieve better accuracy when locating moving sources.

## 3.3 Gamma Camera

Gamma spectroscopy is a powerful non-destructive technique for detecting and identifying radioactive sources in the nuclear industry. GAMPIX, a particular gamma imaging system [76], has been developed by the French Alternative Energies and Atomic Energy Commission (CEA-LIST) for detecting and localizing radioactive materials. Compared with current existing systems, the GAMPIX system offers several advantages, such as higher sensitivity, light weight and easy deployment. Experimental measurements have indicated that the GAMPIX system was able to detect a wide range of $\gamma$-rays, with satisfying sensitivity performances.

Another compact gamma camera aimed at detecting and localizing radioactive sources in large area was developed in [87]. The system used pixelated NaI scintillator detectors together with dedicated electronics for gamma photon detection and data acquisition. Two statistical iterative image reconstruction algorithms, the maximum likelihood expectation maximization (ML-EM) and the basis-pursuit based optimization (BP), have been implemented to improve the spatial resolution and sensitivity for gamma imaging. Although experiments have proved that the gamma camera was able to achieve high angular spatial resolution in localizing radioactive sources, the system lacked real-time dose rate measurement capability.

In [88], a hybrid gamma camera has been proposed to monitor radiation intensity in the environment. The proposed system consists of an optical and a gamma camera, operating in either single or dual-modality mode, where optical and gamma images can be displayed independently or as a fused co-aligned image. Experiments have indicated that the system can accurately localize a radioactive source with a spatial resolution of approximately 11 cm FWHM. The system also can be configured to operate remotely, mounted on a robot platform, to monitor any potential exposure to individuals in complicated environments. However, processing time is still a bottleneck of such systems as it takes about 250 seconds just to determine initial location of the radioactive source, rendering the system useless if the source is moving. By using a larger pinhole diameter, the detection efficiency and processing time can be improved but the spatial resolution will be reduced as a consequence.

Gamma camera imaging with a coded-aperture has been proposed to simplify the process of image reconstruction and improve the accuracy of radioactive source location estimation. A pre-defined coded-aperture (mask) placed on top of a position-sensitive gamma detector can overcome the disadvantage of random distribution of the single pinhole cameras. Any radioactive source placed within the Field of View (FOV) of the camera will illuminate a sub-region of the mask and create shadow patterns on the detector surfaces. Finally, the direction of the source is inferred from the recorded images through the deconvolution process. However, such systems require a high-speed computation module to cross-correlate the binary mask with the measured counts map to estimate the source direction, which will increase the physical size, making these systems bulky, more expensive and limiting their practical applicability [89]. Recently, the development of coded-aperture imaging systems has become more feasible with the development of new and less bulky solid-sate semiconductor detectors which achieve higher energy and spatial resolution.

An example of a coded-aperture gamma camera for localizing radioactive material was described in [90]. The system consisted of two gamma cameras using hybrid CdTe pixel detectors with an FOV of 70x70 degrees. The spatial position of radioactive source is estimated via triangulation with the aid of the directional coordinates provided by each gamma camera. Simulations have indicated the ability of such a system to estimate quickly and accurately the direction of a radioactive source within the order of 1% for STD distances up to 1 m. The only drawback of the system is the requirement of a host

computer to perform an image reconstruction algorithm for estimation of the radioactive source direction. This will reduce the mobility, increase the deployment time, and limit the application of such systems in emergency situations.

In [91], a panoramic coded-aperture gamma camera has been proposed to overcome the limited FOV of the general coded-aperture imaging system. A CdTe detector is used with a MURA pattern-coded aperture to allow better background subtraction during measurement. A method for combining multiple radiation images into a single larger image has been developed, providing a FOV of 360 degrees horizontally and 80 degrees vertically for the camera. A larger such FOV will be most useful in complex decommissioning scenarios such as post-accident, events where the feasibility of autonomously analyzing and quickly characterizing the scene within one single image is a critical issue for the responders.

Recently, gamma cameras have been commercialized by various companies but still present some limitations with the requirements of end-users in terms of sensitivity, mobility, physical dimension and ease of use in comparison. Among these limitations, narrow FOV is the most challenging obstacle which limits the application of gamma cameras [91]. In addition, other aspects also need to be improved: the sensitivity (lower detection threshold), the angular resolution (better location accuracy) together with the reduction of weight and set up duration and the ability to operate in a portable configuration [76].

## 3.4 Portable Dosimeters

In an emergency situation, searching and identifying radioactive sources using a portable dosimeter is often one of the first actions by responders, law enforcement or military personnel [92]. Technological advances in detector fabrication, embedded systems and wireless technology have allowed the development of portable dosimeters with the ability to identify and estimate radioactive source direction. In addition, these dosimeters can connect with a sensor network to allow radioactive sources to be tracked and localized. Such portable dosimeters have small form factor and light weight, with wireless data transmission capability and low power consumption [93].

In order to estimate the source direction, these portable dosimeters often consist of an array of directional detectors. These detectors are directionally sensitive because their surfaces have different orientations with respect to the source direction. To obtain an estimation of the source direction, the measurements from each detector in the array are compared. The ability to estimate source direction is an advantageous aspect of portable dosimeters in many applications including security, surveillance and regulatory control of radioactive materials. In addition, being able to determine source direction will also help to boost and improve the performance of the source localization process [94].

A portable dosimeter for monitoring and locating radioactive sources was presented in [25]. In their research, the authors presented a dosimeter consisting of 9 single-pad solid-state semiconductor detectors CdZnTe arranged into a parallel array. The concept of combining an array of detectors into a row helps to transform a simple monitoring device to a directionally-sensitivity dosimeter. The shielding sheets in between detector pads have been used to reduce the flux of particles after each detector-shield pair and creates the difference in the measured count rate of each detector pad. By comparing radiation density measured by each detector in the array, the radioactive source angular emission can be estimated. Simulations and experimental measurements have proved the ability of the prototype dosimeter to estimate the angular emission of the source to within 9 degrees. Moreover, it is possible to locate a source position in 3D space by combining three rows of detectors or by performing three measurements with one detector row when it is set parallel with the x, y and z axes individually. Unfortunately, by taking advantage of the shielding effect to estimate the direction of radioactive source, the design and performance of the dosimeter will depend on the type of radiation intended to be measured.

The authors in [95] have presented a compact, portable radiation dosimeter system, based on a single chip solution, which can determine both the intensity and the direction of radiation emitted from a radioactive source. The system consists of a sensor section (with three NaI $\gamma$-ray detectors arranged in a spatial configuration) for direction finding and a computational module (single chip solution developed by authors) for source direction estimation. Normally, a dosimeter with one NaI detector will only be able to detect and measure the intensity of a radioactive source without any direction

information. However, the proposed system using multiple NaI crystals with independent detection channels, arranged in a spatial configuration, will be able to perform source direction estimation based on the shadowing effect. Experiments have proved that the system is able to determine the direction of a particular isotope to within 5 degrees. However, the performance of the system still needs to be evaluated at longer STD distance with a higher level of background noise. In addition, power consumption and physical size of the detector also can be decreased by using modern solid-state semiconductor detectors.

Another directionally-sensitive portable dosimeter for detecting and identifying radioactive sources was described in [26]. The dosimeter consists of four NaI detectors, placed side by side in a four-quadrant formation, taking the advantage of shadowing in the occluded array of detectors to create a different measured intensity in each detector depending on the source location. Each source location will have a distinct measured intensity profile for the four detector arrays, which can be used to estimate source direction by a custom fuzzy-logic algorithm. Simulation results have shown that the proposed dosimeter was able to determine the location of a radioactive source within 10.35 degrees from the actual angle. However, by using calibration data to develop initial rule sets for the fuzzy-logic algorithm, the accuracy of the system will be dependent on the calibration process, which is not always consistent in practice. In addition, spatial resolution, processing time and physical dimensions of the system need to be improved to meet the requirement of end users.

In [92], another hand-held radiation detection system was developed by Physical Sciences Inc. (PSI) for localizing radioactive materials. The group proposed a compact and flexible package system, consisting of a real-time threat detection and an isotope identification module with advanced search techniques for source localization. The performance of the system has been validated by field testing and laboratory experiments which have shown its ability to identify and localize a 1 mCi $^{137}Cs$ source from 15 m stand-off range after 15 seconds of data acquisition. However, the effectiveness of the Spin-to-Locate (STL) technique, which uses the shielding effect of the operator's body on the radiation flux to estimate the source azimuth, is also isotope-specific due to energy-dependent attenuation of incident radiation.

Currently, existing portable direction sensitive dosimeters often still rely on a powerful

computation unit, such as a PDA (Personal Digital Assistant) or PC (Personal Computer), to perform data analysis and direction estimation [96]. As a consequence, the use of such systems for long term deployments is limited due to their high-power consumption and their inherently bulky system configurations. Therefore, a low-power consumption and compact dosimeter paradigm (with high angular resolution and short processing time), that is able to perform both radioactive isotope identification and direction estimation, is highly desirable. Such systems will have a range of applications in the radiation industry.

## 3.5 Summary

The chapter reviews the radioactive source localization literature. It includes a detailed report on current developments in directionally-sensitive radiation dosimeters, their strengths and weaknesses, and highlights the need for further research.

# Chapter 4

# Geant4 Package - A Monte Carlo Simulation Toolkit for Radiation Dosimetry

Geant4 is a Monte Carlo simulation toolkit intended for the simulation of the passage of subatomic particles through matter. It is widely used for experiments and projects in a variety of application domains, including high-energy physics, astrophysics and space science, medical physics and radiation protection. Geant4 can describe physics processes and models for particle interactions in matter with a wide energy range from around 100 eV to 10 PeV for electrons, photons, muons, hadrons and ions. In Geant4, users are provided with a number of existing physical model configurations and are also able to create their own configurations to meet their requirements. As an open-source software, Geant4 can be very flexibly used either as an independent toolkit, or incorporated into other applications and frameworks.

In this chapter, an introduction and overview of the Geant4 toolkit will be given, including toolkit fundamentals, main elements of a simulation, and physical processes and materials used for simulation in radiation dosimetry.

## 4.1 Introduction to Geant4 Package

The prototype of Geant4, named RD44, was created in 1994 as a result of the efforts of scientists at CERN (European Council for Nuclear Research) and KEK (High Energy Accelerator Research Organization) to improve the existing FORTRAN-based Geant3 simulation program. At first, the purpose of the RD44 project was to develop a detector simulation program based on modern computing tools. However, the scope of RD44 was soon extended to cover other research areas such as nuclear physics, particle accelerators, space radiation and medical physics. In 1998, the first production release of Geant4 was delivered, followed by several updated versions. These were all under open-source license, enabling Geant4 to derive benefits from various contributors to the Monte Carlo simulation of particle detectors and physical processes [97].

Geant4 is written in the modern object-oriented programming language C++, which compared with the old FORTRAN based Geant3 simulation program, improves the ability to manage all existing physics models. Geant4 allows users to easily create and integrate a new physics model into the toolkit with little or no modification to the existing code, reducing the amount of work and saving time for a user attempting to develop a new application.

## 4.2 Toolkit Fundamentals

### 4.2.1 Geant4 Class Categories

In a large system such as Geant4, it is essential to partition the software into smaller and independent logical units. This will improve software development, because it allows implementation of all units in parallel without cross-interference. In Geant4, class categories are used to create logical units; the relationship and a brief summary of the role of each class category can be seen on Figure 4.1 and Table 4.1 respectively. In the figure, each class category is represented by a box, and the straight lines show their "users" - the relations between classes. The circle at the end of a straight line means the class category which has this circle uses the other (alternate) category [97].

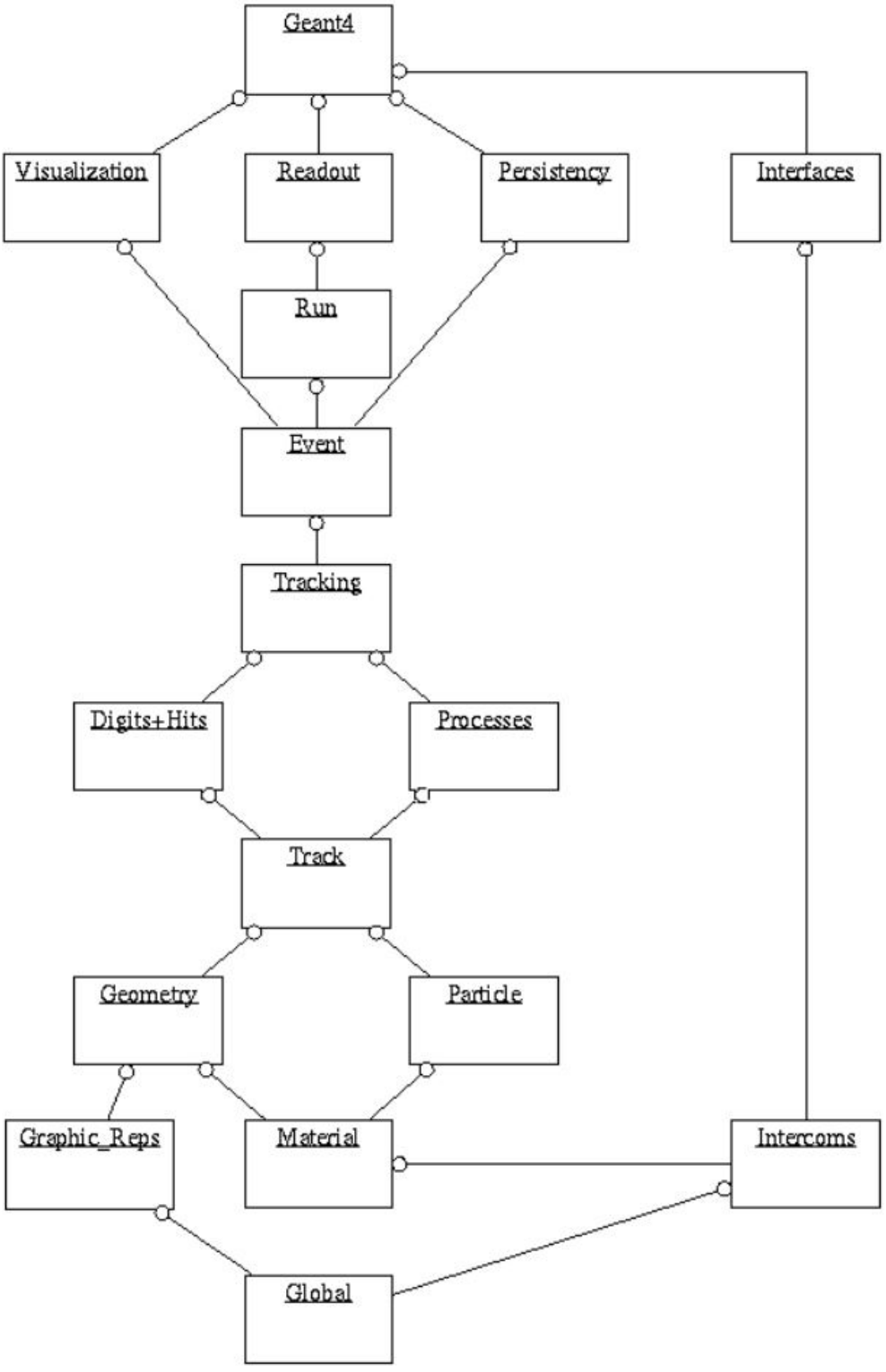


FIGURE 4.1: Geant4 class categories (reproduced from [98]).

| **Geant4 categories** | **Role** |
|---|---|
| Run and Event | Generation of events, interfaces to event generators and any secondary particles produced, provide particles to be tracked to the Tracking Management. |
| Tracking and Track | Propagating a particle by analyzing the factors limiting the step and applying the relevant physics processes. |
| Geometry and Magnetic Field | Manage the geometrical definition of a detector (solid modeling) and the computation of distances to solids (also in a magnetic field). |
| Particle Definition and Matter | Manage the the definition of materials and particles. |
| Physics | Manages all physics processes participating in the interactions of particles in matter. |
| Hits and Digitization | Manage the creation of hits and their use for the digitization phase. |
| Visualization | Manages the visualization of solids, trajectories and hits, and interacts with underlying graphical libraries. |
| Interfaces | Handles the production of the graphical user interface (GUI) and the interactions with external software. |

TABLE 4.1: Summary of the role of each class category in Geant4. [98]

### 4.2.2 System of Units

In Geant4, users can choose and use the preferred units for any quantity from the system library. In addition, new units can be introduced by either extending the system unit library or creating a new one.

### 4.2.3 Run

In Geant4, **Run** is the largest unit of simulation and consists of a sequence of events. Within a **Run**, the detector geometry, the setup of sensitive detectors, and the physics processes used in the simulation should be kept unchanged. **Run** is represented by the **G4Run** class with an identification number, which should be set by the user, and the number of events simulated during the run.

### 4.2.4 Event

**G4Event** class represents an **Event** and contains all inputs and outputs of the simulated event. A **G4Event** object has four major types of information: primary vertexes and primary particles, trajectories, hits collections and digits collections.

### 4.2.5 Track

A **Track** is represented by a **G4Track** class which contains current information of the particle as it travels in space and time. A **Track** has a position, physical quantities (energy, momentum, and time) and a lifetime. The lifetime of a **Track** is started by a generator or a physics process and ended when it leaves the World mother volume, disappears (the particle decays or is absorbed) or the user kills it.

### 4.2.6 Step

The **Step** (**G4Step** class) is the basic unit of simulation. It includes the two endpoints of the step, *PreStepPoint* and *PostStepPoint*, which contain the incremental particle information (energy loss, elapsed time) and the change in track properties between the two points.

## 4.3 Geant4 Simulation Elements

### 4.3.1 The Particle Source

There are three levels of classes to describe particles in Geant4:

- **G4ParticleDefinition**: defines a particle
- **G4DynamicParticle**: describes a particle interacting with materials
- **G4Track**: describes a particle traveling in space and time

Geant4 provides various types of particles, which are derived from a dictionary of particles in the system and organized into six major categories: lepton, meson, baryon,

boson, short-lived and ion. Starting properties of a particle source such as position, direction, momentum, type and energy level need to be defined by the user. All intrinsic properties of the particles used in Geant4 can be accessed from the software database and are processed by an instance of the **G4ParticleGun** class.

### 4.3.2 Detector Geometry

Detector geometry in Geant4 is made of a number of volumes. The World volume, the largest volume, contains all other volumes in the detector geometry. Each volume is created by describing its shape and physical characteristics, and then placing it inside a containing volume. When a volume is placed inside another volume, the former and latter volumes are called the Daughter and Mother volume respectively. The coordinate system of the Mother volume is used to specify the position of the Daughter volume.

The shape of a volume is defined using the concept of a solid, a geometrical object that has a shape and specific values for each dimension of that shape. The properties of each volume consist of the geometrical properties of the solid, together with its physical characteristics such as the material of the volume, sensitive detector elements and the magnetic field.

### 4.3.3 Physics Processes

In Geant4, physics processes describe how particles interact with materials. There are seven major categories of physics processes in Geant4: electromagnetic, hadronic, transportation, decay, optical, photolepton-hadron and parameterisation. All physics processes are treated in the same manner from the tracking point of view. In a simulation, all physics processes are obtained from the **G4VProcess** class.

### 4.3.4 Interactive Session

An interactive session is provided to allow the user to interact with Geant4 simulation by a series of user interface commands. The user can control Geant4 through an interactive session in either a command-line terminal mode, batch mode with a macro file, or a

direct C++ function call. In Geant4, the graphic user interface (GUI) is provided in the **interfaces** category.

### 4.3.5 Visualization

The Geant4 visualization system was developed to provide users with:

- Quick response to study geometries, trajectories and hits
- Exporting high-quality data (in the form of graph, video or picture) for publications
- Flexible angle view to debug complex geometries
- Tools to show volume overlap errors in detector geometries
- Interactive picking to get more information on visualized objects

Simulation data that can be visualized include detector components, hierarchical structure of physical volumes, particle trajectories and tracking steps, hits of particles and scoring data, and some other user-defined objects such as coordinate axes, text, descriptive character strings, comments or titles, scales and logos.

The visualization of Geant4 was designed to be compatible with a variety of graphics systems. Although some graphics software routines use a Geant4 complied library (OpenGL, Qt), others operate as a separate application (HepRApp, DAWN).

### 4.3.6 Data Analysis

The analysis category is aimed at providing users with an analysis tool directly within the Geant4 installation. The category consists of the analysis manager classes, and the **g4tools** package, which allows users to access histograms and n-tuples in several formats such as ROOT, XML AIDA format, CSV (comma-separated values format), and HBOOK, provided by **G4CsvAnalysisManager**, **G4RootAnalysisManager**, **G4XmlAnalysisManager** and **ExG4HbookAnalysisManager** class respectively.

## 4.4 Materials in Geant4

There are three main classes designed to describe materials in Geant4.

- **G4Isotope**: describes the properties of atoms such as atomic number, number of nucleons, atomic mass, and mass per mole
- **G4Element**: describes the properties of elements such as effective atomic number, effective number of nucleons, effective mass per mole, number of isotopes, shell energy, and quantities such as cross-section per atom
- **G4Material**: describes the macroscopic properties of matter such as density, state, temperature, pressure, and macroscopic quantities such as radiation length, mean free path, *dE/dx*

The **G4Material** class is used by the tracking, the geometry, and the physics, and contains all the information related to the elements and isotopes of the material.

### 4.4.1 Building Elements and Materials

There are different ways to define materials in Geant4:

- **Define a single element material** by specifying its name, density, mass per mole, and atomic number
- **Define a molecule** by specifying the number of atoms in the molecule
- **Define a compound** by giving the fractional mass of each component
- **Access the Geant4 material database** to get predefined available materials
- **Define a new material** from the base material available in Geant4 material database

### 4.4.2 Geant4 Materials Database

Geant4 uses a part of the National Institute of Standards (NIST) material database which provides a detailed database of material properties, including density, excitation potential, chemical bounds, element composition and isotope composition with more than 300 isotopes and their properties being tracked.

The Geant4 material database can be accessed easily through **G4NistManager** class and user interface commands. Both **G4Element** and **G4Material** classes can be loaded directly from the database to specify detector or medium layer materials. In addition, a new compound material also can be created by specifying a vector of atomic numbers and weights to retrieve NIST elements.

**Simple Materials (Elements)**

| Z | Name | density(g/cm^3) | I(eV) |
|---|---|---|---|
| 1 | G4_H | 8.3748e-05 | 19.2 |
| 2 | G4_He | 0.000166322 | 41.8 |
| 3 | G4_Li | 0.534 | 40 |
| 4 | G4_Be | 1.848 | 63.7 |
| 5 | G4_B | 2.37 | 76 |
| 6 | G4_C | 2 | 81 |
| 7 | G4_N | 0.0011652 | 82 |
| 8 | G4_O | 0.00133151 | 95 |
| 9 | G4_F | 0.00158029 | 115 |
| 10 | G4_Ne | 0.000838505 | 137 |
| 11 | G4_Na | 0.971 | 149 |
| 12 | G4_Mg | 1.74 | 156 |
| 13 | G4_Al | 2.699 | 166 |
| 14 | G4_Si | 2.33 | 173 |
| 15 | G4_P | 2.2 | 173 |
| 16 | G4_S | 2 | 180 |
| 17 | G4_Cl | 0.00299473 | 174 |
| 18 | G4_Ar | 0.00166201 | 188 |
| 19 | G4_K | 0.862 | 190 |
| 20 | G4_Ca | 1.55 | 191 |
| 21 | G4_Sc | 2.989 | 216 |
| 22 | G4_Ti | 4.54 | 233 |
| 23 | G4_V | 6.11 | 245 |
| 24 | G4_Cr | 7.18 | 257 |
| 25 | G4_Mn | 7.44 | 272 |

FIGURE 4.2: A part of Geant4 material database table (reproduced from [99]).

## 4.5 Development of Geant4

Geant4 exploits advanced software engineering techniques based on the Booch/UML Object Oriented Methodology and follows the evolution of the ESA Software Engineering Standards for the development process. A Geant4 development process often starts with user requirements being collected, followed by analysis and design procedure.

Geant4 is actively and continuously developed and maintained by the International Geant4 Collaboration. In addition, as an open software, Geant4 also benefits from a strong contribution by third-party organizations, researchers and users world-wide.

## 4.6 Summary

This chapter has provided an introduction and overview of the Geant4 software toolkit, including its history, toolkit fundamentals, and the main elements of a simulation, as well as the development of the toolkit. Geant4 has application in a variety of settings; its functionality, modelling capabilities and performance continue to be extended and enhanced.

# Chapter 5

# Wearable Directionally-sensitive Radiation Dosimeters

The ability to determine the emission direction of a radioactive source is a critical requirement in the regulatory control of ionizing radiation sources and has been shown to improve the process of tracking and localizing radioactive isotopes. The development of low-cost solid-state semiconductor radiation detectors with excellent energy resolution, fast and linear energy response, and low voltage supply has enabled the design of light weight, portable directionally-sensitive dosimeters.

This chapter begins by providing detailed information regarding the proposed active and wearable directionally-sensitive radiation dosimeter using multiple solid-state CdZnTe semiconductor detectors, including detector geometry and simulation configuration. Secondly, an algorithm to estimate the emission direction of a radioactive source, based on the number of interacting particles recorded in the four closest detectors of a circular array of eight detectors, will be introduced. This is then followed by an analysis and discussion of the efficiency and accuracy of the proposed dosimeter for determining the direction of radioactive sources of different detector shapes and at different STD distances. Finally, a brief evaluation of the performance of the proposed dosimeter in a 3D environment will be presented.

## 5.1 System Requirements

Currently, a variety of radiation detectors with different properties are available to choose from. However, because the aim of this research is to design a wearable dosimeter, any detector selected for this application will have to satisfy some specific requirements as below:

1. **Sensitivity**: the proposed dosimeter is designed as a wearable device. To increase safety to its users, its detectors need to have high sensitivity, enabling the detection of distant or low energy radioactive sources.

2. **Energy Range**: because $\gamma$-rays are the most penetrating radiation and can have an adverse effect on living tissue, the selected detector needs to cover the energy range of $\gamma$-rays from a few hundred keV up to 10 MeV.

3. **Energy Resolution**: to increase the accuracy of identifying existing radioactive isotopes, the selected detector is expected to have high energy resolution (finer than 3 %).

4. **Response Time**: to increase the speed of dose rate measurement and source direction estimation of the proposed dosimeter, it is desirable that the selected detector have a fast time response (less than 5 ns when exposed to X-rays or electron beams).

5. **Linearity**: in order to achieve a consistent and accurate measurement, it is expected that the selected detector reading is linear within the measurement energy range.

6. **Operating Voltage**: to satisfy the safety requirement of a wearable electronic device, it is preferable that the detector operate with a low power supply voltage (under 5 VDC(Volts Direct Current)).

7. **Physical Dimension**: to make it easier and more convenient for users, it is desirable that the selected detector has small physical dimensions.

8. **Weight**: the selected detector is expected to be light-weight: the total weight of the whole dosimeter (including detectors and other electronic, and mechanical parts) is intended to be under 500 g.

Based on the above requirements, a survey was conducted to compare available radiation detectors. Among those available, the best to satisfy those requirements is the CdZnTe solid-state semiconductor detector, as it has the most advantages for a radiation detector: high energy resolution and detection efficiency, good room-temperature performance and low power-supply voltage [57].

## 5.2 Detector Geometry

The proposed dosimeter uses a circular array (see Figure 5.1 below) of eight CdZnTe detectors (*D1* (green colour) to *D8*). Each detector is considered box-shaped, 10 cm high, 5 cm wide and 1 cm deep. The rationale for the circular arrangement is based on the intention either to attach all detectors to a belt or to integrate them into a (wearable) lab coat.

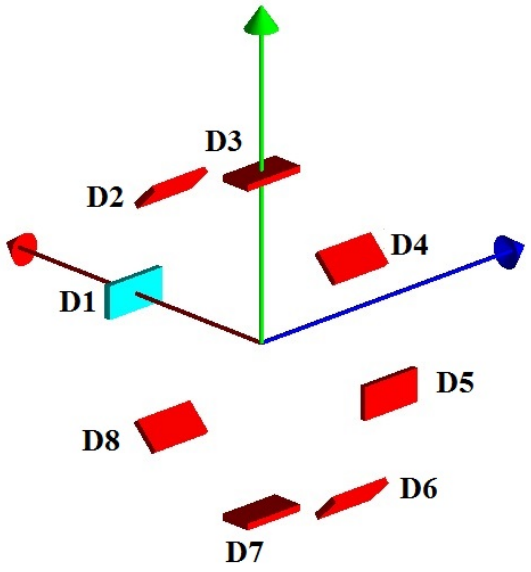


FIGURE 5.1: Layout of the proposed dosimeter in Geant4.

## 5.3 Simulation Setup

In order to evaluate the performance of the proposed dosimeter, simulation using the Geant4 toolkit has been set up with conditions as follows:

1. **The World Volume**: in our simulation setup, the world volume was modelled as a 15 m x 15 m x 3 m cubic volume of air, which replicates a surveillance area where the dosimeter might well be used in practice.

2. **The Sensitive Volume**: to allow the number of hits in each detector to be collected independently each detector is defined as one sensitive volume.

3. **The Primary Particle Source**: this is an isotropic point source of $^{137}_{55}Cs$ radioactive isotope.

4. **Physical Process**: this is the natural radioactive decay process of $^{137}_{55}Cs$ isotope.

5. **Source-to-detector (STD) Distance**: the primary particle source was placed 75 cm from the centre of the dosimeter, as shown in Figure 5.2.

6. **Data Output**: simulation data, which are the number of interacting particles recorded in each detector, are printed to the screen (Figure 5.3) and saved to a ROOT (or CVS) file for further analysis.

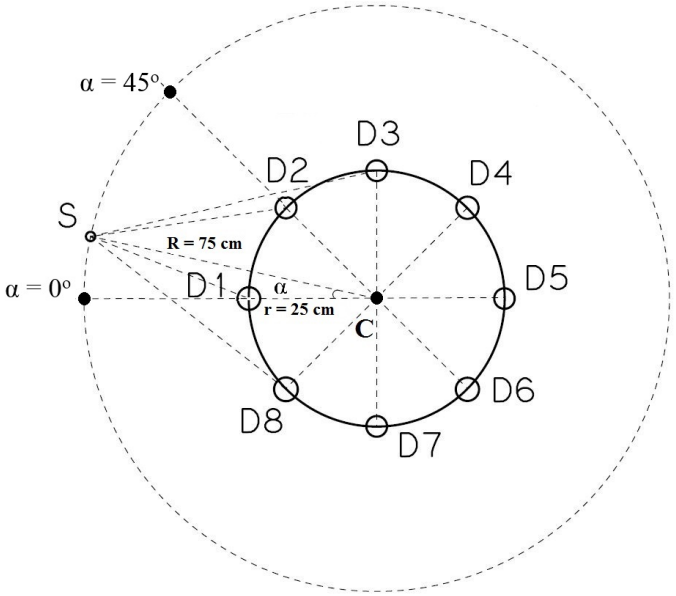


FIGURE 5.2: Simulation setup in Geant4.

```
 Run terminated.
Run Summary
  Number of events processed : 5000000
  User=1022.1s Real=0s Sys=0.063s

--------------------End of Global Run-----------------------
 The run was 5000000 events
 Nb of events with energy deposit in detector 1: 4499
------------------------------------------------------------
 Nb of events with energy deposit in detector 2: 3187
------------------------------------------------------------
 Nb of events with energy deposit in detector 3: 1178
------------------------------------------------------------
 Nb of events with energy deposit in detector 4: 661
------------------------------------------------------------
 Nb of events with energy deposit in detector 5: 639
------------------------------------------------------------
 Nb of events with energy deposit in detector 6: 546
------------------------------------------------------------
 Nb of events with energy deposit in detector 7: 848
------------------------------------------------------------
 Nb of events with energy deposit in detector 8: 1990
... write Root file : TR.root - done
```

FIGURE 5.3: Simulation results shown on screen.

## 5.4 Radioactive Source Direction Estimation

### 5.4.1 Determining Four Closest Detectors

In the proposed dosimeter, the process of estimating the direction of a radioactive source $S$ commences by establishing the four detectors that are closest to the source $S$ in the circular array of eight detectors. These four detectors are identified based on the number of interacting photons recorded by each detector during the measurement interval. At the end of each measurement cycle, the recorded number of interacting particles in each detector will be compared, and the four detectors with highest reading are selected to be the detectors closest to the source $S$. The main reasons for the difference in the number of hits recorded by each detector are the different STD distances from source $S$ to each detector, and the 'shadow effect', in which the front detectors will cover and limit the number of photons that interact with the rear detectors.

An illustrative example can be seen in Figure 5.2. With eight detectors (*D1* to *D8*) in the circular array, the number of particles released by the source *S*, interacting with each of the detectors will be different. In this example, detectors *D1*, *D2*, *D3* and *D8* will record the highest number of interacting particles compared to other detectors, due to their closer proximity to the source *S*. Furthermore, the four rear detectors (*D3*, *D4*, *D5* and *D7*) are shadowed by the four front detectors (*D1*, *D2*, *D3* and *D8*) and the medium inside the dosimeter (which can be air, as in our simulation, or, in practice, the human body or other materials). This leads to a lower number of hits collected in the four rear detectors; therefore, in this case *D1*, *D2*, *D3* and *D8* are considered as the four closest detectors.

### 5.4.2 Estimating Source Direction

In the proposed system, the direction of a radioactive source $S$ is defined as the angle $\alpha$ which is created by the line from the source to the centre of the dosimeter with the horizontal axis of the dosimeter as shown in Figure 5.2. When the direction of the source $S$ (angle $\alpha$) increases from 0 to 45 degrees (Figure 5.2), the number of hits collected in two pairs of detectors *D1*, *D8* (and *D2*, *D3*) will be decreased (and increased, respectively) as the distance from source $S$ to these detector pairs is changed. That relationship

is expected to be linear when the primary particle source is an isotropic point source, that radiates uniformly in all directions over a sphere centred on the source. Simulation using the Geant4 tools has helped establish the relationship between radioactive source direction and radiation intensity (number of collected hits) measured by the four closest detectors.

In the simulation, the primary particle source is an isotropic point source of $^{137}_{55}Cs$ whose main physical process is natural radioactive decay. This is aimed at simulating a man-made radioactive source in the environment, required to be detected and localized by the proposed dosimeter. Simulation was run with the source $S$ releasing 5 million particles, which is equivalent to the dosimeter being irradiated by a $10\mu$Ci $^{137}_{55}Cs$ radioactive source for about 14 seconds. That will allow the closest detector to collect approximately 5000 to 6000 interacting particles when the source $S$ is placed 75 cm from the centre of the dosimeter, 50 cm away from each detector (see Figure 5.2).

Measurement data was collected at every 5 degrees as radioactive source $S$ was moved clockwise from 0 to 45 degrees. Each detector (sensitive volume) will independently and simultaneously measure and record the radiation intensity released from the source *S*. The number of interacting photons collected by each of the detectors will be displayed on the screen for observation and also saved to a file for use in the next step to estimate the direction of radioactive source *S*. An example of the simulation results (the number of interacting particles in each pair of closest detectors *D1*, *D8* and *D2*, *D3*) is shown in Figure 5.4 and Figure 5.5 respectively.

As can be seen from Figure 5.4 and Figure 5.5, when the direction (angle $\alpha$) of radioactive source $S$ is increased from 0 to 45 degrees, the number of collected hits is decreased in detectors *D1* and *D8*, but increased in detectors *D2* and *D3*. This is consistent with Newton's Inverse Square Law, in which the intensity of radiation decreases when the distance from the detector to the source increases, and vice versa [100]. It is clear that, as expected, the relationship between the direction of radioactive source $S$ and the number of interacting photons in two pairs of detectors *D1*, *D8* and *D2*, *D3*, is almost linear.

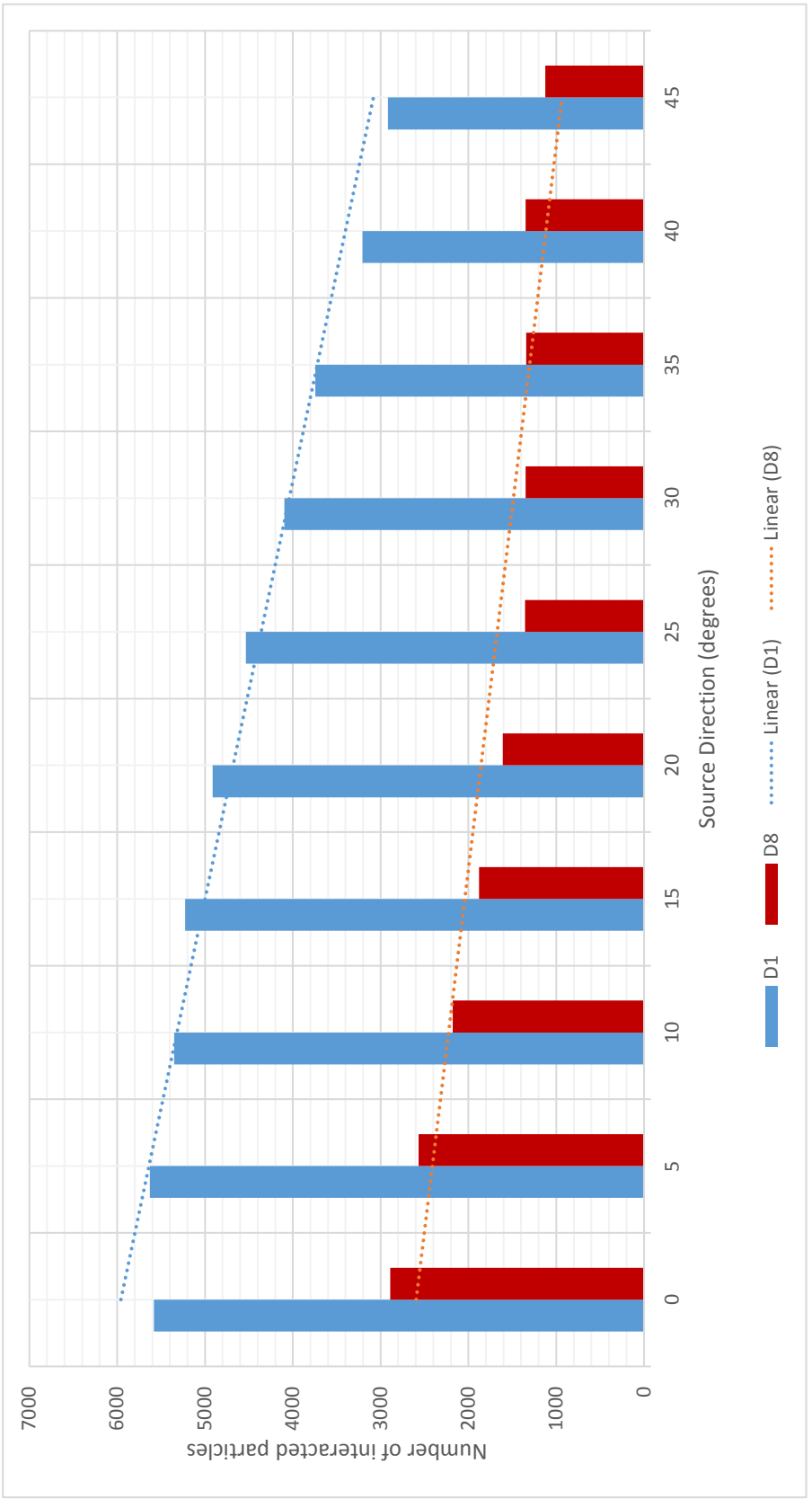


FIGURE 5.4: Number of interacting particles in detectors *D1* and *D8* (STD = 50 cm).

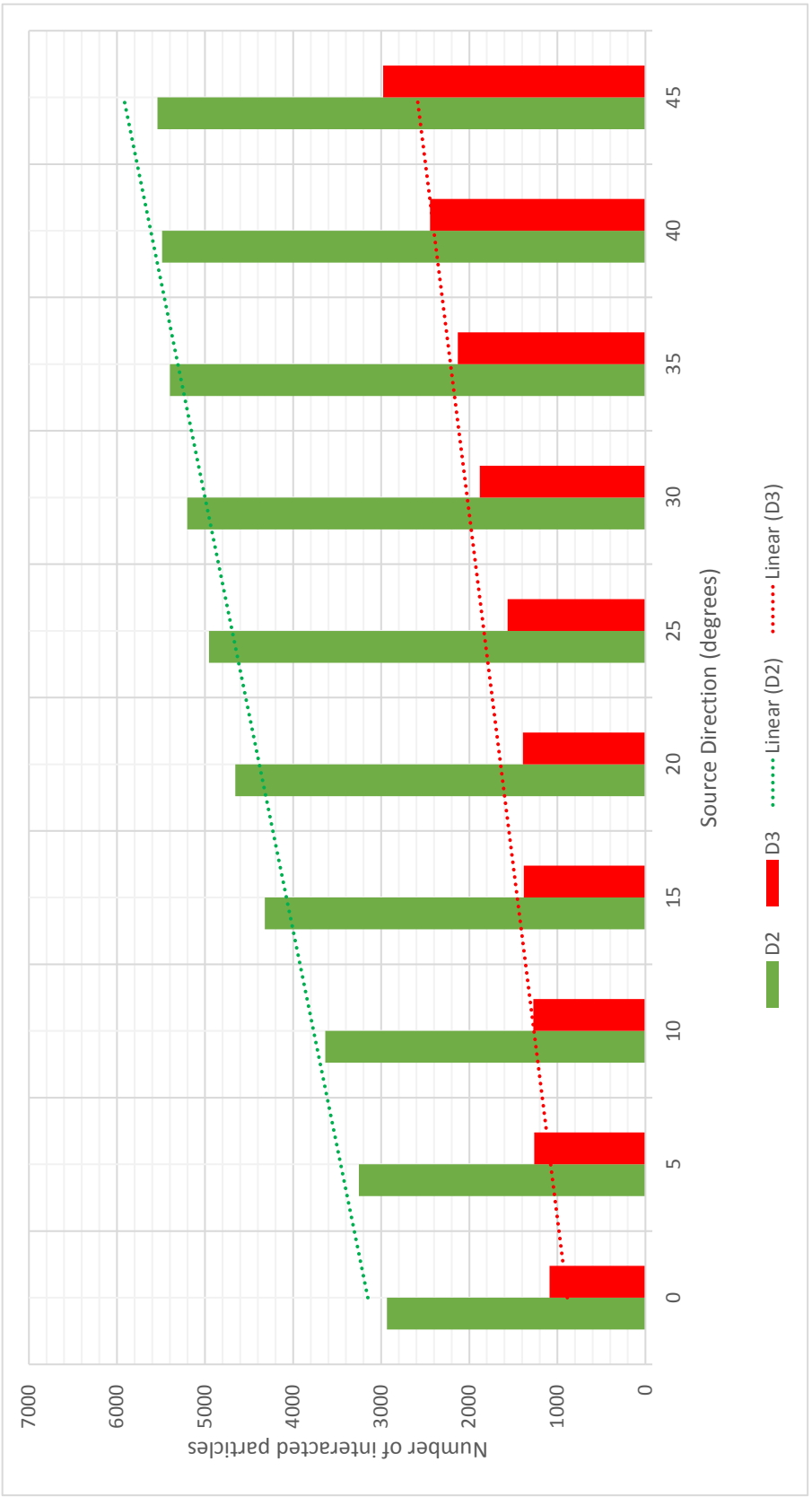


FIGURE 5.5: Number of interacting particles in detectors *D2* and *D3* (STD = 50 cm).

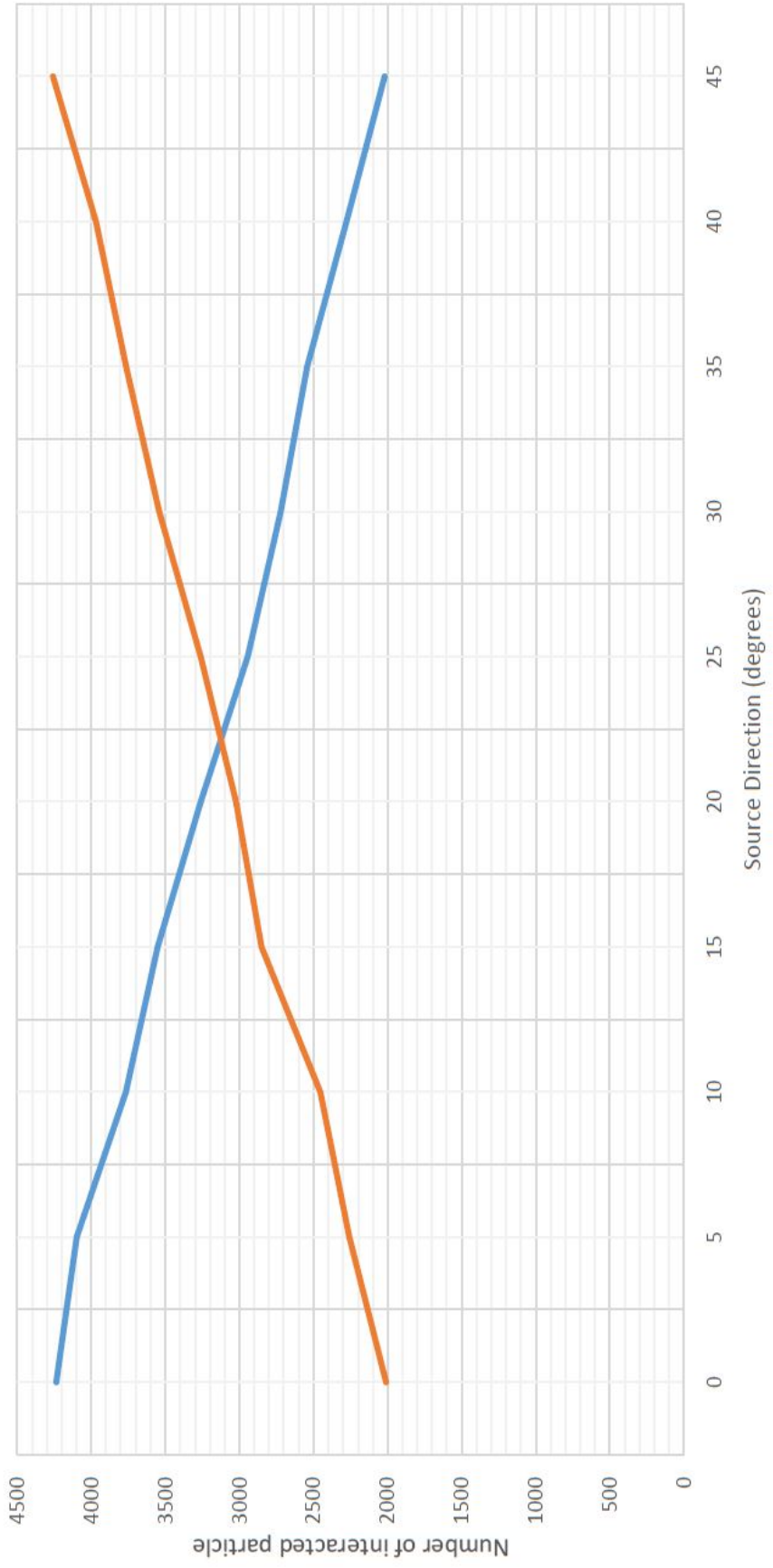


FIGURE 5.6: Average number of interacting particles in 2 pairs of detectors 1,8($D18$) and 2,3($D23$) (STD = 50 cm).

In order to obtain a more linear relationship between radioactive source $S$ direction and the number of interacting photons in these detectors, the average number of hits in each pair of detectors 1,8(*D18*) and 2,3(*D23*) will be used to form the equation which represents that relationship. As shown in Figure 5.6, by using the average number of hits in each pair of detectors, a better relationship is achieved compared to that shown in Figure 5.4 and Figure 5.5, when the number of interacting photons in each detector was used separately. Based on that improvement, a relationship to estimate the angle $\alpha$ of radioactive source $S$ using the average number of hits (radiation intensity) collected in each pair of closest detectors is proposed as below:

$$\alpha = A(I_{18\_\alpha} - I_{23\_\alpha}) + B \tag{5.1}$$

where:

$$I_{18\_\alpha} = \frac{I_{1\_\alpha} + I_{8\_\alpha}}{2} \tag{5.2}$$

and

$$I_{23\_\alpha} = \frac{I_{2\_\alpha} + I_{3\_\alpha}}{2} \tag{5.3}$$

where $I_{1\_\alpha}, I_{8\_\alpha}, I_{2\_\alpha}, I_{3\_\alpha}$ are the number of hits (radiation intensity) collected at detector *D1*, *D8*, *D2*, *D3* respectively when the radioactive source $S$ is at $\alpha$ degrees.

When the radioactive source $S$ is at angle $\alpha = 22.5$ (in the middle of the arc from 0 to 45 degrees), the average radiation intensity measured by two pairs of detectors *D18* ($I_{18\_22.5}$) and *D23* ($I_{23\_22.5}$) will be equal, because the distances from the source $S$ to detectors *D1*, *D2* and *D3*, *D8* are equal (assuming that there is no left-right ambiguity in the detectors). Applying that condition to Equation (5.1) we find:

$$22.5 = A(I_{18\_22.5} - I_{23\_22.5}) + B \tag{5.4}$$

Hence: $B = 22.5$

Additionally, $A$ will be determined using measurement results when the radioactive source $S$ is at an angle of 0 or 45 degrees. Firstly, when the source $S$ is at 0 degrees ($\alpha = 0$) we find:

$$0 = A_0(I_{18\_0} - I_{23\_0}) + 22.5 \tag{5.5}$$

$$A_0 = \frac{22.5}{I_{23\_0} - I_{18\_0}} \tag{5.6}$$

Secondly, when the source $S$ is at 45 degrees ($\alpha = 45$) we obtain:

$$45 = A_{45}(I_{18\_45} - I_{23\_45}) + 22.5 \tag{5.7}$$

$$A_{45} = \frac{22.5}{I_{18\_45} - I_{23\_45}} \tag{5.8}$$

Then $A$ will be the average:

$$A = \frac{A_0 + A_{45}}{2} \tag{5.9}$$

Finally, by applying Equations 5.6, 5.8 and 5.9 in Equation 5.1, the equation to estimate the angle $\alpha$ of radioactive source $S$ is:

$$\alpha = \frac{\frac{22.5}{I_{23\_0} - I_{18\_0}} + \frac{22.5}{I_{18\_45} - I_{23\_45}}}{2}(I_{18\_\alpha} - I_{23\_\alpha}) + 22.5 \tag{5.10}$$

where $I_{18\_0}, I_{23\_0}, I_{18\_45}, I_{23\_45}$ are the average radiation intensities measured by two detector pairs *D18* and *D23* when the radioactive source $S$ is at an angle of 0 and 45 degrees respectively.

## 5.5 Results and Discussion

Using data obtained from simulation, the direction (angle $\alpha$) of a radioactive source $S$ has been estimated by Equation 5.10. A comparison between the real and estimated angles of the radioactive source $S$ can be seen in Figure 5.7 and Table 5.1. The results were promising, showing that the proposed dosimeter can accurately estimate the direction of a radioactive source within a short measurement duration with high angular resolution. In our simulation, the proposed dosimeter has satisfactorily estimated the direction of a radioactive source $S$ to within 2 degrees at a distance of 70 cm from the source to the centre of the dosimeter (STD = 50 cm).

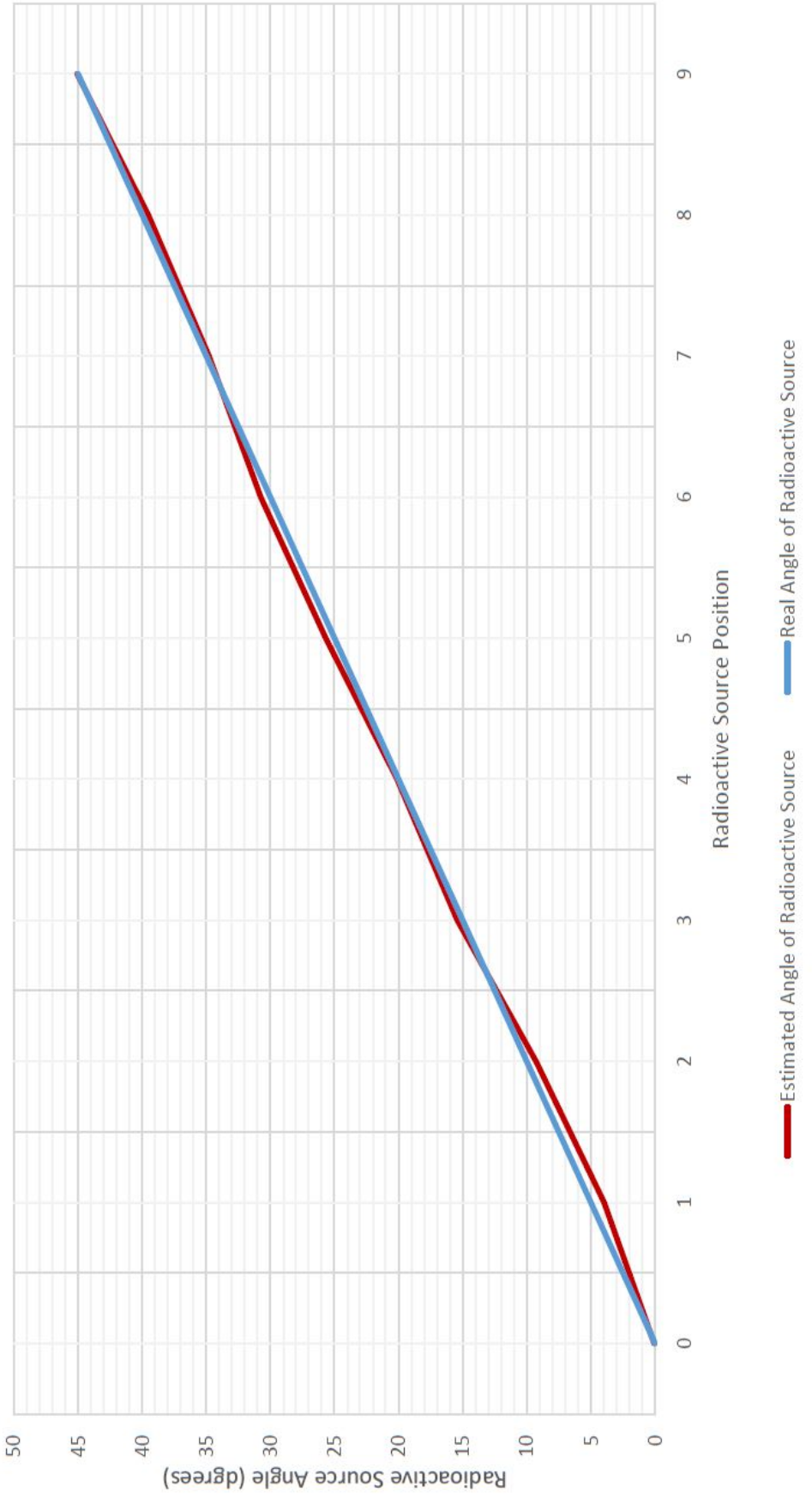


FIGURE 5.7: A comparison between the real and estimated angle of the radioactive source S (STD = 50 cm).

| **Source Position** | **Real Angle (degrees)** | **Estimated Angle (degrees)** |
|---|---|---|
| 0 | 0 | **0.0655** |
| 1 | 5 | **3.9667** |
| 2 | 10 | **9.2691** |
| 3 | 15 | **15.423** |
| 4 | 20 | **20.116** |
| 5 | 25 | **25.671** |
| 6 | 30 | **30.761** |
| 7 | 35 | **34.793** |
| 8 | 40 | **39.526** |
| 9 | 45 | **45.066** |

TABLE 5.1: Real and estimated angle of radioactive source S (STD = 50 cm)

Ideally, the proposed dosimeter is expected to be able to estimate the direction of a radioactive source at a longer distance as in practical working conditions. Therefore, in order to evaluate the performance of the proposed dosimeter, the simulation was repeated with the STD distance increased to 100 cm, 200 cm and 500 cm. All simulation conditions and setup, such as detector geometry, physical process and primary particle source were kept the same as when the STD distance was 50 cm, but to give each detector a reasonable number of interacting particles, the number of events was increased in proportion to the increase in STD distance.

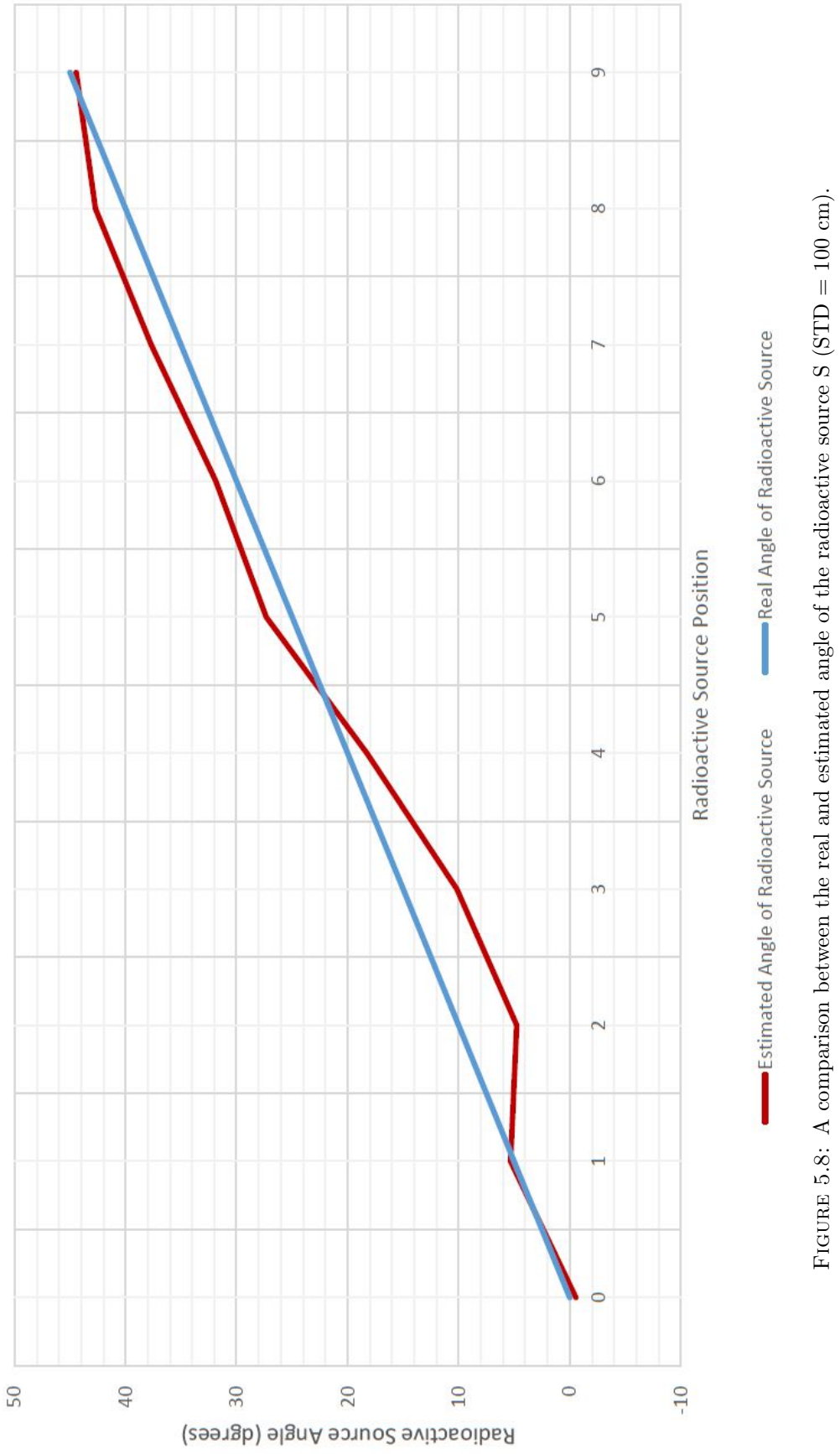


FIGURE 5.8: A comparison between the real and estimated angle of the radioactive source S (STD = 100 cm).

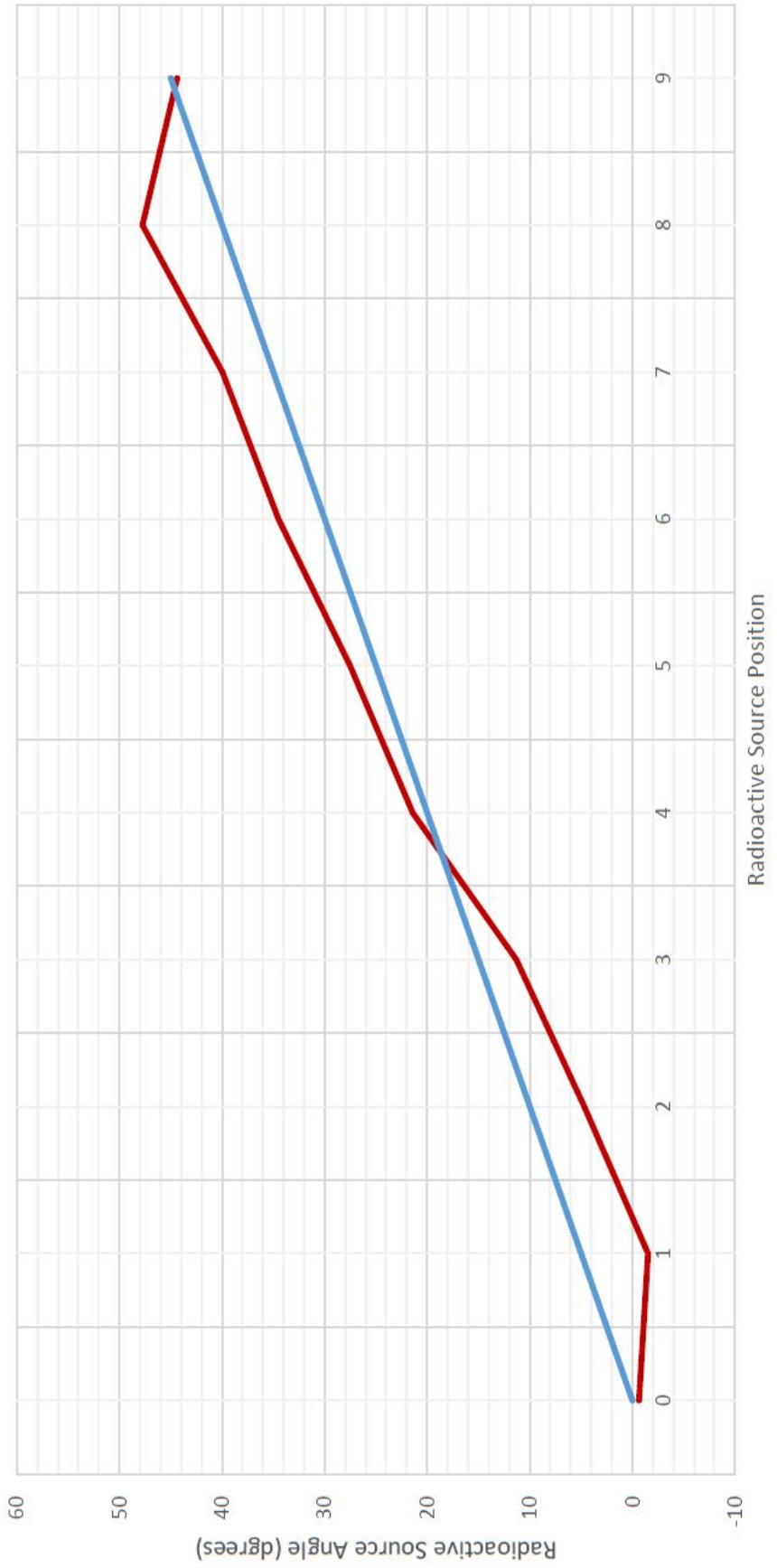


FIGURE 5.9: A comparison between the real and estimated angle of the radioactive source S (STD = 2 m).

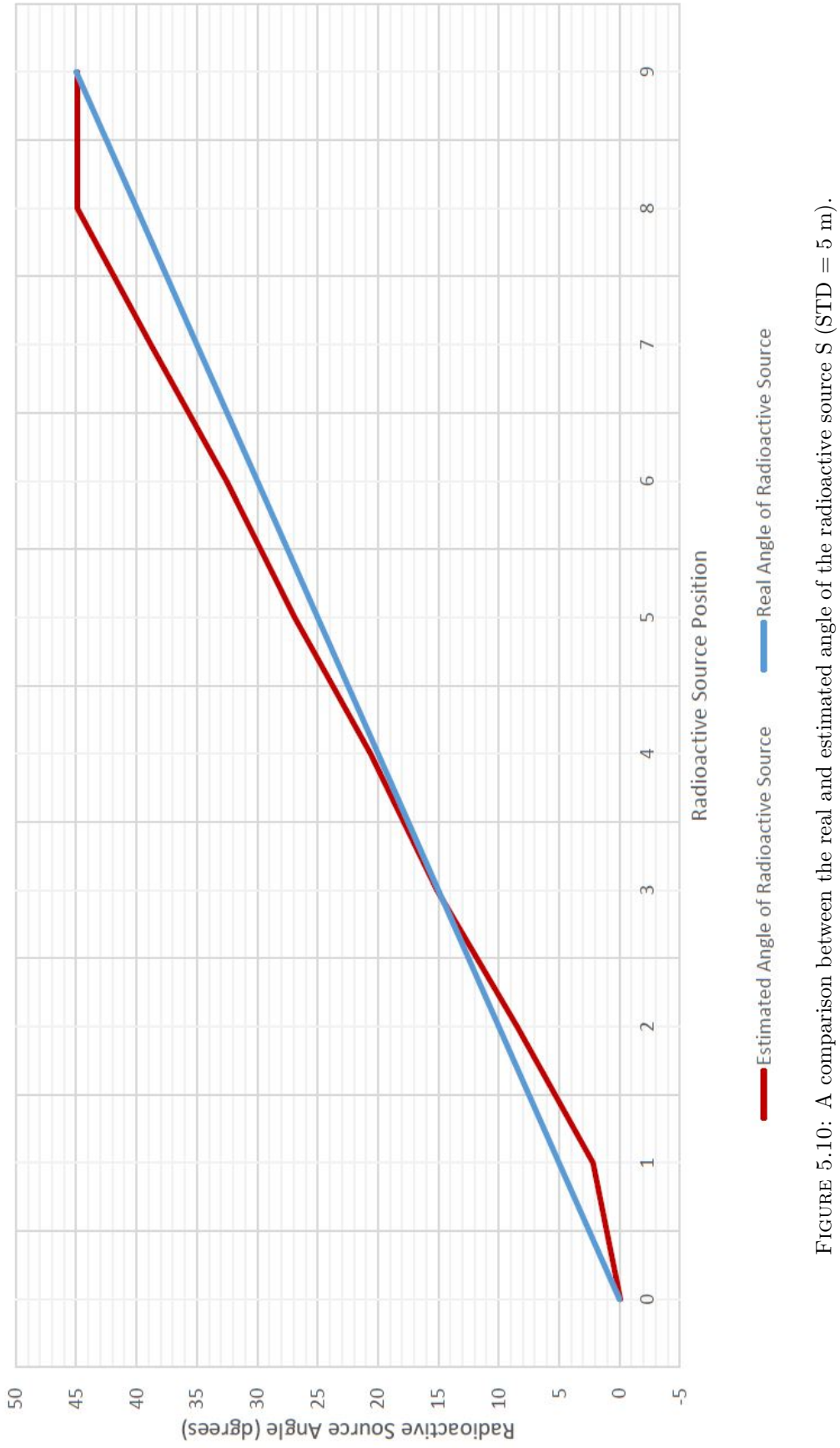


FIGURE 5.10: A comparison between the real and estimated angle of the radioactive source S (STD = 5 m).

| **Source Position** | **Real Angle (degrees)** | **Estimated Angle at Different STD Distance (degrees)** | | | |
|---|---|---|---|---|---|
| | | **50 cm** | **100 cm** | **2 m** | **5 m** |
| 0 | 0 | **0.0655** | **-0.553** | **-0.636** | **-0.084** |
| 1 | 5 | **3.9667** | **5.3257** | **-1.526** | **2.1893** |
| 2 | 10 | **9.2691** | **4.7807** | **4.6813** | **8.4712** |
| 3 | 15 | **15.4234** | **10.164** | **11.307** | **15.123** |
| 4 | 20 | **20.116** | **18.256** | **21.402** | **20.614** |
| 5 | 25 | **25.671** | **27.339** | **27.504** | **26.912** |
| 6 | 30 | **30.761** | **31.879** | **34.513** | **32.537** |
| 7 | 35 | **34.793** | **37.693** | **39.953** | **38.819** |
| 8 | 40 | **39.526** | **42.713** | **47.763** | **44.916** |
| 9 | 45 | **45.066** | **44.447** | **44.364** | **44.916** |

TABLE 5.2: Real and estimated angle of radioactive source S at different STD

Simulation results with the STD distance increased to 100 cm, 2 m and 5 m can be seen in Figures 5.8, 5.9 and 5.10 respectively. In addition, a comparison between estimated and real angles of the radioactive source $S$ at different STD distances, can be found in Table 5.2 and Figure 5.11. The results have demonstrated the ability of the dosimeter to estimate radioactive source direction consistently at different distances using Equation 5.10.

Simulation data also show that the accuracy of estimated source direction is decreased when the STD distance increases. According to Newton's Inverse Square Law [100], radiation intensity is inversely proportional to the distance from the source, which causes a significant decrease of measured intensity when STD distance is increased while the detector's sensitive volume remains unchanged. Therefore, in our simulation, when the STD distance is increased, the number of recorded interacting particles in each detector reduces sharply. This leads to an increase in the uncertainty as well as a decrease in the probability of whether the detectors can accurately detect and record all interacting particles. Consequently, the accuracy of the proposed dosimeter will decrease in proportion to the increase of STD distance. In practice, increasing the measurement time will be necessary and is the simplest method to improve the accuracy of source direction estimation when the STD distance is large.

These comparisons have shown a better estimation of radioactive source direction in the middle range of angles (between 10 and 40 degrees). The error is highest when the source direction is within the two boundary areas (i.e. close to 0 and 45 degrees). This happens when the source is at the boundary area: there might be two possible combinations of four closest detectors of either *D1*, *D2*, *D3*, *D8* or *D1*, *D2* and *D7*, *D8* (when the source is at 0 degrees), for which extra and/or repeated calculations might be necessary in order to achieve more accurate results. The situation of the radioactive source direction being within the boundary area can be detected when two out of four closest detectors have very similar numbers of collected hits, for example *D1* and *D3* or *D2* and *D8* when the source is close to 0 or 45 degrees respectively (Figure 5.2).

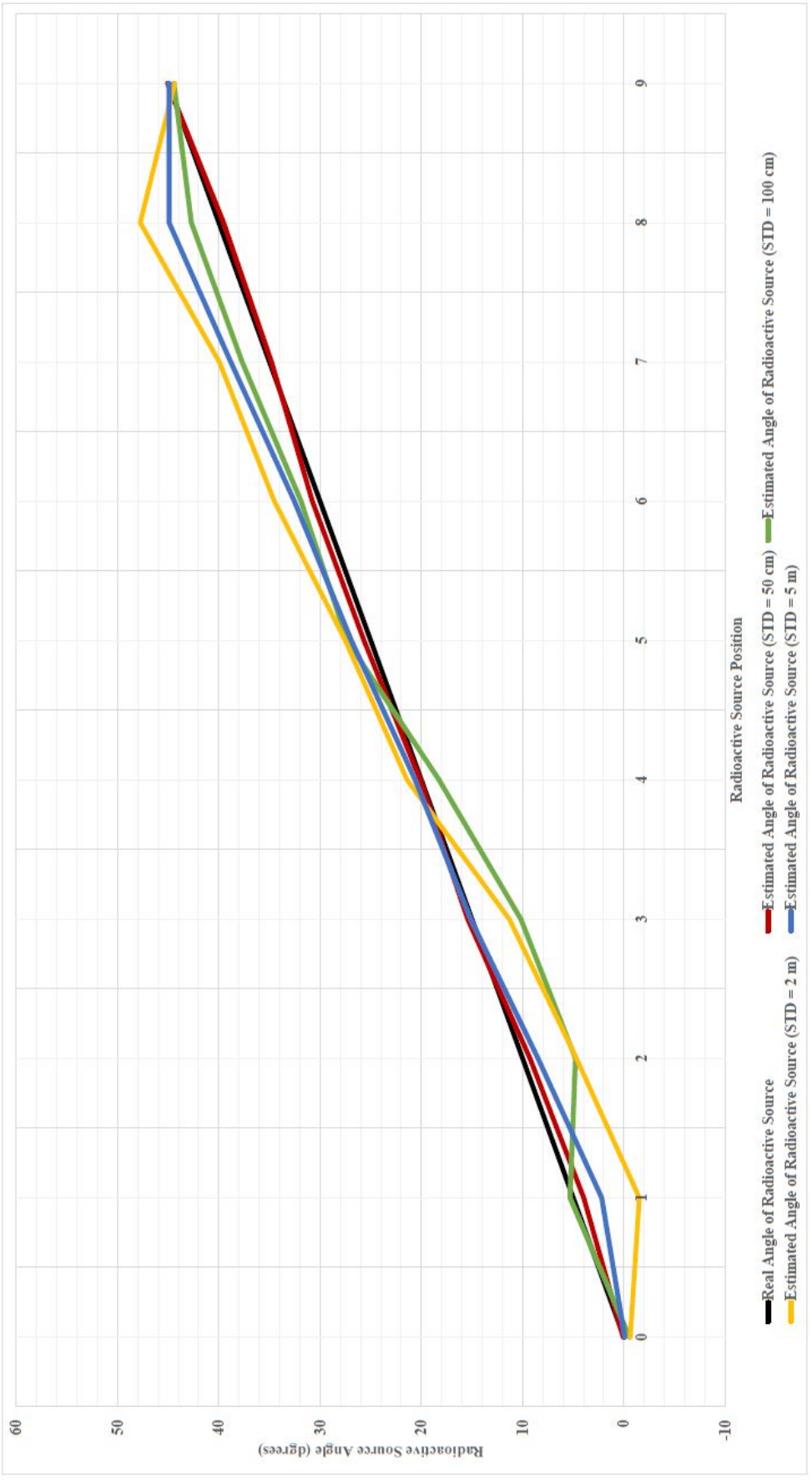


FIGURE 5.11: A comparison between the real and estimated angle of the radioactive source S at all simulation STD distances.

## 5.6 Estimation of Source Direction in 3D Environment

In terms of radiation security concerns, the ability to estimate the emission direction of radioactive sources in a 3D environment will be a key advantage of modern directionally-sensitive dosimeters. In fact, radioactive sources are not always in the same plane as the detectors, and surveillance areas can vary substantially from the simplest case of an empty field, to a complex area with many obstacles (such as buildings, trees, cars ... and even humans) of different shapes, dimension and materials. In such scenarios, it might be impossible to place the detectors close to or in the same plane as the sources. Consequently, it is expected that the proposed dosimeter will be able to detect and estimate the emission direction of radioactive sources in a 3D environment.

To improve the ability of the proposed dosimeter to estimate radioactive source direction in 3D, two other direction sensitive detectors in addition to the box shape, have been suggested and evaluated by simulation using Geant4 package. These new detectors (namely semi-tube and hemisphere) are designed with the same materials (CdZnTe), thickness and total sensitive volume as the initial box shape detector. The layout of these detectors in Geant4 package can be seen in Figure 5.12 and 5.13.

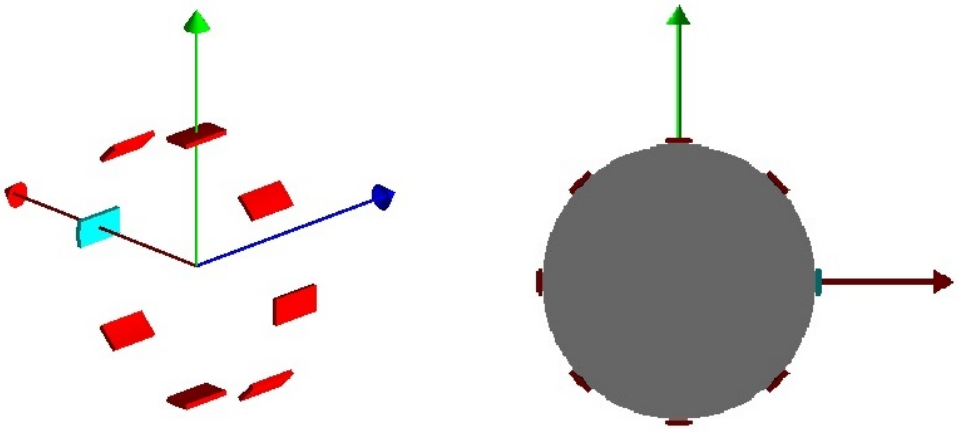

FIGURE 5.12: Layout of the proposed dosimeter using a semi-tube shape in Geant4.

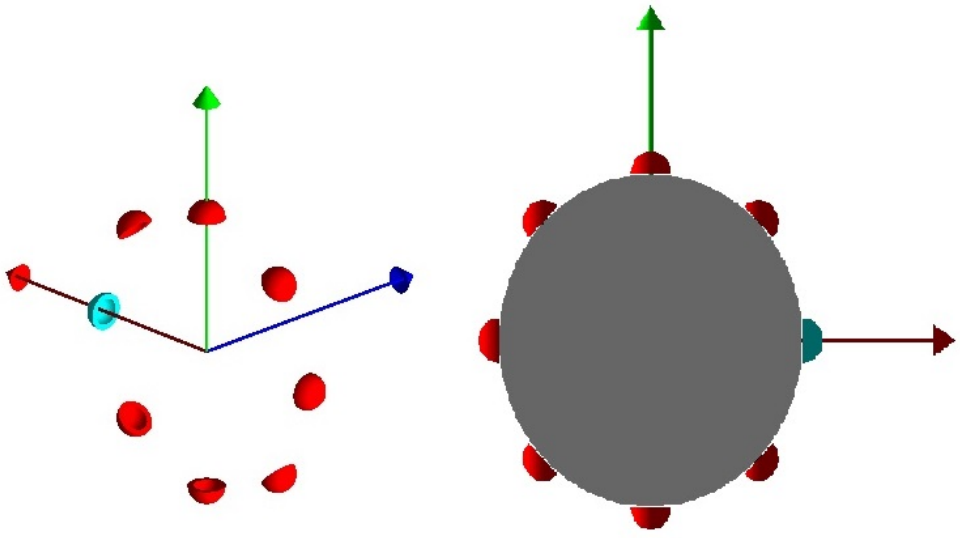

FIGURE 5.13: Layout of the proposed dosimeter using a hemispherical shape in Geant4.

Simulations using the Geant4 package have been performed to evaluate the efficiency of the proposed dosimeter with the new detectors' physical shapes. With the semi-tube and hemispherical detectors, all of the simulation conditions are maintained exactly the same as for box shape detectors. Comparison of estimated radioactive source emission direction obtained by different detector shapes at four STD distances (50 cm, 100 cm, 200 cm and 500 cm) are shown in Figure 5.14, 5.15, 5.16 and 5.17 respectively.

These comparisons clearly show that, similar to the box shape detector, in semi-tube and hemispherical detectors the accuracy obtained for estimating the source direction is reduced when the STD distance is increased. In general, the performance of the hemispherical detector is worse than the other two detector shapes: this is due to its smaller physical dimensions as its sensitive volume remains the same with the box shape detector. On the other hand, for the semi-tube detector, there is an improvement in performance as a result of its curve surface, which increases the probability of collecting more emission particles from an isotropic source, compared to the box shape detector. This improvement is actually only minor when the detectors are close to the source but becomes more significant at longer STD distance.

Figures 5.18, 5.19 and 5.20 show another performance comparison at different STD distances for each detector shape. The results indicate that at longer STD distances although it is less accurate than box and semi-tube shape detectors (due to smaller physical dimensions), a hemispherical detector obtains better precision. This is due to its own 3D structure which allows it to collect more radiation (compared to box and semi-tube shape detectors) from an isotropic radioactive source (emitting particles in 360 degrees). In addition, at shorter STD distances (particularly at STD distance of 50 cm), hemispherical shape detectors also achieve better accuracy, which confirms its advantage over other detector shapes in a 3D environment.

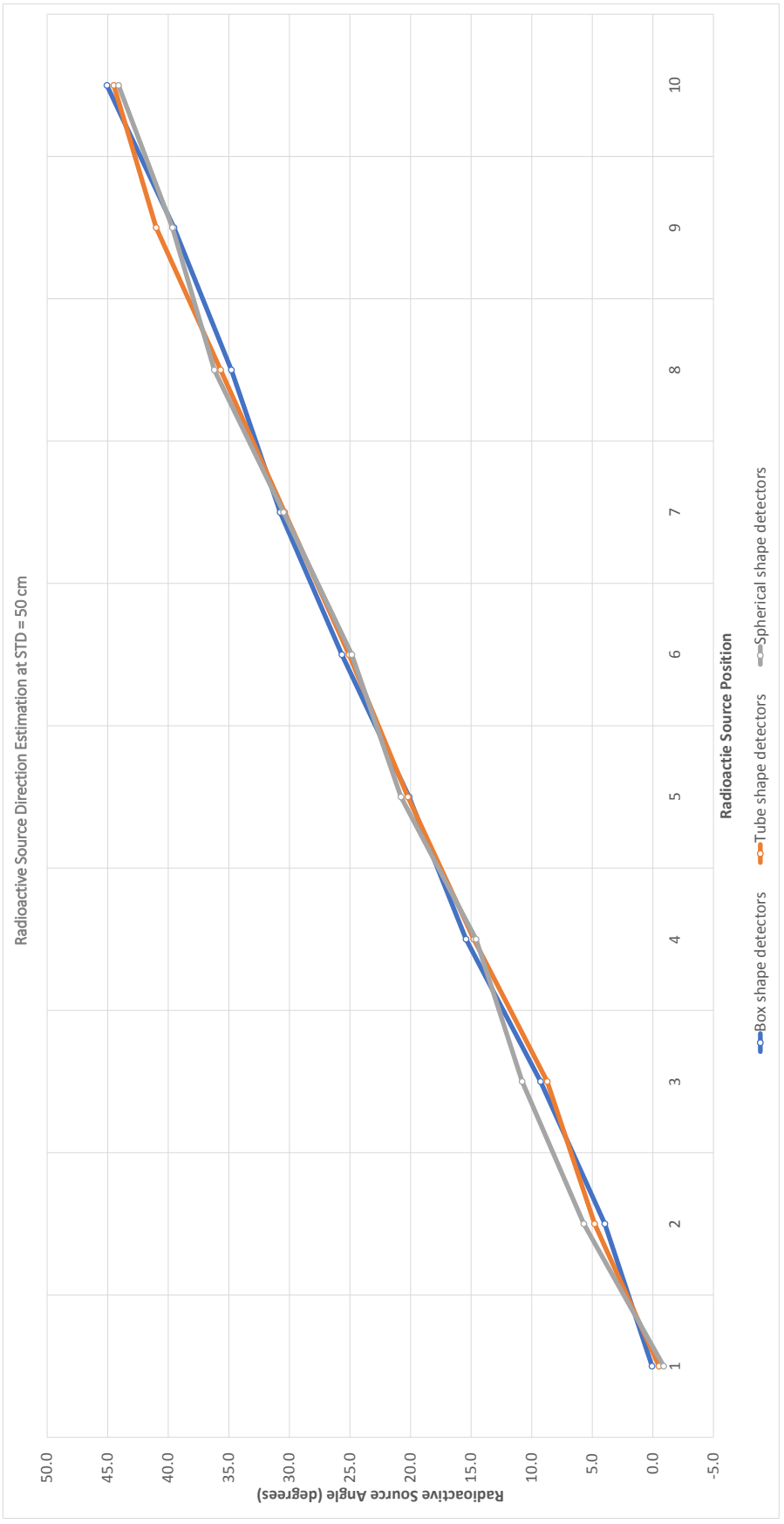


FIGURE 5.14: Radioactive source direction estimation by different detector shape at STD = 50 cm.

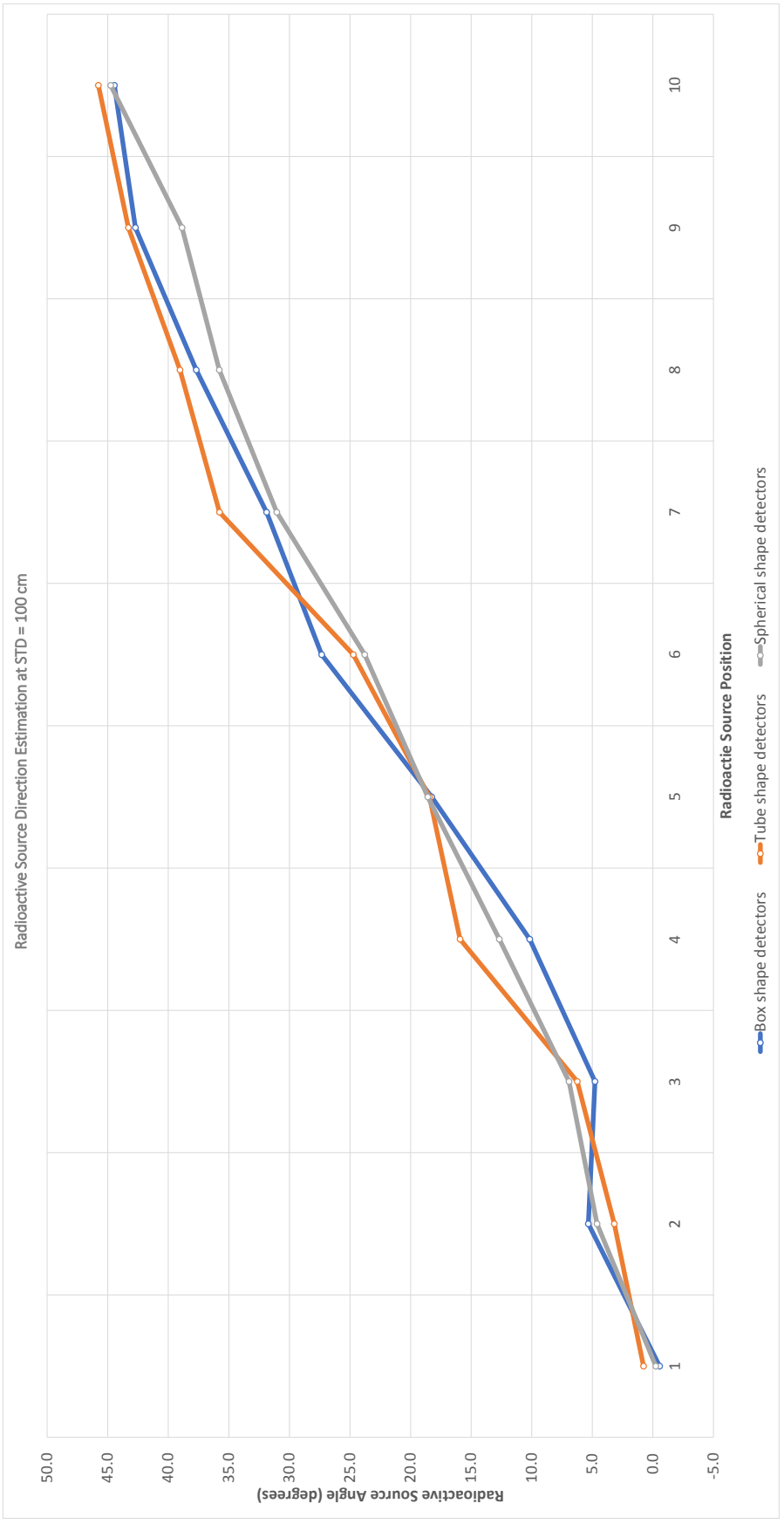


FIGURE 5.15: Radioactive source direction estimation by different detector shape at STD = 100 cm.

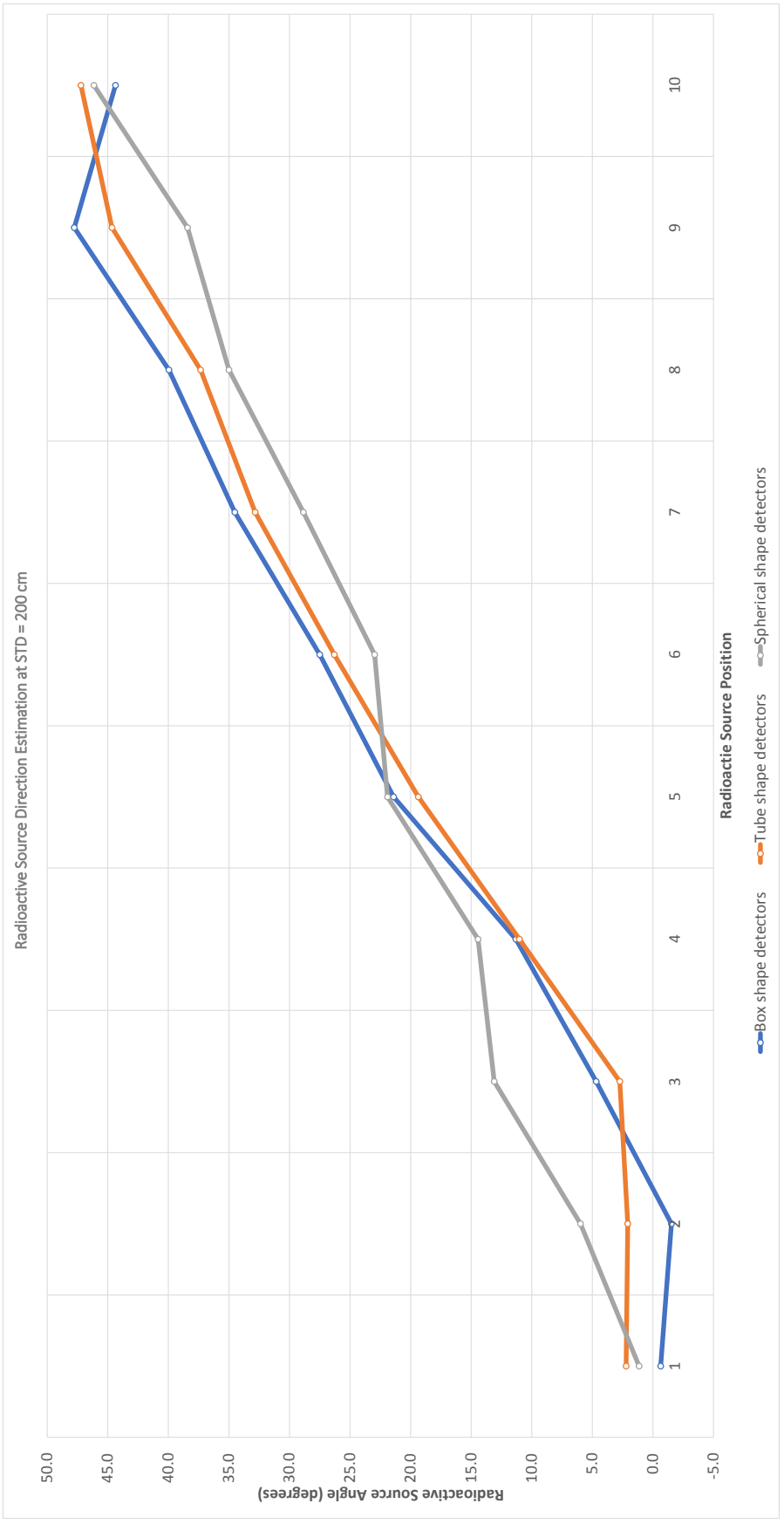


FIGURE 5.16: Radioactive source direction estimation by different detector shape at STD = 200 cm.

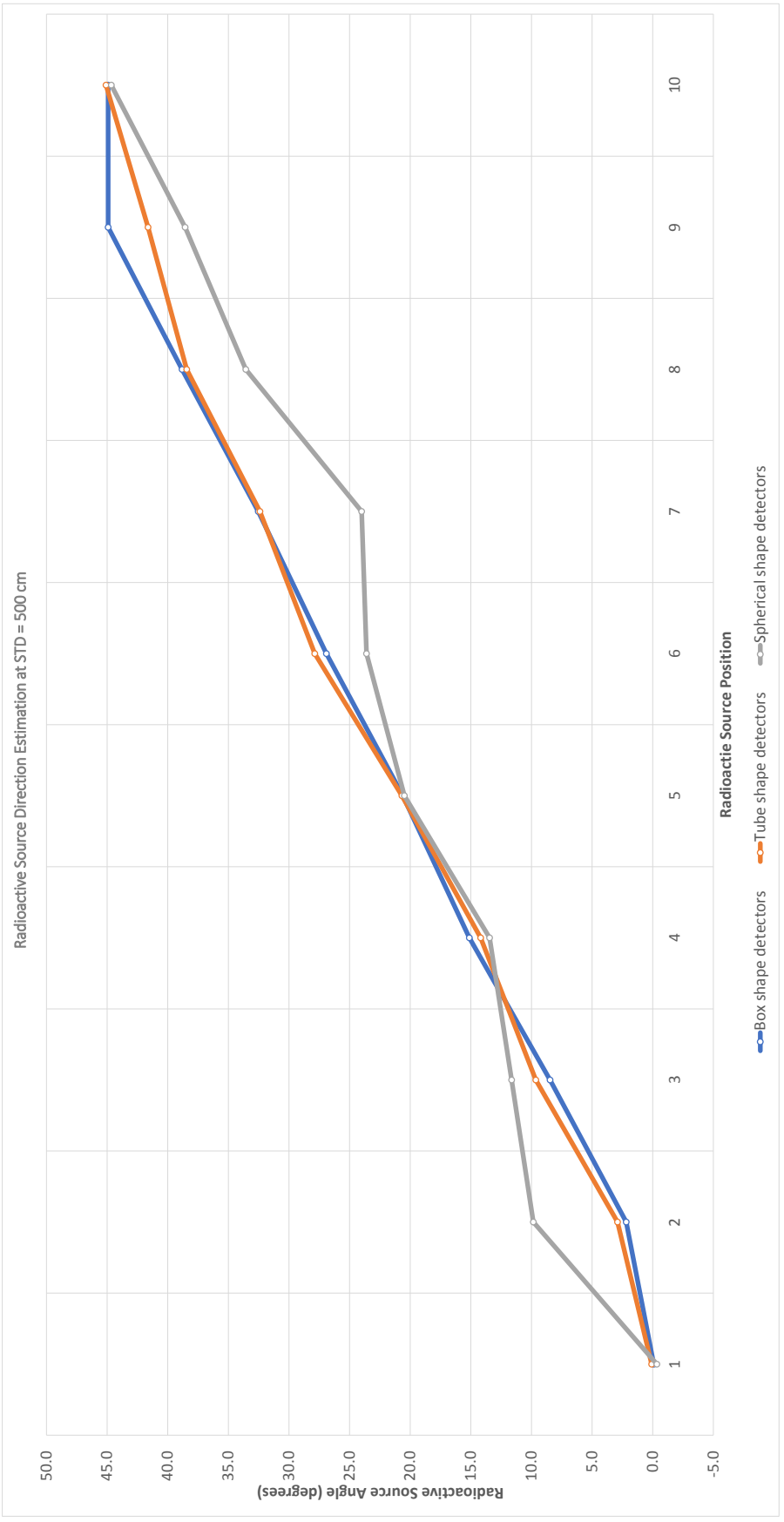


FIGURE 5.17: Radioactive source direction estimation by different detector shape at STD = 500 cm.

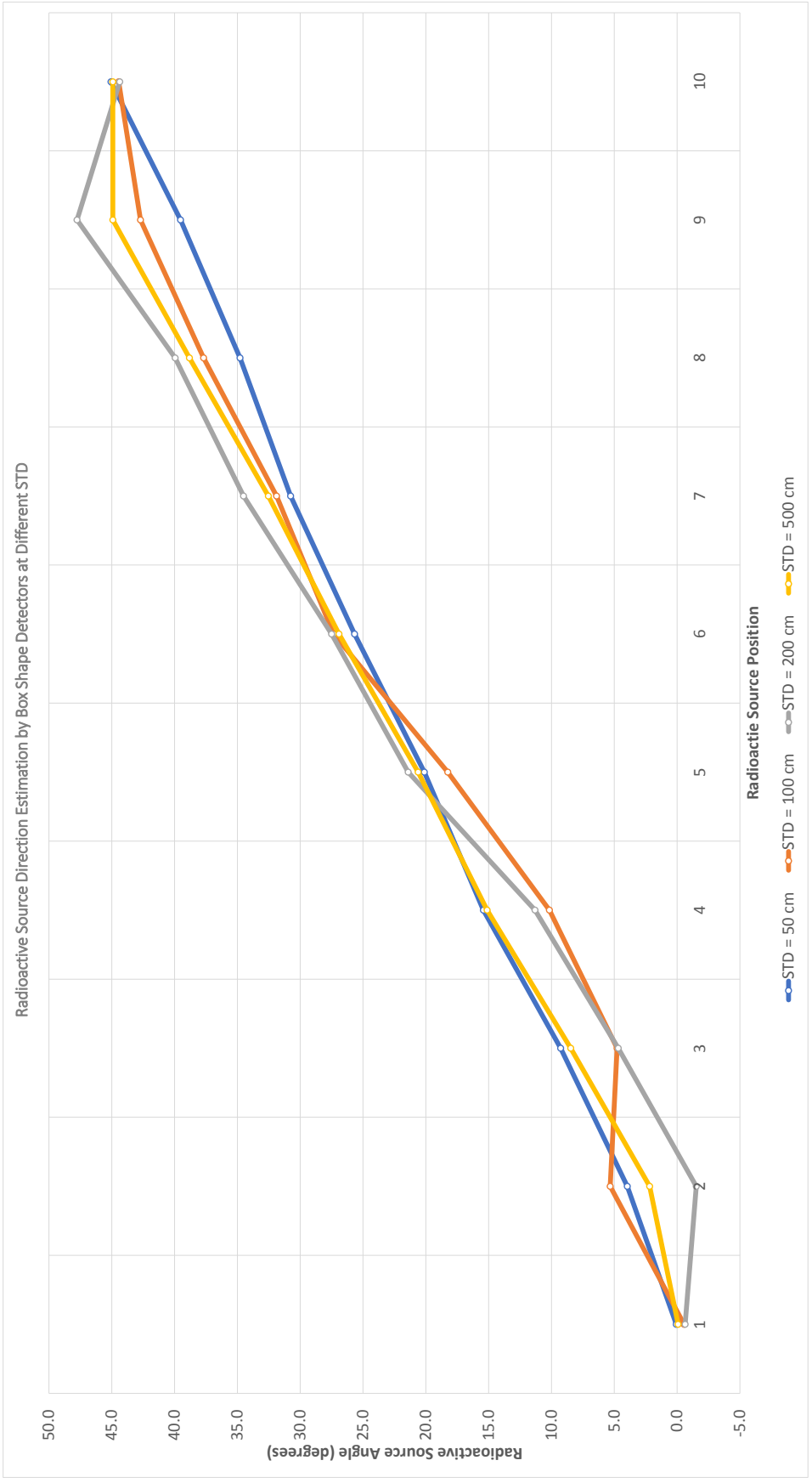


FIGURE 5.18: Radioactive source direction estimation by box shape detectors at different STD.

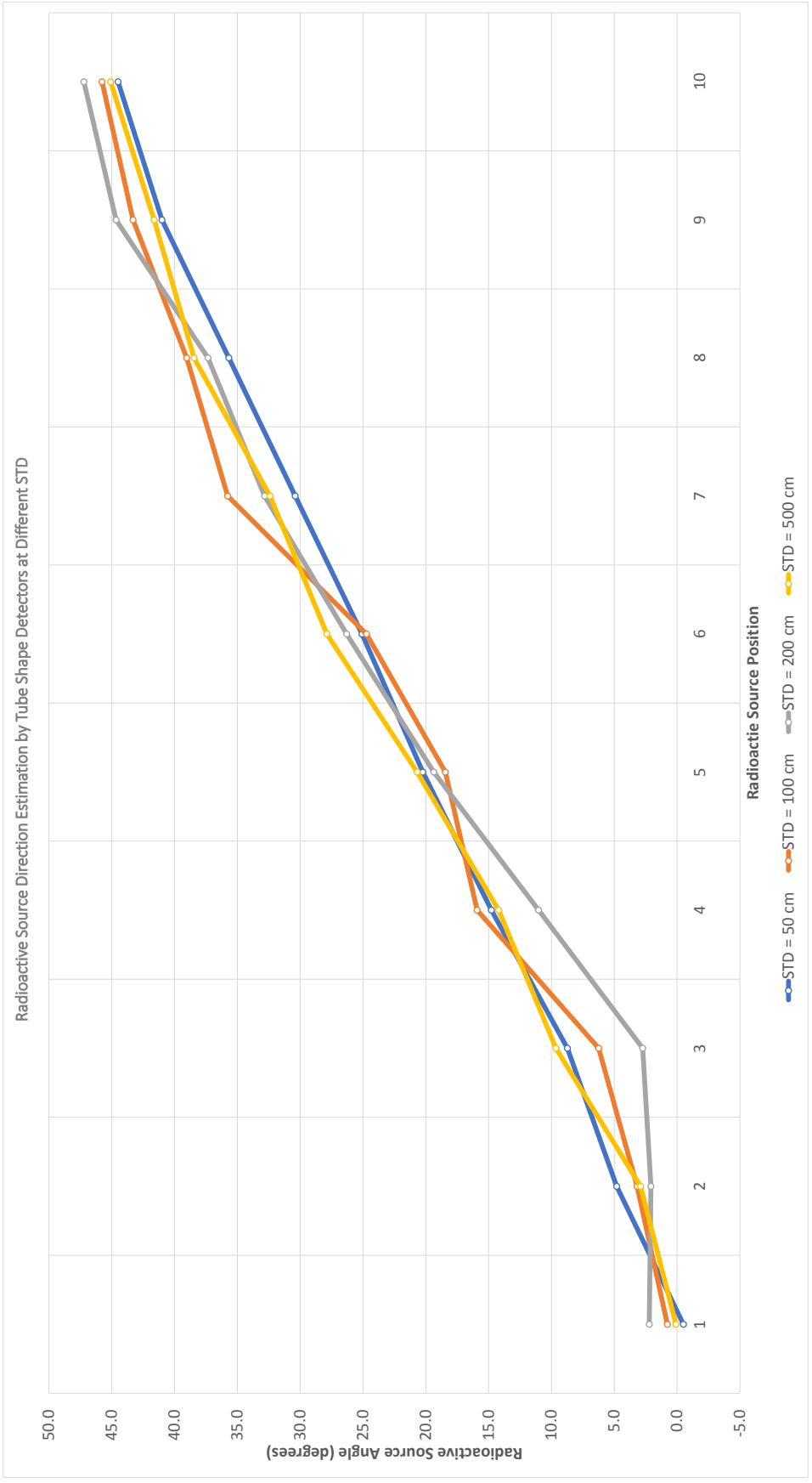


FIGURE 5.19: Radioactive source direction estimation by tube shape detectors at different STD.

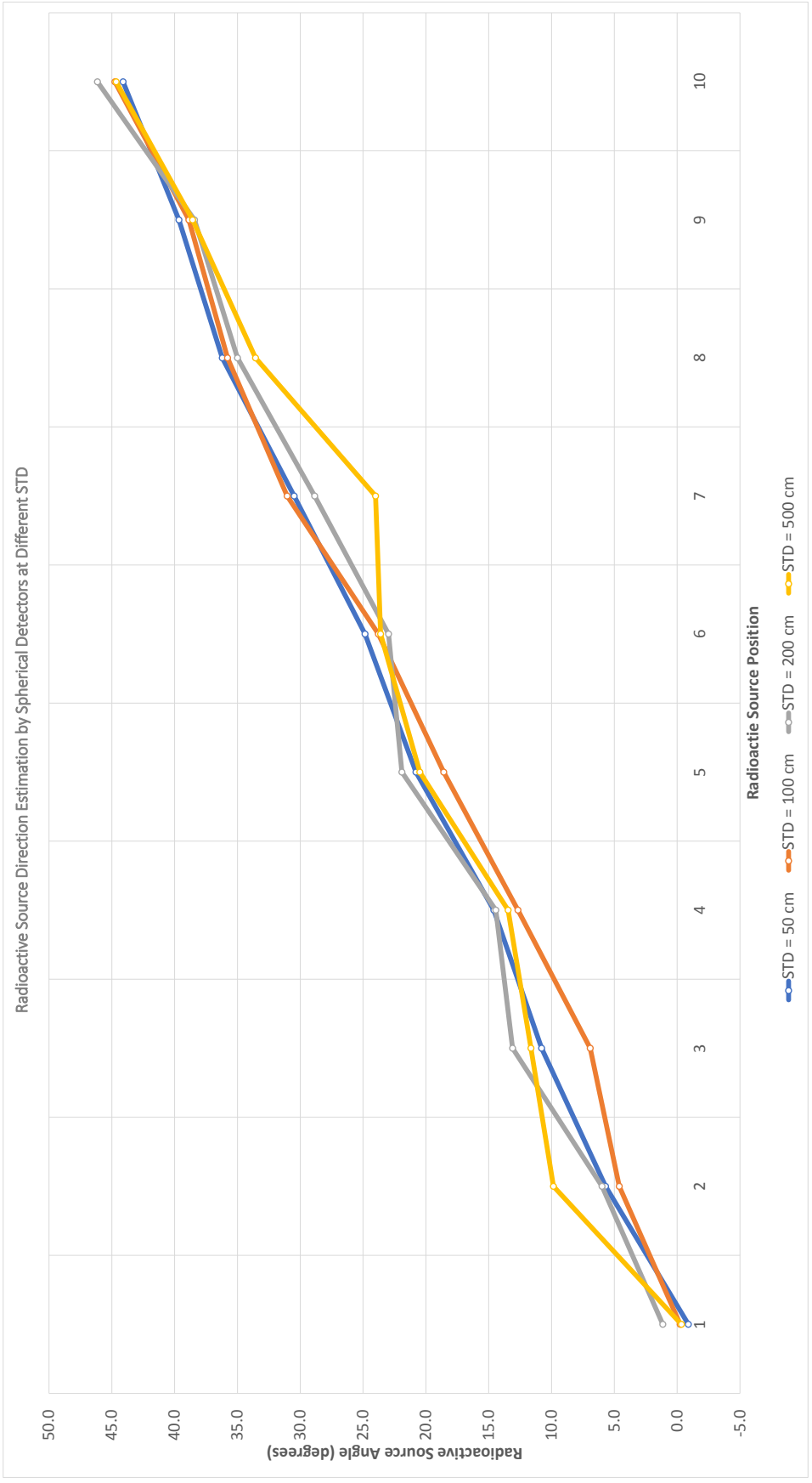


FIGURE 5.20: Radioactive source direction estimation by hemispherical shape detectors at different STD.

Simulation results have shown that the proposed dosimeter is able to better estimate the emission direction of a radioactive source in 3D when using 3D-structure detectors (hemispherical shape). It also suggests that the accuracy of an estimated direction at longer STD distances can be improved by increasing the physical dimensions of the detector. Consequently, in practice there is always a trade-off between accuracy, physical size, convenience of use and cost when designing a directionally-sensitive dosimeter: this can only be determined based on its particular application.

## 5.7 Summary

This chapter has presented detailed information regarding active wearable directionally-sensitive radiation dosimetry using multiple CdZnTe detectors, including detector geometry, materials, physical processes and simulation setup. In addition, an equation to estimate direction of the radioactive source has been proposed, based on the linear relationship between source direction and the number of interacted particles recorded by the four closest detectors. The chapter has also provided simulation results of estimated source direction at various STD distances, and the performance of the proposed dosimeter has been evaluated by comparison with the estimation equation. Simulation has also confirmed the ability of the proposed dosimeter to perform source emission direction estimation in a 3D environment using 3D shaped detectors. In general, the simulation results were consistent and promising, verifying the ability of the proposed dosimeter to estimate the direction of a radioactive source accurately.

# Chapter 6

# Critical Findings and Contributions

This chapter summarizes the critical findings and observations from the thesis.

So far, the thesis has presented the hardware structure together with an algorithm and techniques used to create a novel wearable directionally-sensitive radiation dosimeter system which has the capability to detect radioactive sources, measure the radiation intensity, and identify and estimate the emission direction.

In recent years, the threat posed to public safety and homeland security from a possible radiation attack by terrorists has increased dramatically. This has put a high pressure on authorities in charge of managing radioactive sources, not only to manage all existing sources strictly, but also to localize and identify any unknown sources quickly in the case of an emergency. Localizing radioactive sources is also a critical requirement in the nuclear power industry, including the decommissioning of nuclear power plants, and waste management to eliminate any loss or misuse of radioactive materials.

Despite the expenditure of considerable engineering effort, the ability of current commercially available radiation detectors to localize a radioactive source accurately is still limited. The main factors influencing this are: background noise, variation in source concentrations and compositions, as well as the limited performance of current commercially available radiation detectors.

The main aim of this thesis was to create a wearable radiation dosimeter to provide operators with a real-time radiation intensity measurement as well as an estimation of the emission direction of a radioactive source. The proposed dosimeter takes advantage of the shadow effect, which creates different measured intensity in each detector in an array of detectors, to establish the relationship between a radioactive source emission direction and radiation intensity measurement by each of the individual detectors in the array. Based on that theory, the system consists of three fundamental steps: determining the four closest detectors, establishing the linear relationship between source emission direction and the average number of interacting particles recorded by these detectors, and then estimating the emission direction of the radioactive source by linear interpolation.

Simulation using Geant4 package have proved the advantages of the proposed dosimeter in compare to other current maket available devices. The proposed dosimeter was able to provide faster, more accuracy and efficiency radioactive sources measurement and localization by taking the advantages of new radiation detector fabrication methods, incorporated with a proposed interpolation algorithm. Radioactive source emission direction estimated by the proposed dosimeter was achieved with better angular resolution as well as shorter measurement duration.

Within the thesis, simulations have been conducted using different detectors' physical shapes, which show that the accuracy of estimated emission direction of radioactive source is also affected by detectors' physical structure. In particular, by using a 3D structure detector (hemispherical shape) for an isotropic point source, the accuracy of direction estimation can be improved at long STD distances. Additionally, using directionally-sensitive detectors (of hemispherical shape) will boost the performance of the dosimeter in 3D, as it will require only one measurement instead of having to perform multiple measurements if using non-directional detectors.

## 6.1 Research Contribution

The main contributions and achievements of this research are summarized below:

- A literature review regarding commercially available radiation detectors in terms of type, material, physical dimensions, and cost as well as their characteristics and scope of application.

- The review of the current state of the art in radiation dosimeters (in particular, directionally-sensitive dosimeters), including their properties and physical structure, and a method for estimating source emission direction. The report has analyzed their advantages and pointed out their limitations, highlighting the need for further research and improvement.

- The proposal of a novel wearable directionally-sensitive radiation dosimeter that exploits the advantage of the shadow effect between individual detectors in a circular array to estimate the emission direction of a radioactive source accurately.

- Successful establishment of the linear relationship between emission direction of a radioactive source and the average number of interacting particles recorded by individual detectors in the array, using linear interpolation.

- Successful development of a simulation program using the Geant4 package to simulate the operation and evaluate the performance of the proposed wearable directionally-sensitive radiation dosimeter for measuring and estimating the emission direction of a radioactive source. With only minor modifications, the source code can be extended further to develop a platform for simulating the operation of other similar radiation dosimeters.

- Successfully simulating the operation, analyzing the efficiency and accuracy of the proposed dosimeter in estimating the emission direction of a radioactive source; evaluating the performance of the dosimeter in 3D using different directionally-sensitive detector shapes (semi-tube and hemispherical).

# Chapter 7

# Limitations, Future Work and Conclusion

This chapter shows the limitations of the study, indicates directions for future research and adds some conclusions.

## 7.1 Limitations

Within the thesis, evaluation has been limited to a study based solely on simulation to develop, validate and confirm the conceptual design. Anticipated forthcoming advancements in detector technology and fabrication to reduce the price of currently prohibitively-expensive detectors will be a major factor in the viability of experimental investigation for enabling a detailed assessment of the practical performance of the proposed dosimeter. It can be expected that further research may lead to the eventual development of a system with affordability suitable for commercialization.

## 7.2 Future Work

The overall performance of the dosimeter depends mostly on the properties of detectors. As a result, improvement in the fabrication process of detectors will be crucial in any effort to improve the estimation results of the proposed dosimeter. Improvement of the detector properties can be achieved by either developing a new fabrication method or

creating new material to achieve better detector sensitivity, energy and spatial resolution. Such improvements of detectors would enable an increase in accuracy as well as decreasing the time duration of the estimation process.

In addition, the speed and accuracy of the estimation process might also be improved by integrating an optical camera into the proposed system, to provide a visual aid which allows the operator to determine the source emission direction even faster and more easily. The directional estimation accuracy can be improved by displaying the source direction provided by the dosimeter, overlaid on a visual image of the detecting area created by such an optical camera.

Radioactive source identification capability can be included in the proposed dosimeter via a predefined library of the energy spectra of known radioactive sources. By comparing the energy spectrum of a suspect source with the spectrum library, source identification can be determined together with its emission direction estimation. The ability to identify specific radioactive sources would provide responders with detailed information about that particular type of radioactive source, enabling more suitable and efficient methods of evacuation, isolation, or other response.

## 7.3 Conclusion

This thesis proposes a novel wearable directionally-sensitive radiation dosimeter that can provide real-time radiation intensity measurement as well as estimation of the emission direction of radioactive sources. The simulation results indicate that the proposed dosimeter can accurately estimate the direction of emission of a radioactive source within a short time interval. The estimation algorithm is straightforward, based on a linear relationship between radioactive source emission direction and the radiation intensity measured by an array of detectors, which is optimal for the limited computational capability of a wearable device. By using direction-orientated detectors (hemispheric detectors), the proposed dosimeter is also able to estimate the emission direction of radioactive sources in 3D environments. Although the proposed dosimeter is intended for human use, with minor modifications, it can be adapted to use in other platforms (such as a robot) to meet the requirements of different situations.

# Appendix A

# Appendix A - Geant4 Simulation Program Source Code

This appendix provides source code of the Geant4 simulation program which has been used throughout this thesis.

## A.1 Main Function

The *"Main function"* is used to construct or derive all mandatory classes and define graphic user interface (GUI) session.

```
#ifdef   G4MULTITHREADED
#include "G4MTRunManager.hh"
#else
#include "G4RunManager.hh"
#endif
#include "G4UImanager.hh"
#include "Randomize.hh"
#include "TRDetectorConstruction.hh"
#include "TRPhysicsList.hh"
#include "TRActionInitialization.hh"
#include "G4Timer.hh"
#ifdef   G4VIS_USE
```

```
#include "G4VisExecutive.hh"
#endif
#ifdef   G4UI_USE
#include "G4UIExecutive.hh"
#endif
/*********************************************************/
int main(int argc, char** argv)
 {
 //Instantiate the G4Timer object, to monitor the CPU
 //time spent for the entire execution
 G4Timer* theTimer = new G4Timer();
 //Start the benchmark
 theTimer->Start();
 //Choose the Random engine
 G4Random::setTheEngine(new CLHEP::RanecuEngine);
 //Construct the default run manager. Pick the proper
 //run manager depending if the multi-threading option is
 //active or not.
 #ifdef G4MULTITHREADED
  G4MTRunManager* runManager = new G4MTRunManager;
 #else
  G4RunManager* runManager = new G4RunManager;
 #endif
 //Set mandatory initialization classes
 runManager->
        SetUserInitialization(new TRDetectorConstruction);
 runManager->SetUserInitialization(new TRPhysicsList);
 //Set user action initialization
 runManager->
        SetUserInitialization(new TRActionInitialization());
 // Initialize Geant4 kernel
 runManager->Initialize();
 #ifdef G4VIS_USE
```

```
// Initialize visualization
G4VisManager* visManager = new G4VisExecutive;
//G4VisExecutive can take a verbosity argument
//- see /vis/verbose guidance.
//G4VisManager* visManager = new G4VisExecutive("Quiet");
visManager->Initialize();
#endif
//Get the pointer to the User Interface manager
G4UImanager* UImanager = G4UImanager::GetUIpointer();
//if an argument is given after the name of the
//executable (i.e. argc > 1), then take the argument
//as a Geant4 macro and execute it
if (argc != 1)   // batch mode
    {
      G4String command = "/control/execute ";
      G4String fileName = argv[1];
      UImanager->ApplyCommand(command + fileName);
    }
//otherwise (only the executable is given), start a user
//interface session. An initialization macro is executed
//by default. The macro which is executed depends on the
//activation (or not) of the visualization
else
    {//interactive mode : define UI session
#ifdef G4UI_USE
 G4UIExecutive* ui = new G4UIExecutive(argc, argv);
#ifdef G4VIS_USE
 UImanager->ApplyCommand("/control/execute init_vis.mac");
#else
 UImanager->ApplyCommand("/control/execute init.mac");
#endif
//start the session here: make the Geant4 prompt Idle>
//available to the user
```

```
      ui->SessionStart();
      delete ui;
#endif
    }
  //Stop the benchmark here
  theTimer->Stop();
  G4cout << "The simulation took: " << theTimer->
  GetRealElapsed() << " s to run (real time)" << G4endl;
  //Job termination
  //Free the store: user actions, physics_list and detector
  //description are owned and deleted by the run manager,
  //so they should not be deleted in the main() program !
#ifdef G4VIS_USE
  delete visManager;
#endif
  delete runManager;
  return 0;
}
```

## A.2 Action Initialization

The *"Action Initialization"* routine will initialize all mandatory classes that will be used by the program.

```
#include "TRActionInitialization.hh"
#include "TRPrimaryGeneratorAction.hh"
#include "TRRunAction.hh"
#include "TRStackingAction.hh"
/*************************************************************/
TRActionInitialization::TRActionInitialization()
  : G4VUserActionInitialization()
 {}
/*************************************************************/
TRActionInitialization::~TRActionInitialization()
 {}
/*************************************************************/
void TRActionInitialization::BuildForMaster() const
 {
        SetUserAction(new TRRunAction);
 }
/*************************************************************/
void TRActionInitialization::Build() const
 {
        SetUserAction(new TRPrimaryGeneratorAction);
        SetUserAction(new TRRunAction);
        SetUserAction(new TRStackingAction);
 }
```

## A.3 Detector Construction

The *"Detector Constuction"* class will construct the geometry and materials of all detectors that are used in the program.

```
#include "TRDetectorConstruction.hh"
#include "G4NistManager.hh"
#include "G4Box.hh"
#include "G4Tubs.hh"
#include "G4Sphere.hh"
#include "G4LogicalVolume.hh"
#include "G4PVPlacement.hh"
#include "G4RotationMatrix.hh"
#include "G4Transform3D.hh"
#include "G4SDManager.hh"
#include "G4MultiFunctionalDetector.hh"
#include "G4VPrimitiveScorer.hh"
#include "G4PSEnergyDeposit.hh"
#include "G4VisAttributes.hh"
#include "G4PhysicalConstants.hh"
#include "G4SystemOfUnits.hh"
/*************************************************/
TRDetectorConstruction::TRDetectorConstruction()
 : G4VUserDetectorConstruction(),
   fCheckOverlaps(true)
 {
  //**Material definition**
  DefineMaterials();
 }
/*************************************************/
TRDetectorConstruction::~TRDetectorConstruction()
 { }
/*************************************************/
void TRDetectorConstruction::DefineMaterials()
```

```
 {
 G4NistManager* man = G4NistManager::Instance();
 G4bool isotopes = false;
 G4Element*  Cd = man->FindOrBuildElement("Cd", isotopes);
 G4Element* Zn = man->FindOrBuildElement("Zn", isotopes);
 G4Element* Te = man->FindOrBuildElement("Te", isotopes);
 G4Material* CdZnTe = new G4Material("CdZnTe",5.78*g/cm3,3);
 CdZnTe->AddElement(Cd, 0.9);
 CdZnTe->AddElement(Zn, 0.1);
 CdZnTe->AddElement(Te, 1);
 }
/*****************************************************/
G4VPhysicalVolume* TRDetectorConstruction::Construct()
 {
 G4NistManager* nist = G4NistManager::Instance();
 G4double density;
 G4int ncomponents;
 //**Retrieve Nist Materials**
 G4Material* default_mat = nist->FindOrBuildMaterial("G4_AIR");
 G4Material* body_mat = nist->FindOrBuildMaterial("G4_AIR");
 G4Material* cryst_mat = nist->FindOrBuildMaterial("CdZnTe");
 //***** World *****
 //Create the world volume as a box. This is big enough to
 //contain all the detector setup
 G4double world_sizeXY = 1500*cm;
 G4double world_sizeZ = 300*cm;
 G4Box* solidWorld = new G4Box("World",0.5*world_sizeXY,
    0.5*world_sizeXY,0.5*world_sizeZ);
 //World Logical Volume definition
 G4LogicalVolume* logicWorld =
        new G4LogicalVolume(solidWorld,    //its solid
                            default_mat,   //its material
                            "World");      //its name
```

```
 // World Physical Volume Placement at (0,0,0)
G4VPhysicalVolume* physWorld =
   new G4PVPlacement(0,              //no rotation
                     G4ThreeVector(),//at (0,0,0)
                     logicWorld,     //its logical volume
                     "World",        //its name
                     0,              //its mother  volume
                     false,          //no boolean operation
                     0,              //copy number
                     fCheckOverlaps);// checking overlaps
  // ***** Detectors crystal *****
  G4double inch = 2.54*cm;
  G4double innerRadius = 0.*cm;
  G4double outerRadius = 3*inch/2.;
  G4double height = 3.*inch;
  G4double cryst_dX = 20.3*cm, cryst_dY = 20.3*cm,
  cryst_dZ = 10*mm;
  G4int nb_cryst = 8;//No of detectors
  G4double dPhi = twopi / nb_cryst, half_dPhi = 0.5*dPhi;
  //G4double cosdPhi = std::cos(half_dPhi);
  G4double tandPhi = std::tan(half_dPhi);
  G4double phi0 = 0;//icrys: 0 to No of detectors nb_crys
  G4double ring_R1 = 0.5*cryst_dY / tandPhi;
  G4RotationMatrix rotm0 = G4RotationMatrix();
  rotm0.rotateY(90*deg);//90 box and spherical
  rotm0.rotateZ(phi0);//for boxs detector
  G4ThreeVector uz0 = G4ThreeVector(std::cos(phi0),
  std::sin(phi0), 0.);
  G4ThreeVector position0 = (ring_R1 + 0.5*cryst_dZ)*uz0;
  G4Transform3D transform0 = G4Transform3D(rotm0, position0);
  G4double gap = 15.3*cm;//a gap for wrapping
  G4double gapY = 10.3 cm;
  G4double dX = cryst_dX - gapY, dY = cryst_dY - gap;
```

```
//8 detectors for simulation 0 to 7
//***** Detector 0 *****
//G4Tubs* CdZnTeSolid = new G4Tubs("CdZnTeSolid", 25*cm,
//26*cm, 5*cm, 1.968173*pi, pi/15.71);
G4Box* CdZnTeSolid = new G4Box("CdZnTeSolid", dX/2, dY/2,
cryst_dZ/2);
//G4Sphere* CdZnTeSolid = new G4Sphere("CdZnTeSolid",
//3.306*cm, 0*degree, 360*degree, 0*degree, 90*degree);
//Logical Volume definition
G4LogicalVolume* CdZnTeLogical =
  new G4LogicalVolume(CdZnTeSolid,     //its solid
                      cryst_mat,    //its material
                      "CdZnTeLV");     //its name
//Physical Volume Placement at (0,0,0)
  new G4PVPlacement(transform0,     //spherical section
                    CdZnTeLogical,     //its logical volume
                    "CdZnTe",          //its name
                    logicWorld,     //its mother  volume
                    false,          //no boolean operation
                    0,              //copy number
                    fCheckOverlaps);// checking overlaps
//***** Detector 1 *****
G4double phi1 = dPhi;
G4RotationMatrix rotm1 = G4RotationMatrix();
rotm1.rotateY(90*deg);
rotm1.rotateZ(phi1);
G4ThreeVector uz1 = G4ThreeVector(std::cos(phi1),
std::sin(phi1), 0.);
G4ThreeVector position1 = (ring_R1 + 0.5*cryst_dZ)*uz1;
G4Transform3D transform1 = G4Transform3D(rotm1, position1);
//G4Tubs* CdZnTeSolid2 = new G4Tubs("CdZnTeSolid2", 25*cm,
//26*cm, 5*cm, 0.218173*pi, pi/15.71);
G4Box* CdZnTeSolid2 = new G4Box("CdZnTeSolid2", dX/2, dY/2,
```

```
cryst_dZ/2);
//G4Sphere* CdZnTeSolid2 = new G4Sphere("CdZnTeSolid2",
//3.306*cm, 0*degree, 360*degree, 0*degree, 90*degree);
//Logical Volume definition
G4LogicalVolume* CdZnTeLogical2 =
  new G4LogicalVolume(CdZnTeSolid2,   //its solid
                      cryst_mat,   //its material
                      "CdZnTeLV2");   //its name
//Physical Volume Placement at (0,0,0)
  new G4PVPlacement(transform1,    //spherical section
                    CdZnTeLogical2,   //its logical volume
                    "CdZnTe2",        //its name
                    logicWorld,    //its mother  volume
                    false,         //no boolean operation
                    0,             //copy number
                    fCheckOverlaps);// checking overlaps
//***** Detector 2 *****
G4double phi2 = 2*dPhi;
G4RotationMatrix rotm2 = G4RotationMatrix();
rotm2.rotateY(90*deg);
rotm2.rotateZ(phi2);
G4ThreeVector uz2 = G4ThreeVector(std::cos(phi2),
std::sin(phi2), 0.);
G4ThreeVector position2 = (ring_R1 + 0.5*cryst_dZ)*uz2;
G4Transform3D transform2 = G4Transform3D(rotm2, position2);
//G4Tubs* CdZnTeSolid3 = new G4Tubs("CdZnTeSolid3", 25*cm,
//26*cm, 5*cm, 0.218173*pi, pi/15.71);
G4Box* CdZnTeSolid3 = new G4Box("CdZnTeSolid3", dX/2, dY/2,
cryst_dZ/2);
//G4Sphere* CdZnTeSolid3 = new G4Sphere("CdZnTeSolid3",
//3.306*cm, 0*degree, 360*degree, 0*degree, 90*degree);
//Logical Volume definition
G4LogicalVolume* CdZnTeLogical3 =
```

```
    new G4LogicalVolume(CdZnTeSolid3,    //its solid
                        cryst_mat,    //its material
                        "CdZnTeLV3");    //its name
  //Physical Volume Placement at (0,0,0)
    new G4PVPlacement(transform2,    //spherical section
                      CdZnTeLogical3,    //its logical volume
                      "CdZnTe3",         //its name
                      logicWorld,    //its mother  volume
                      false,          //no boolean operation
                      0,              //copy number
                      fCheckOverlaps);// checking overlaps
  //***** Detector 3 *****
  G4double phi3 = 3*dPhi;
  G4RotationMatrix rotm3 = G4RotationMatrix();
  rotm3.rotateY(90*deg);
  rotm3.rotateZ(phi3);
  G4ThreeVector uz3 = G4ThreeVector(std::cos(phi3),
  std::sin(phi3), 0.);
  G4ThreeVector position3 = (ring_R1 + 0.5*cryst_dZ)*uz3;
  G4Transform3D transform3 = G4Transform3D(rotm3, position3);
  //G4Tubs* CdZnTeSolid4 = new G4Tubs("CdZnTeSolid4", 25*cm,
  //26*cm, 5*cm, 0.218173*pi, pi/15.71);
  G4Box* CdZnTeSolid4 = new G4Box("CdZnTeSolid4", dX/2, dY/2,
  cryst_dZ/2);
  //G4Sphere* CdZnTeSolid4 = new G4Sphere("CdZnTeSolid4",
  //3.306*cm, 0*degree, 360*degree, 0*degree, 90*degree);
  //Logical Volume definition
  G4LogicalVolume* CdZnTeLogical4 =
    new G4LogicalVolume(CdZnTeSolid4,    //its solid
                        cryst_mat,    //its material
                        "CdZnTeLV4");    //its name
  //Physical Volume Placement at (0,0,0)
    new G4PVPlacement(transform3,    //spherical section
```

```
                    CdZnTeLogical4,   //its logical volume
                    "CdZnTe4",        //its name
                    logicWorld,    //its mother  volume
                    false,         //no boolean operation
                    0,             //copy number
                    fCheckOverlaps);// checking overlaps
//***** Detector 4 *****
G4double phi4 = 4*dPhi;
G4RotationMatrix rotm4 = G4RotationMatrix();
rotm4.rotateY(90*deg);
rotm4.rotateZ(phi4);
G4ThreeVector uz4 = G4ThreeVector(std::cos(phi4),
std::sin(phi4), 0.);
G4ThreeVector position4 = (ring_R1 + 0.5*cryst_dZ)*uz4;
G4Transform3D transform4 = G4Transform3D(rotm4, position4);
//G4Tubs* CdZnTeSolid5 = new G4Tubs("CdZnTeSolid5", 25*cm,
//26*cm, 5*cm, 0.218173*pi, pi/15.71);
G4Box* CdZnTeSolid5 = new G4Box("CdZnTeSolid5", dX/2, dY/2,
cryst_dZ/2);
//G4Sphere* CdZnTeSolid5 = new G4Sphere("CdZnTeSolid5",
//3.306*cm, 0*degree, 360*degree, 0*degree, 90*degree);
//Logical Volume definition
G4LogicalVolume* CdZnTeLogical5 =
  new G4LogicalVolume(CdZnTeSolid5,   //its solid
                      cryst_mat,   //its material
                      "CdZnTeLV5");   //its name
//Physical Volume Placement at (0,0,0)
  new G4PVPlacement(transform4,    //spherical section
                    CdZnTeLogical5,   //its logical volume
                    "CdZnTe5",        //its name
                    logicWorld,    //its mother  volume
                    false,         //no boolean operation
                    0,             //copy number
```

```
                    fCheckOverlaps);// checking overlaps
//***** Detector 5 *****
G4double phi5 = 5*dPhi;
G4RotationMatrix rotm5 = G4RotationMatrix();
rotm5.rotateY(90*deg);
rotm5.rotateZ(phi5);
G4ThreeVector uz5 = G4ThreeVector(std::cos(phi5),
std::sin(phi5), 0.);
G4ThreeVector position5 = (ring_R1 + 0.5*cryst_dZ)*uz5;
G4Transform3D transform5 = G4Transform3D(rotm5, position5);
//G4Tubs* CdZnTeSolid6 = new G4Tubs("CdZnTeSolid6", 25*cm,
//26*cm, 5*cm, 0.218173*pi, pi/15.71);
G4Box* CdZnTeSolid6 = new G4Box("CdZnTeSolid6", dX/2, dY/2,
cryst_dZ/2);
//G4Sphere* CdZnTeSolid6 = new G4Sphere("CdZnTeSolid6",
//3.306*cm, 0*degree, 360*degree, 0*degree, 90*degree);
//Logical Volume definition
G4LogicalVolume* CdZnTeLogical6 =
  new G4LogicalVolume(CdZnTeSolid6,   //its solid
                      cryst_mat,   //its material
                      "CdZnTeLV6");   //its name
//Physical Volume Placement at (0,0,0)
  new G4PVPlacement(transform5,    //spherical section
                    CdZnTeLogical6,   //its logical volume
                    "CdZnTe6",        //its name
                    logicWorld,    //its mother  volume
                    false,         //no boolean operation
                    0,             //copy number
                    fCheckOverlaps);// checking overlaps
//***** Detector 6 *****
G4double phi6 = 6*dPhi;
G4RotationMatrix rotm6 = G4RotationMatrix();
rotm6.rotateY(90*deg);
```

```
rotm6.rotateZ(phi6);
G4ThreeVector uz6 = G4ThreeVector(std::cos(phi6),
std::sin(phi6), 0.);
G4ThreeVector position6 = (ring_R1 + 0.5*cryst_dZ)*uz6;
G4Transform3D transform6 = G4Transform3D(rotm6, position6);
//G4Tubs* CdZnTeSolid7 = new G4Tubs("CdZnTeSolid7", 25*cm,
//26*cm, 5*cm, 0.218173*pi, pi/15.71);
G4Box* CdZnTeSolid7 = new G4Box("CdZnTeSolid7", dX/2, dY/2,
cryst_dZ/2);
//G4Sphere* CdZnTeSolid7 = new G4Sphere("CdZnTeSolid7",
//3.306*cm, 0*degree, 360*degree, 0*degree, 90*degree);
//Logical Volume definition
G4LogicalVolume* CdZnTeLogical7 =
  new G4LogicalVolume(CdZnTeSolid7,   //its solid
                      cryst_mat,   //its material
                      "CdZnTeLV7");   //its name
//Physical Volume Placement at (0,0,0)
  new G4PVPlacement(transform6,    //spherical section
                    CdZnTeLogical7,   //its logical volume
                    "CdZnTe7",        //its name
                    logicWorld,    //its mother  volume
                    false,         //no boolean operation
                    0,             //copy number
                    fCheckOverlaps);// checking overlaps
//***** Detector 7 *****
G4double phi8 = 8*dPhi;
G4RotationMatrix rotm8 = G4RotationMatrix();
rotm8.rotateY(90*deg);
rotm8.rotateZ(phi8);
G4ThreeVector uz8 = G4ThreeVector(std::cos(phi8),
std::sin(phi8), 0.);
G4ThreeVector position8 = (ring_R1 + 0.5*cryst_dZ)*uz8;
G4Transform3D transform8 = G4Transform3D(rotm8, position8);
```

```
//G4Tubs* CdZnTeSolid8 = new G4Tubs("CdZnTeSolid8", 25*cm,
//26*cm, 5*cm, 0.218173*pi, pi/15.71);
G4Box* CdZnTeSolid8 = new G4Box("CdZnTeSolid8", dX/2, dY/2,
cryst_dZ/2);
//G4Sphere* CdZnTeSolid8 = new G4Sphere("CdZnTeSolid8",
//3.306*cm, 0*degree, 360*degree, 0*degree, 90*degree);
//Logical Volume definition
G4LogicalVolume* CdZnTeLogical8 =
  new G4LogicalVolume(CdZnTeSolid8,   //its solid
                      cryst_mat,   //its material
                      "CdZnTeLV8");   //its name
//Physical Volume Placement at (0,0,0)
  new G4PVPlacement(transform7,    //spherical section
                    CdZnTeLogical8,   //its logical volume
                    "CdZnTe8",        //its name
                    logicWorld,    //its mother  volume
                    false,         //no boolean operation
                    0,             //copy number
                    fCheckOverlaps);// checking overlaps
G4VisAttributes* boxVisAtt =
 new G4VisAttributes(G4Colour(1.0, 0.0, 0.0));
G4VisAttributes* chamberVisAtt =
 new G4VisAttributes(G4Colour(1.0, 1.0, 0.0));
G4VisAttributes* boxVisAtt1 =
 new G4VisAttributes(G4Colour(0.0, 1.0,1.0));
G4VisAttributes* chamberVisAtt1 =
 new G4VisAttributes(G4Colour(0.0, 1.0, 0.0));
CdZnTeLogical->SetVisAttributes(boxVisAtt1);
CdZnTeLogical2->SetVisAttributes(boxVisAtt);
CdZnTeLogical3->SetVisAttributes(boxVisAtt);
CdZnTeLogical4->SetVisAttributes(boxVisAtt);
CdZnTeLogical5->SetVisAttributes(boxVisAtt);
CdZnTeLogical6->SetVisAttributes(boxVisAtt);
```

```
CdZnTeLogical7->SetVisAttributes(boxVisAtt);
CdZnTeLogical8->SetVisAttributes(boxVisAtt);
//Print materials
G4cout << *(G4Material::GetMaterialTable()) << G4endl;
//return the physical World
return physWorld;
```

## A.4 Physics List

The *"Physic List"* class will define all necessary particles, assign physic process to proper particles and cut-off ranges of all particles.

```
#include "TRPhysicsList.hh"
#include "G4DecayPhysics.hh"
#include "G4RadioactiveDecayPhysics.hh"
#include "G4EmStandardPhysics.hh"
#include "G4EmStandardPhysics_option3.hh"
#include "G4Scintillation.hh"
#include "G4ProcessManager.hh"
#include "G4EmLivermorePhysics.hh"
#include "G4ParticleDefinition.hh"
#include "G4ParticleTypes.hh"
#include "G4ParticleTable.hh"
#include "G4LossTableManager.hh"
#include "G4EmSaturation.hh"
#include "G4RadioactiveDecay.hh"
#include "G4UAtomicDeexcitation.hh"
#include "G4PhysicsListHelper.hh"
/*****************************************************/
TRPhysicsList::TRPhysicsList()
 : G4VModularPhysicsList()
 {
  // Create a modular physics list and register only a
  // few modules for it: EM interactions, decay of
  // particles and radioactive decay.
  SetVerboseLevel(1);
  //Default Decay Physics
  RegisterPhysics(new G4DecayPhysics());
  //Default Radioactive Decay Physics
  RegisterPhysics(new G4RadioactiveDecayPhysics());
  //Standard EM Physics
```

```
  RegisterPhysics(new G4EmStandardPhysics());
 }
/*****************************************************/
TRPhysicsList::~TRPhysicsList()
 { }
/*****************************************************/
void TRPhysicsList::SetCuts()
 {
  //The method SetCuts() is mandatory in the interface.
  //Here, one just use the default SetCuts() provided
  //by the base class.
  G4VUserPhysicsList::SetCuts();
  //In addition, dump the full list of cuts for the
  //materials used in the setup.
  DumpCutValuesTable();
 }
```

## A.5 Primary Generator Action

The *"Primary Generator Action"* class is used to generate the primary particles source in the program.

```
#include "TRPrimaryGeneratorAction.hh"
#include "G4RunManager.hh"
#include "G4Event.hh"
#include "G4ParticleGun.hh"
#include "G4ParticleTable.hh"
#include "G4IonTable.hh"
#include "G4ParticleDefinition.hh"
#include "G4ChargedGeantino.hh"
#include "G4SystemOfUnits.hh"
#include "Randomize.hh"
#include "G4GeneralParticleSource.hh"
/*************************************************/
TRPrimaryGeneratorAction::TRPrimaryGeneratorAction()
 : G4VUserPrimaryGeneratorAction(),
    fParticleGun(0)
 {
  G4int n_particle = 1;
  fParticleGun = new G4ParticleGun(n_particle);
  // default particle kinematic
  G4ParticleTable* particleTable =
   G4ParticleTable::GetParticleTable();
  G4ParticleDefinition* particle =
   particleTable->FindParticle("chargedgeantino");
  fParticleGun->SetParticleDefinition(particle);
  fParticleGun->SetParticleEnergy(1.*eV);
 }
/*************************************************/
TRPrimaryGeneratorAction::~TRPrimaryGeneratorAction()
 {
```

```
  delete fParticleGun;
 }
/**************************************************/
void TRPrimaryGeneratorAction
 ::GeneratePrimaries(G4Event* anEvent)
 {
  G4ParticleDefinition* particle =
   fParticleGun->GetParticleDefinition();
  if (particle == G4ChargedGeantino::ChargedGeantino())
 {
  //Cs-137
  G4int Z = 55, A = 137; //Z = 55, A = 137;
  G4double ionCharge = 0.*eplus;
  G4double excitEnergy = 0.*keV;
  G4ParticleDefinition* ion
  = G4IonTable::GetIonTable()->GetIon(Z, A, excitEnergy);
  fParticleGun->SetParticleDefinition(ion);
  fParticleGun->SetParticleEnergy(0.*eV); //at rest
  fParticleGun->SetParticleCharge(ionCharge);
 }
  //isotropic source: flat in cosTheta and phi
  //Randomize it
  G4double cosTheta = G4UniformRand();
  //cosTheta in [0,1] --> theta in [0,pi/2]
  G4double phi = G4UniformRand()*360*deg;//flat in[0,2pi]
  G4double sinTheta = std::sqrt(1. - cosTheta*cosTheta);
  G4ThreeVector dir(sinTheta*std::cos(phi),
  sinTheta*std::sin(phi), cosTheta);
  fParticleGun->SetParticleMomentumDirection(dir);
  //create vertex
  fParticleGun->GeneratePrimaryVertex(anEvent);
 }
```

## A.6 Run

The *"Run"* class will detect and record interaction in the sensitive volume of detectors.

```
#include "TRRun.hh"
#include "G4RunManager.hh"
#include "G4Event.hh"
#include "G4SDManager.hh"
#include "G4HCofThisEvent.hh"
#include "G4THitsMap.hh"
#include "G4SystemOfUnits.hh"
#include "TRAnalysis.hh"
/*************************************************************/
TRRun::TRRun()
 : G4Run(),
   fCollID_cryst(-1),
   fCollID_cryst2(-1),
   fCollID_cryst3(-1),
   fCollID_cryst4(-1),
   fCollID_cryst5(-1),
   fCollID_cryst6(-1),
   fCollID_cryst7(-1),
   fCollID_cryst8(-1),
   fPrintModulo(10000000),
   fGoodEvents(0),
   fGoodEvents2(0),
   fGoodEvents3(0),
   fGoodEvents4(0),
   fGoodEvents5(0),
   fGoodEvents6(0),
   fGoodEvents7(0),
   fGoodEvents8(0)
 { }
/*************************************************************/
```

```
/clearpage
TRRun::~TRRun()
 { }
/**************************************************/
/// Called at the end of each event
void TRRun::RecordEvent(const G4Event* event)
 {
  //Retrieve the collectionID corresponding to hits in
  //the crystal.
  if (fCollID_cryst < 0) { fCollID_cryst = G4SDManager
   ::GetSDMpointer()->GetCollectionID("crystal/edep");}
  if (fCollID_cryst2 < 0) {fCollID_cryst2 = G4SDManager
   ::GetSDMpointer()->GetCollectionID("crystal2/edep2");}
  if (fCollID_cryst3 < 0) { fCollID_cryst3 = G4SDManager
   ::GetSDMpointer()->GetCollectionID("crystal3/edep3");}
  if (fCollID_cryst4 < 0) { fCollID_cryst4 = G4SDManager
   ::GetSDMpointer()->GetCollectionID("crystal4/edep4");}
  if (fCollID_cryst5 < 0) { fCollID_cryst5 = G4SDManager
   ::GetSDMpointer()->GetCollectionID("crystal5/edep5");}
  if (fCollID_cryst6 < 0) { fCollID_cryst6 = G4SDManager
   ::GetSDMpointer()->GetCollectionID("crystal6/edep6");}
  if (fCollID_cryst7 < 0) { fCollID_cryst7 = G4SDManager
   ::GetSDMpointer()->GetCollectionID("crystal7/edep7");}
  if (fCollID_cryst8 < 0) { fCollID_cryst8 = G4SDManager
   ::GetSDMpointer()->GetCollectionID("crystal8/edep8");}
  G4int evtNb = event->GetEventID();
   if (evtNb%fPrintModulo == 0)
   {G4cout << "\n---> end of event: " << evtNb << G4endl;}
  //Hits (interactions) collections
  //Get all hits-collections available for this events.
  G4HCofThisEvent* HCE = event->GetHCofThisEvent();
  if (!HCE) return;
  //Energy in crystal : identify 'good events'
```

```
//retrieve the hits-collection in the crystals.
//This comes from a Geant4 multiscorer of type
//"G4PSEnergyDeposit", which scores energy deposit.
G4THitsMap<G4double>* evtMap = static_cast<G4THitsMap
 <G4double>*>(HCE->GetHC(fCollID_cryst));
std::map<G4int, G4double*>::iterator itr;
G4double totEdep = 0.;
for (itr = evtMap->GetMap()->begin(); itr !=
 evtMap->GetMap()->end(); itr++)
{
 G4double edep = *(itr->second);
 totEdep += edep;
}
//Retrieve the HC
G4THitsMap<G4double>* evtMap2 = static_cast<G4THitsMap
 <G4double>*>(HCE->GetHC(fCollID_cryst2));
std::map<G4int, G4double*>::iterator itr2;
G4double totEcrystal2 = 0.;
//Loop over all entries
for (itr2 = evtMap2->GetMap()->begin(); itr2 !=
 evtMap2->GetMap()->end(); itr2++)
{
G4double edep2 = *(itr2->second);
totEcrystal2 += edep2;
}
G4THitsMap<G4double>* evtMap3 = static_cast<G4THitsMap
 <G4double>*>(HCE->GetHC(fCollID_cryst3));
std::map<G4int, G4double*>::iterator itr3;
G4double totEcrystal3 = 0.;
//Loop over all entries
for (itr3 = evtMap3->GetMap()->begin(); itr3 !=
 evtMap3->GetMap()->end(); itr3++)
{ G4double edep3 = *(itr3->second);
```

```
  totEcrystal3 += edep3; }
G4THitsMap<G4double>* evtMap4 = static_cast<G4THitsMap
 <G4double>*>(HCE->GetHC(fCollID_cryst4));
std::map<G4int, G4double*>::iterator itr4;
G4double totEcrystal4 = 0.;
//Loop over all entries
for (itr4 = evtMap4->GetMap()->begin(); itr4 != evtMap4->
 GetMap()->end(); itr4++)
{ G4double edep4 = *(itr4->second);
      totEcrystal4 += edep4; }
G4THitsMap<G4double>* evtMap5 = static_cast<G4THitsMap
 <G4double>*>(HCE->GetHC(fCollID_cryst5));
std::map<G4int, G4double*>::iterator itr5;
G4double totEcrystal5 = 0.;
//Loop over all entries
for (itr5 = evtMap5->GetMap()->begin(); itr5 != evtMap5->
 GetMap()->end(); itr5++)
{ G4double edep5 = *(itr5->second);
      totEcrystal5 += edep5; }
G4THitsMap<G4double>* evtMap6 = static_cast<G4THitsMap
 <G4double>*>(HCE->GetHC(fCollID_cryst6));
std::map<G4int, G4double*>::iterator itr6;
G4double totEcrystal6 = 0.;
//Loop over all entries
for (itr6 = evtMap6->GetMap()->begin(); itr6 != evtMap6->
 GetMap()->end(); itr6++)
{ G4double edep6 = *(itr6->second);
      totEcrystal6 += edep6; }
G4THitsMap<G4double>* evtMap7 = static_cast<G4THitsMap
 <G4double>*>(HCE->GetHC(fCollID_cryst7));
std::map<G4int, G4double*>::iterator itr7;
G4double totEcrystal7 = 0.;
//Loop over all entries
```

```
for (itr7 = evtMap7->GetMap()->begin(); itr7 != evtMap7->
 GetMap()->end(); itr7++)
{ G4double edep7 = *(itr7->second);
      totEcrystal7 += edep7; }
G4THitsMap<G4double>* evtMap8 = static_cast<G4THitsMap
 <G4double>*>(HCE->GetHC(fCollID_cryst8));
std::map<G4int, G4double*>::iterator itr8;
G4double totEcrystal8 = 0.;
//Loop over all entries
for (itr8 = evtMap8->GetMap()->begin(); itr8 != evtMap8->
 GetMap()->end(); itr8++)
{ G4double edep8 = *(itr8->second);
      totEcrystal8 += edep8; }
```

## A.7 RunAction

The *"RunAction"* class is used to manage the collected data.

```
#include "TRRunAction.hh"
#include "TRPrimaryGeneratorAction.hh"
#include "TRRun.hh"
#include "G4Run.hh"
#include "G4RunManager.hh"
#include "G4UnitsTable.hh"
#include "G4SystemOfUnits.hh"
#include "TRAnalysis.hh"
/*************************************************************/
TRRunAction::TRRunAction()
 : G4UserRunAction()
 {;}
/*************************************************************/
TRRunAction::~TRRunAction()
 {
  delete G4AnalysisManager::Instance();
 }
/*************************************************************/
G4Run* TRRunAction::GenerateRun()
 { return new TRRun; }
/*************************************************************/
void TRRunAction::BeginOfRunAction(const G4Run* run)
 {
  G4cout << "### Run "
   << run->GetRunID() << " start." << G4endl;
  //Create analysis manager
  //Notice: it must be done the same way
  //in master and workers
  G4AnalysisManager* analysisManager =
   G4AnalysisManager::Instance();
```

```
  analysisManager->SetVerboseLevel(1);
  const G4int kMaxHisto = 8;
  const G4String id[] = { "0", "1", "2", "3", "4",
   "5", "6", "7"};
  const G4String title[] =
  {"Detector 0",
   "Detector 1",
   "Detector 2",
   "Detector 3",
   "Detector 4",
   "Detector 5",
   "Detector 6",
   "Detector 7"
  };
  //Default values (to be reset via /analysis/h1/set command)
  G4int nbins = 150.;
  G4double vmin = 0.;
  G4double vmax = 1500.;
  //Create all histograms as inactivated
  //as we have not yet set nbins, vmin, vmax
  for (G4int k = 0; k<kMaxHisto; k++)
   { G4int ih = analysisManager->CreateH1(id[k], title[k],
    nbins, vmin, vmax); }
  analysisManager->OpenFile("TR");
  //inform the runManager to save random number seed
  G4RunManager::GetRunManager()->SetRandomNumberStore(false);
        }
/**************************************************/
void TRRunAction::EndOfRunAction(const G4Run* run)
 {
  //retrieve the number of events produced in the run
  G4int nofEvents = run->GetNumberOfEvent();
  //do nothing, if no events were processed
```

```
if (nofEvents == 0) return;
const TRPrimaryGeneratorAction* generatorAction =
 static_cast<const TRPrimaryGeneratorAction*>(
G4RunManager::GetRunManager()
 ->GetUserPrimaryGeneratorAction());
G4String partName;
if (generatorAction)
 {
  G4ParticleDefinition* particle =
   generatorAction->GetParticleGun()
    ->GetParticleDefinition();
  partName = particle->GetParticleName();
 }
//results
const TRRun* theRun = static_cast<const TRRun*>(run);
G4int nbGoodEvents = theRun->GetNGoodEvents();
G4int nbGoodEvents2 = theRun->GetNGoodEvents2();
G4int nbGoodEvents3 = theRun->GetNGoodEvents3();
G4int nbGoodEvents4 = theRun->GetNGoodEvents4();
G4int nbGoodEvents5 = theRun->GetNGoodEvents5();
G4int nbGoodEvents6 = theRun->GetNGoodEvents6();
G4int nbGoodEvents7 = theRun->GetNGoodEvents7();
G4int nbGoodEvents8 = theRun->GetNGoodEvents8();
//print out to the screen
if (IsMaster())
{
 G4cout
<< "\n----------------End of Global Run-----------------"
<< " \n The run was " << nofEvents << " events ";
}
else
{
 G4cout
```

```
  << "\n----------------End of Local Run--------------------"
  << " \n The run was " << nofEvents << " " << partName;
  }
  G4cout
  << "\n Nb of events with energy deposit in detector 0: "
   << nbGoodEvents
  << "\n-------------------------------------------------\n"
  << " Nb of events with energy deposit in detector 7: "
   << nbGoodEvents8
  << "\n -------------------------------------------------\n"
  << " Nb of events with energy deposit in detector 1: "
   << nbGoodEvents2
  << "\n-------------------------------------------------\n"
  << " Nb of events with energy deposit in detector 2: "
   << nbGoodEvents3
  << "\n-------------------------------------------------\n"
  << G4endl;
  //save histograms
  G4AnalysisManager* man = G4AnalysisManager::Instance();
  man->Write();
  man->CloseFile();
 }
```

## A.8 StackingAction

The *"StackingAction"* class prepare and classify the tracking priority control of new events as well as managing the stack.

```
#include "TRStackingAction.hh"
#include "G4Track.hh"
#include "G4NeutrinoE.hh"
/*************************************************************/
TRStackingAction::TRStackingAction()
 { }
/*************************************************************/
TRStackingAction::~TRStackingAction()
 { }
/*************************************************************/
G4ClassificationOfNewTrack
 TRStackingAction::ClassifyNewTrack(const G4Track* track)
 {
  //kill secondary neutrino
  if (track->GetDefinition() == G4NeutrinoE::NeutrinoE() &&
  track->GetParentID()>0)
  return fKill;
  //otherwise, return what Geant4 would have returned
  //by itself
  else
  return G4UserStackingAction::ClassifyNewTrack(track);
 }
```

# References


[1] World Health Organization. Health risk assessment from the nuclear accident after the 2011 Great East Japan earthquake and tsunami, based on a preliminary dose estimation. pages 1–172, 2013.

[2] TIME (World). Inside the uranium underworld: Dark secrets, dirty bombs. [Online]. Available: `http://time.com/4728293/uranium-underworld-dark-secrets-dirty-bombs/`.

[3] International Atomic Energy Agency (IAEA). Inadequate control of world's radioactive sources. [Online]. Available: `https://www.iaea.org/newscenter/pressreleases/inadequate-control-worlds-radioactive-sources`.

[4] G. Thoreson, E. Schneider, H. Armstrong, and C. Hoeven. The application of neutron transport green's functions to threat scenario simulation. *IEEE Transactions On Nuclear Science*, 62(1):236–249, 2015.

[5] The White House Office of the Press Secretary (2009 April 05). Remarks by President Barack Obama in Prague as delivered. [Online]. Available: `https://obamawhitehouse.archives.gov/the-press-office/remarks-president-barack-obama-prague-delivered`.

[6] A.C. Madden, P.F. Bloser, J.S. Legere, M.L. McConnell, and J.M. Ryan. Enhanced data analysis for an imaging neutron/gamma-ray spectrometer. *Nuclear Science Symposium and Medical Imaging Conference (NSS/MIC)*, pages 1–6, 2014.

[7] Atomic Archive - Enhanced Edition (atomicarchive.com). Radiation effects on humans. [Online]. Available: `http://www.atomicarchive.com/Effects/effects15.shtml`.

[8] R. Warry-BBC News (Health). Health effects of radiation exposure. [Online]. Available: `http://www.bbc.com/news/health-12722435`.

[9] World Health Organization-Media centre (Fact sheet). Ionizing radiation, health effects and protective measures. [Online]. Available: `http://www.who.int/mediacentre/factsheets/fs371/en/`.

[10] G.F. Knoll. *Radiation Detection and Measurement*. John Wiley & Sons, Inc., United States of America, 2000.

[11] F.H. Attix. *Introduction to Radiological Physics and Radiation Dosimetry*. John Wiley & Sons, Inc., United States of America, 1986.

[12] HyperPhysics (C.R.Nave). Compton scattering equation. [Online]. Available: `http://hyperphysics.phy-astr.gsu.edu/hbase/quantum/compeq.html`.

[13] S.Jr. Hastings and L.C. Marcia. *Passive Nondestructive Assay of Nuclear Materials*, chapter 3. Los Alamos National Laboratory, United States of America, 1991.

[14] Innovation Australia Government-Department of Industry and Science (Resources). Australian radioactive waste management framework. [Online]. Available: `https://www.industry.gov.au/sites/default/files/2019-04/australian_radioactive_waste_management_framework.pdf`.

[15] C. Jren-chit, S.V.R. Nageswara, K.Y.Y. David, S. Mallikarjun, Y. Yong, and C.H. Jennifer. Identification of low-level point radioactive sources using a sensor network. *ACM Transactions on Sensor Networks*, 7(3):1–35, 2008.

[16] K. Shoukat, A.T. Syed, A. Reyaz, R. Tanveer, M. Ajaz, and F.A. Jan. Radioactive waste management in a hospital. *International Journal of Health Sciences*, 4(1):39–46, 2010.

[17] United State Nuclear Regulatory Commission (U.S.NRC). Detecting radiation. [Online]. Available: `https://www.nrc.gov/about-nrc/radiation/health-effects/detection-radiation.html`.

[18] H. Toivonen, Ph. Holm, K. Perajarvi, T. Ilander, and S. Ihantola. Radioactive source localization with spectrometric data. *Matine*, 846(7):1–7, 2013.

[19] P. Kumpa, B. Er-Wei, Ch. Kung-Sik, and E. William. Detection of shielded radionuclides from weak and poorly resolved spectra using group positive rival. *Radiation Measurements*, 48:18–28, 2013.

[20] P. Fehlau. Comparing a recursive digital filter with the movingaverage and sequential probability-ratio detection methods for snm portal monitors. *Nuclear Science, IEEE Transactions*, 40:143–146, 1993.

[21] D. Budhaditya, J.A.F. Ross, I.Ch. Adrian, and M.J. Hartman. Radioactive source estimation using a system of directional and non-directional detectors. *Nuclear Science, IEEE Transactions*, 58:3281–3290, 2011.

[22] H.E. Baidoo-Williams, M. Raghuraman, B. Er-Wei, and D. Sudeb. Some theoretical limits on nuclear source localization and tracking. *2015 Information Theory and Applications Workshop (ITA)*, pages 270–274, 2015.

[23] I. Orion, A. Pernick, D. Ilzycer, and H. Zafrir. Locating gamma radiation source by self collimating bgo detector system. *Israel Nuclear Society, Conference of the Israel Nuclear Societies*, pages 1–4, 1996.

[24] L.J. Matteson, M.A. Capote, R.T. Skelton, J.G. Batinica, S. Edwin, E.R. Rothschild, H. George, G. Tom, and R.M. Pelling. A directional gamma radiation spectrometer based on pixelated czt arrays and coded mask apertures. *Nuclear Science Symposium Conference Record, 2006. IEEE*, pages 87–92, 2006.

[25] J. Uher, C. Frojdh, J. Jakubek, S. Pospisil, G. Thungstrom, and Z. Vykydal. Directional radiation detector. *Nuclear Science Symposium Conference Record, 2007. NSS '07. IEEE*, pages 1162–1165, 2007.

[26] J.M. Willis, E.S. Skutnik, and L.H. Hall. Detection and positioning of radioactive sources using a four-detector response algorithm. *Nuclear Instruments and Methods in Physics Research, Section A: Accelerators, Spectrometers, Detectors and Associated Equipment*, 767:445–452, 2014.

[27] J.E. Martin. *Physics for Radiation Protection.* John Wiley & Sons, Inc., United States of America, 2006.

[28] S.N. Ahmed. *Physics and Engineering of Radiation Detection.* Elsevier, Great Britain, 2007.

[29] J. Seco, B. Clasie, and M. Partridge. Review on the characteristics of radiation detectors for dosimetry and imaging. *Physics in Medicine and Biology*, pages 303–347, 2014.

[30] L.A. DeWerda and L.K. Wagner. Characteristics of radiation detectors for diagnostic radiology. *Applied Radiation and Isotopes*, pages 125–136, 1999.

[31] Radiation and Nuclear Detection Capability Area Process Action Team (RN CAPAT). For radiation detection systems – specific methods. [Online]. Available: `https://www.nist.gov/sites/default/files/documents/2017/05/09/global_docs_TECMIPT_TTOP_Radiation-Detection-Systems-Specific-Methods.pdf`.

[32] European Nuclear Society (ENS). Ionization chamber. [Online]. Available: `https://www.euronuclear.org/info/encyclopedia/i/ionizationchamber.htm`.

[33] Images Scientific Instruments (ISI). Geiger counter tube. [Online]. Available: `https:http://www.imagesco.com/geiger/geiger-counter-tube.html`.

[34] Scintillator Materials Group (SMG). What are scintillator materials? [Online]. Available: `https://web.stanford.edu/group/scintillators/scintillators.html`.

[35] M. Nikl. Scintillation detectors for x-rays. *Measurement Science and Technology*, 17:37–54, 2006.

[36] A.H.F. Muggleton. Semiconductor devices for gamma ray, x ray and nuclear radiation detection. *Journal of Physics E: Scientific Instruments*, 5:390–404, 1972.

[37] R.P. Parker. Semiconductor nuclear radiation detectors. *Physics in Medicine & Biology*, 15(4):605–620, 1970.

[38] G. Dearnaley. Nuclear radiation detection by solid state devices. *Journal of Physics E: Scientific Instruments*, 43:869–877, 1966.

[39] United States Nuclear Regulatory Commission (U.S.NRC). Measuring radiation. [Online]. Available: `https://www.nrc.gov/about-nrc/radiation/health-effects/measuring-radiation.html`.

[40] Institute for Energy and Environmental Research (IEER). Measuring radiation: Terminology and units. [Online]. Available: https://ieer.org/resource/classroom/measuring-radiation-terminology/.

[41] The Editors of Encyclopædia Britannica (Britannica Articles). Radioactivity. [Online]. Available: https://www.britannica.com/science/activity-radioactivity.

[42] Centers for Disease Control and Prevention (CDC). Measuring radiation. [Online]. Available: https://www.cdc.gov/nceh/radiation/emergencies/measurement.htm?CDC_AA_refVal=https%3A%2F%2Femergency.cdc.gov%2Fradiation%2Fmeasurement.asp.

[43] Australian Radiation Protection and Nuclear Safety Agency (ARPANSA). Units of ionizing radiation measurement. [Online]. Available: https://www.arpansa.gov.au/understanding-radiation/what-is-radiation/radiation/measurement.

[44] S. Mattsson and M. Soderberg. *Radiation Protection in Nuclear Medicine*, chapter 2, pages 7–18. Springer Berlin Heidelberg, Berlin, Heidelberg, 2013.

[45] International Commission on Radiological Protection (ICRP). The 2007 recommendations of the international commission on radiological protection. ICRP publication 103. Ann. ICRP 37. [Online]. Available: http://journals.sagepub.com/doi/pdf/10.1177/ANIB_37_2-4.

[46] International Atomic Energy Agency (IAEA). Radiation protection. [Online]. Available: https://www.iaea.org/topics/radiation-protection.

[47] P. Mora and M. Acuna. Assessment of medical occupational radiation doses in costa rica. *Radiation Protection Dosimetry*, 147(1-2):230–232, 2011.

[48] T. Yuan, Z. Liang, and J. Yongjian. Dose level of occupational exposure in china. *Radiation Protection Dosimetry*, 128(4):491–495, 2008.

[49] Australia Radiation Protection and Nuclear Safety Agency (ARPANSA). Statement on changes to occupational dose limit for lens of the eye (November 2011). [Online]. Available: https://www.arpansa.gov.au/sites/g/files/net3086/f/rhc-statement-occupational-dose-limit-for-eye.pdf.

[50] The National Occupational Health and Safety Commission (NOHSC:1013(1995)). National standard for limiting occupational exposure to ionizing radiation. [Online]. Available: `https://www.safeworkaustralia.gov.au/system/files/documents/1702/nationalstandardforlimitingoccupationalexposure_ionizingradiation_nohsc1013-1995_archivepdf.pdf`.

[51] Australian Radiation Protection and Nuclear Safety agency (ARPANSA). Radiation protection in planned exposure situations. [Online]. Available: `https://www.arpansa.gov.au/sites/g/files/net3086/f/legacy/pubs/rps/rpsc-1.pdf`.

[52] International Atomic Energy Agency (IAEA). Radiation protection of the public and the environment. [Online]. Available: `https://www.iaea.org/publications/11183/radiation-protection-of-the-public-and-the-environment`.

[53] United States Environmental Protection Agency (EPA). Protecting yourself from radiation. [Online]. Available: `https://www.epa.gov/radiation/protecting-yourself-radiation#timedistanceshielding`.

[54] J. Seco, B. Clasie, and M. Partridge. Review on the characteristics of radiation detectors for dosimetry and imaging. *Physics in Medicine & Biology*, 59:303–347, 2014.

[55] K. Gregory, G. Bibbo, and J. Pattison. A standard approach to measurement uncertainties for scientists and engineers in medicine. *Australasian Physical & Engineering Sciences in Medicine*, 28(2):131–139, 2005.

[56] E.B. Podgorsak. *Radiation oncology physics : a handbook for teachers and students*. International Atomic Energy Agency, Vienna, Austria, 2005.

[57] S.D. Sordo, L. Abbene, E. Caroli, A.M. Mancini, A. Zappettini, and P. Ubertini. Progress in the development of CdTe and CdZnTe semiconductor radiation detectors for astrophysical and medical applications. *Sensors*, 9(5):3491–3526, 2009.

[58] X. Li, J. Chu, L. Li, N. Dai, S. Zhang, and F. Zhang. Fabrication and characterization of room temperature nuclear radiation CdZnTe 3x3 pixel array detector. *Photonics and Optoelectronics (SOPO)*, pages 1–3, 2012.

[59] GE Healthcare White Paper (GE). CZT technology: Fundamentals and applications. [Online]. Available: `https://www3.gehealthcare.co.uk/~/media/downloads/uk/education/nm%20white%20papers/czt_technology_white_paper1.pdf?Parent=%7BDB182D8D-D63F-4D8A-B66B-0D1A42BBDC70%7D`.

[60] R. Redus (AMPTEK). Application note ANCZT-2 Rev.3 Charge trapping in XR-100T-CdTe and -CZT detectors. [Online]. Available: `https://amptek.com/pdf/anczt2.pdf`.

[61] A. Bolotnikov (BNL). New developments in wide bandgap CdZnTe (CZT) semiconductor detectors. [Online]. Available: `http://enpl.mephi.ru/download/seminars/2012-05-20_02-39-09_a.bolotnikov_2012_05_18.pdf`.

[62] T.E. Schlesinger, T.E. Toney, H. Yoon, E.Y. Lee, B.A. Brunett, L. Franks, and R.B. James. Cadmium zinc telluride and its use as a nuclear radiation detector material. *Materials Science and Engineering*, 32:103–189, 2001.

[63] T. Takahashi and S. Watanabe. Recent progress in CdTe and CdZnTe detectors. *IEEE Transaction on Nuclear Science*, 48(4):950–959, 2001.

[64] M. Fiederle, V. Babentsov, J. Franc, A. Fauler, and J.P. Konrath. Growth of high resistivity CdTe and (Cd,Zn)Te crystals. *Crystal Research and Technology*, 38:588–597, 2003.

[65] H. Chen, S.A. Awadalla, J. Mackenzie, R. Redden, G. Bendley, A.E. Bolotnikov, G.S. Camarda, G. Carini, and R.B. James. Characterization of Traveling Heater Method (THM) grown $Cd_{0.9}Zn_{0.1}Te$ crystals. *IEEE Transaction on Nuclear Science*, 54(4):811–816, 2007.

[66] A.E. Bolotnikov, G.S. Camarda, G.A. Carini, Y. Cui, K.T. Kohman, L Li, M.B. Salomon, and R.B. James. Performance-limiting defects in CdZnTe detectors. *IEEE Transaction on Nuclear Science*, 54:821–827, 2007.

[67] M. Fiederle. Crystal growth and characterization of detector grade (Cd,Zn)Te crystals. *IEEE Transaction on Nuclear Science*, 54:769–772, 2007.

[68] G. Li, S. Shih, Y. Huang, T. Wang, and W. Jie. Nanostructures of defects in CdZnTe single crystals. *Journal of Crystal Growth*, 311:85–89, 2008.

[69] C. Szeles, S.E. Cameron, J.O. Ndap, and W. Chalmers. Advances in the crystal growth of semi-insulating CdZnTe for radiation detector applications. *IEEE Transaction on Nuclear Science*, 49(5):2535–2540, 2002.

[70] T. Asahi, O. Oda, Y. Taniguchi, and A. Koyama. Growth and characterization of 100 mm diameter CdZnTe single crystals by the Vertical Gradient Freezing method. *Journal of Crystal Growth*, 161(14):20–27, 1996.

[71] J. Franc, P. Moravec, Hlidek, E. Belas, P. oschl, R. Grill, and A. Sourek. Development of inclusion free CdZnTe substrates from crystals grown by the Vertical Gradient Freezing method. *Journal of Electronic Materials*, 32(7):761–765, 2003.

[72] K. Grasza, U. Zuzga-Grasza, A. Jedrzejczak, R. Galazka, J. Maajewski, A. Szadkowski, and E. Grodzicka. A novel method of crystal growth by Physical Vapour Transport and its application to CdTe. *Journal of Crystal Growth*, 161(14):20–27, 1996.

[73] U.N. Roy, O.S. Babalola, J.Jones, Y. Cui, T. Mounts, A. Zavalin, S. Morgan, and A. Burger. Uniform $cd^{\text{ffl}}$ doping of Physical Vapour Transport grown $CdS_xSe_{1-x}$ crystals. *Journal of Electronic Materials*, 34(1):19, 2005.

[74] U.S. Department of Homeland Security (NAT). Civil defense and homeland security: A short history of national preparedness efforts. [Online]. Available: `https://training.fema.gov/hiedu/docs/dhs%20civil%20defense-hs%20-%20short%20history.pdf`.

[75] R. Vilim and R. Klann. Radrac: A system for detecting, localizing and tracking radioactive sources in real time. *Nuclear Technology*, 168(1):61–73, 2009.

[76] F. Carrel, R. A. Khalil, S. Colas, D. de Toro, G. Ferrand, E. Gaillard-Lecanu, M. Gmar, D. Hameau, S. Jahan, F. Lainé, A. S. Lalleman, F. Lemasle, C. Mahé, J. E. Maurer, N. Menaa, S. Normand, H. Onillon, N. Saurel, V. Schoepff, and H. Toubon. Gampix: a new gamma imaging system for radiological safety and homeland security purposes. *IEEE Nuclear Science Symposium and Medical Imaging Conference (NSS/MIC)*, pages 4739–4744, 2011.

[77] B. Deb, J. A. F. Ross, A. Ivan, and M. Hartman. Radioactive source estimation using a system of directional and non-directional detectors. *IEEE Transaction on Nuclear Science*, 58:3281–3290, 2011.

[78] C.P. Lambropoulos, T. Aoki, J. Crocco, E. Dieguez, C. Disch, A. Fauler, M. Fiederle, D. Hatzistratis, V.A. Gnatyuk, K.Karafasoulis, L.A. Kosyachenko, S.N. Levytskyi, D. Loukas, O.L. Maslyanchuk, A. Medvids, T. Orphanoudakis, I. Papadakis, A. Papadimitriou, K. Papakonstantinou, C. Potiriadis, T. Schulman, V.V. Sklyarchuk, K. Spartiotis, G. Theodoratos, O.I. Vlasenko, K. Zachariadou, and E. Zervakis. The COCAE detector: An instrument for localization—identification of radioactive sources. *IEEE Transaction on Nuclear Science*, 58(5):2363–2370, 2011.

[79] L. Hermine, A. Khalil, A.K. Roger, A. Jean-Claude, B. Florent, D.T. Daniel, C. Frédérick, G. Olivier, G. Mehdi, M. Nabil, M. Yves, N. Stéphane, P. Audrey, S. Vincent, T. Philippe, and T. Tebug. Implementation of an imaging spectrometer for localization and identification of radioactive sources. *2013 3rd International Conference on Advancements in Nuclear Instrumentation, Measurement Methods and their Applications (ANIMMA)*, pages 1–5, 2013.

[80] A. Gunatilaka, B. Ristic, C. Mendis, S. Karunasekera, and A. Skvortsov. The effect of data collection geometry on radiological source localisation. *2009 International Conference on Intelligent Sensors, Sensor Networks and Information Processing (ISSNIP)*, pages 145–150, 2009.

[81] R.J. Nemzek, J.S. Dreicer, and D.C. Torney. Distributed sensor networks for detection of mobile radioactive sources. *IEEE Transactions on Nuclear Science*, 51(4):1693–1700, 2004.

[82] B. Deb. Iterative estimation of location and trajectory of radioactive sources with a networked system of detectors. *IEEE Transactions on Nuclear Science*, 60(2):1315–1326, 2013.

[83] U. Bhattacharyya and C. Baum. Estimating the location of a nuclear source in a three-dimensional environment using a two-stage adaptive algorithm. *2018 IEEE 8th Annual Computing and Communication Workshop and Conference (CCWC)*, pages 8–14, 2018.

[84] C. Jren-chit, D.K.Y. Yau, R.S.V. Nageswara, Y. Yong, C.Y.T Ma, and S. Mallikarjun. Accurate localization of low-level radioactive source under noise and measurement errors. *Proceedings of the 6th ACM conference on Embedded network sensor systems*, 8(14):183–196, 2008.

[85] R. Li, Z. Fang, B. Hao, and F. Yang. Research on indoor wireless localization system for radioactive sources based on zigbee. *2010 International Conference on Computing, Control and Industrial Engineering*, pages 359–362, 2010.

[86] J.S. Clair. Radioactive source localization in urban environments with sensor networks and the internet of things. *IEEE lntemational Conference on Multisensor Fusion and Integration for Intelligent Systems (MFI)*, pages 384–388, 2016.

[87] S. Chen, T. Ma, F. He, Y. Liu, and S. Wang. A new compact gamma camera with super resolution capability and high sensitivity for monitoring sparse radioactive sources in large area. *2013 IEEE Nuclear Science Symposium and Medical Imaging Conference (2013 NSS/MIC)*, pages 1–4, 2013.

[88] J.E. Lees, S.L. Bugby, A.P. Bark, D.J. Bassford, P.E. Blackshawb, and A.C. Perkins. A hybrid camera for locating sources of gamma radiation in the environment. *Journal of Instrumentation*, 8(10):1–11, 2013.

[89] S. Huh, J. Maltz, D. Gunter, L. Mihailescu, and K. Vetter. Real-time radioactive source localization with a moving coded-aperture detector system at low count rates. *IEEE Nuclear Science Symposiwn and Medical Imaging Conference Record (NSS/MIC)*, pages 666–673, 2012.

[90] C. Papadimitropoulos, I. Kaissas, C. Potiriadis, K. Karafasoulis, D. Loukasd, and C.P. Lambropoulos. Radioactive source localization by a two detector system. *17th International Workshop on Radiation Imaging Detectors*, pages 1–9, 2015.

[91] V. Paradiso, K. Amgarou, N. Blanc De Lanaute, V. Schoepff, G. Amoyal, C. Mahe, O. Beltramello, and E. Liénard. A panoramic coded aperture gamma camera for radioactive hotspots localization. *Journal of Instrumentation*, 12(11):1–16, 2017.

[92] K.N. Shokhirev, D. Konno, T.M. Schmit, V. Ziskin, and B.R. Cosofret. Man-portable radiation detector based on advanced source detection, identification, and localization algorithms. *2015 IEEE Nuclear Science Symposium and Medical Imaging Conference (NSS/MIC)*, pages 1–5, 2015.

[93] D. Magalotti, P. Placidi, M. Dionigi, A. Scorzoni, L. Bissi, and L. Servoli. A wireless personal sensor node for the dosimetry of interventional radiology operators. *IEEE International Symposium on Medical Measurements and Applications (MeMeA)*, pages 1–6, 2015.

[94] Z. Liu and A. Nehorai. Detection of particle sources with directional detector arrays and a mean-difference test. *IEEE Transaction on Signal Processing*, 53(12):4472–4484, 2005.

[95] N. Schemm, S. Balkır, M.W. Hoffman, and M. Bauer. A directional gamma ray detector using a single chip computational sensor. *2011 IEEE SENSORS Proceedings*, pages 1760–1763, 2011.

[96] E. Conti, P. Placidi, D. Magalotti, L. Bissi, M. Paolucci, A. Scorzoni, and L. Servoli. A portable dosimetric system based on a cmos image sensor for radiation protection in interventional radiology. pages 288–292, 2014.

[97] Geant4 Collaboration (CERN). Introduction to geant4. [Online]. Available: `http://geant4.web.cern.ch/geant4/UserDocumentation/UsersGuides/IntroductionToGeant4/html/index.html`.

[98] Geant4 Collaboration (CERN). Geant4 user's guide for application developers. [Online]. Available: `http://geant4.web.cern.ch/geant4/UserDocumentation/UsersGuides/ForApplicationDeveloper/html/`.

[99] Geant4 Collaboration (CERN). Geant4 material database. [Online]. Available: `http://geant4.web.cern.ch/geant4/UserDocumentation/UsersGuides/ForApplicationDeveloper/BackupVersions/V10.2/html/apas06.html`.

[100] Freely Accessible Remote Laboratories (FarLabs). Radiation and the "Inverse-Square" Law. [Online]. Available: `https://www.farlabs.edu.au/nuclear/explain-inverse-square-law/`.